Study on Creep Behavior of Semi-Solid A356 Alloy Produced by the GISS Process

Yi Zhou

A Thesis Submitted in Fulfillment of the Requirements for the Degree of

Master of Engineering in Materials Engineering

Prince of Songkla University

2011

Thesis Title	Study on Creep Behavior of Semi-Solid A356 Alloy Produced by the GISS Process
Author	Mr. Yi Zhou
Major Program	Materials Engineering

Major Advisor

…….....

(Asst. Prof. Dr. Thawatchai Plookphol)

Co-Advisors

…….....

(Assoc.Prof.Dr.Sirikul Wisutmethangoon)

…….....

(Asst. Prof. Dr. Jessada Wannasin)

Examining Committee

……..…..…..….....Chairperson

(Asst. Prof. Dr. Prapas Muangjunburee)

……....…….....

(Asst. Prof. Thawatchai Plookphol)

……..…….....

(Assoc. Prof. Dr.Sirikul Wisutmethangoon)

…….....

(Assoc. Prof. Dr. Chaowalit Limmaneevichitr)

The Graduate School, Prince of Songkla University, has approved this thesis as partial fulfillment of the requirements for the Master of Engineering Degree in Materials Engineering.

……...……..……

(Prof. Dr. Amornrat Phongdara)

Dean of Graduate School

Thesis Title	Study on Creep Behavior of Semi-Solid A356 Alloy Produced by the GISS Process
Author	Mr. Yi Zhou
Major Program	Materials Engineering
Academic Year	2011

ABSTRACT

The A356 alloy is a class of aluminum alloy widely applied in automotive industries because of its high strength, good heat treatability, and excellent castability. Gas Induced Semi-Solid (GISS) process is a kind of semi-solid preparation process which has been developed by a Thai and US researcher team at the Department of Mining and Materials Engineering, Prince of Songkla University, Thailand. In the GISS, non-dendrite, globular, semi-solid metal slurry can be obtained via using flowing gas bubbles through a porous graphite diffuser into the molten metal at a temperature between its liquidus point and solidus point to get semi-solid slurry with 10~70% solid fraction before cast into the molds in order to get less gas porosity, smaller solid shrinkage, better heat treatability and higher ductility with shorter cycle times. Nowadays there are many parts of automotive and aeroplane are replaced by aluminum alloys to reduce weight and save energy, however many of them have to expose at high temperature and endure high stress conditions, where time-dependent plastic deformation and fracture process always take place, this phenomenon was first referred to as stretch by Philips and viscous flow by Andrade, later became known as creep. Therefore, it is vital to learn creep properties before design for high temperature application of those aluminum alloys.

In this study, a tensile creep test machine has been designed and fabricated by the author and his team. Primary A356 alloy pieces were produced by squeeze casting with and without the GISS process, and further improved by the T6 heat treatment. Tensile and creep properties of the A356 alloy with different cast process and T6 heat treatment were investigated, microstructures of the alloys were observed by OM, SEM and TEM, and mechanical composition of them were tested

by OES and EDX. Large primary stage of creep was observed and several numerical models were discovered to describe and simulate the creep curves.

Keywords: GISS process, SSM A356 alloy, high temperature properties, creep.

ACKNOWLEDGEMENT

First of all, the author would like to express his sincere gratitude to his advisors, Asst. Prof. Dr. Thawatchai Plookphol, Assoc. Prof. Dr. Sirikul Wisutmethangoon and Asst. Prof. Dr. Jessada Wannasin, and also extend his heartfelt thanks to Asst. Prof. Dr. Prapas Muangjunburee for his help and guidance.

High tribute shall be paid to the external committee, Assoc. Prof. Dr. Chaowalit Limmaneevichitr.

The author would like to express his thanks to the semi-solid group, heat treatment group and welding group of Department of Mining & Materials Engineering, Prince of Songkla University.

Last but not least, the author would like to thank Mr. Suchart Chanratamanee, Mrs. Narissara Mahathaninwong, Mr. Sarawut Gonsrang, Mr. Phairote Sungkhaphaitoon and all of his friends in the Department of Mining & Materials Engineering, Faculty of Engineering, Prince of Songkla Unierisity.

This research program was partially supported by the Graduate School of Prince of Songkla of University and the National Research University (NRU) project of Thailand's Office of Higher Education Commission (NO. ENG540551d).

Yi Zhou

TABLE OF CONTENTS

LIST OF TABLES

LIST OF FIGURES

Chapter 1. Introduction

1.1. Background of the A356 aluminum casting alloy

Casting alloy is defined as alloys used for productions which are produced by the shape casting. Casting aluminum alloys nowadays has a wide range of applications and shares a big portion in the worldwide metallic materials market because of its lightweight (around 2.7g/mm^2), high strength (above 200MPa) and good ductility, according to different reports of estimation, 20~30% of all aluminum products in the world are produced by shape casting [1].

A356 (Al-7Si-0.3Mg) is a class of aluminum-silicon based casting alloy widely applied in automotive industries [2], for example hub of wheel (Fig. 1-1), engine block (Fig. 1-2) and engine cover (Fig. 1-3), because of its high strength, good heat treat-ability, and excellent castability.

Eutectic point of the Al-Si binary eutectic system is 12.6 wt.% Si [3]. The typical microstructure of hypoeutectic Al-Si alloys at room temperature is featured by soft and ductile primary aluminum phase α surrounded by hard and brittle eutectic silicon phase [2].

Chemical composition limits of this grade of alloy was defined by the ASTM B108 Standard [4], which contains silicon 6.5-7.5%, iron ≤ 0.20%, copper ≤ 0.20%, manganese ≤ 0.10%, magnesium 0.25-0.45%, zinc ≤ 0.10%, titanium ≤ 0.20%, others except aluminum each ≤ 0.05% and total ≤ 0.15%, and balance is aluminum.

Fig. 1-1 Yokohama hub made from A356 aluminum alloy.
[*http://blog.xuite.net/atenzatt/2008/34382237*]

Fig. 1-2 Fontana engine block made from A356 aluminum alloy.
[*http://www.fontana-automotive.com/index.php/products/new-generation-engine*]

Fig. 1-3 Fontana engine cover made from A356 aluminum alloy.
[*http://www.fontana-automotive.com/index.php/products/new-generation-engine*]

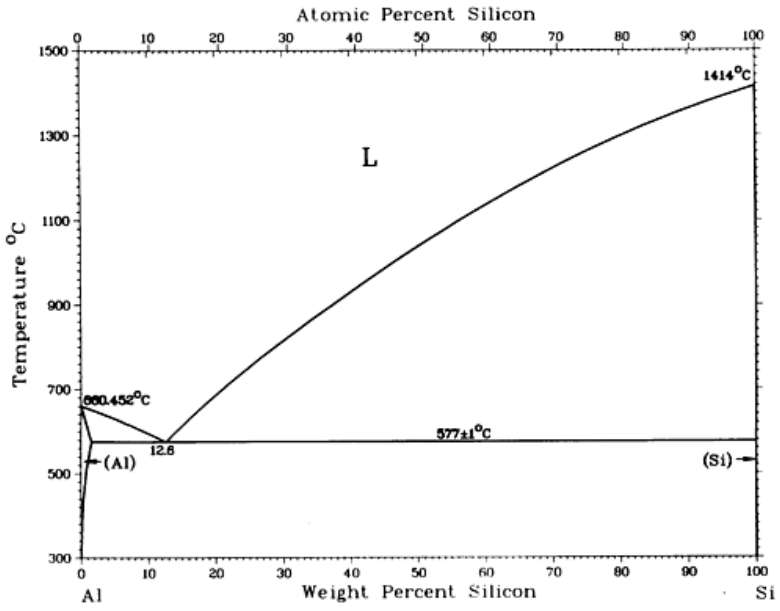

Fig. 1-4 Phase diagram of Al-Si binary alloy. [3]

1.2. Background of the gas-induced semi-solid casting

Semi-solid metal (SSM) casting is an advanced process, invented and identified in the Massachusetts Institute of Technology in early 1970s, for producing near-net shape non-ferrite alloy products for industrial applications such as automobile engine parts, aeronautic parts and so forth [9]. The SSM process is done by hold the alloy at a temperature between its liquidus and solidus temperature, with 10~70% solid fraction, for creating globular primary phase distributing in the liquid phase, then a low viscous slurry could get before casting or forming. There are many advantages of the SSM process compared with the conventional liquid casting have been reported in the past, for example less gas porosity, smaller solid shrinkage, better heat treat-ability, higher ductility and shorter cycle times.

However, there is still a cost disadvantage with the conventional SSM process because of its complex equipment and working process, to improve the situation, a novel process named Gas-Induced Semi-Solid (GISS) process has been developed by a Thai and US researcher team at the Department of Mining and Materials Engineering, Prince of Songkla University, Thailand [10]. In the GISS, non-dendrite, globular, semi-solid metal slurry can be obtained via using flowing gas bubbles through a porous graphite diffuser into the molten metal at a temperature between its liquidus point and solidus point to get semi-solid slurry (Fig. 1-5). Fig. 1-6 and Fig. 1-7 show a comparison of a typical dendritic structure of A356 alloy produced by the conventional liquid casting and globular structure of semi-solid A356 alloy produced by the GISS process.

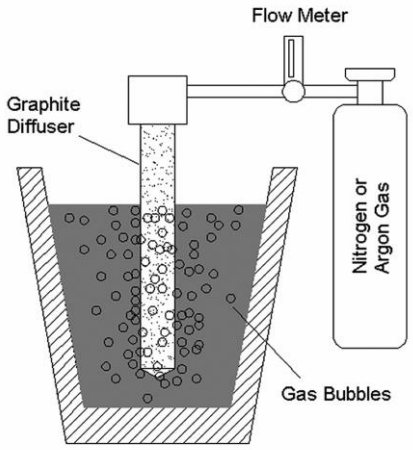

Fig. 1-5 A schematics of the GISS process. [11]

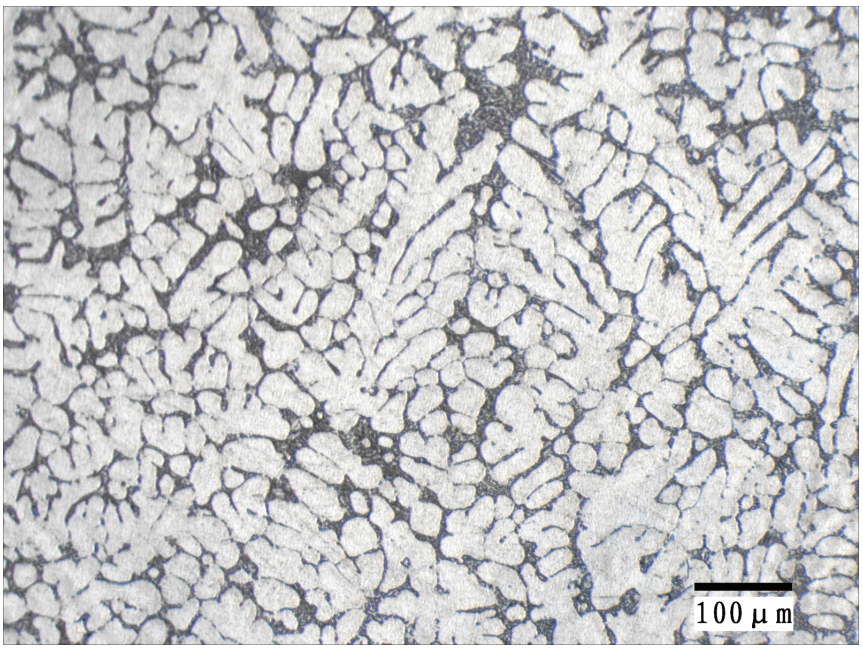

Fig. 1-6 A typical dendritic structure of as cast A356 alloy produced by conventional liquid casting.

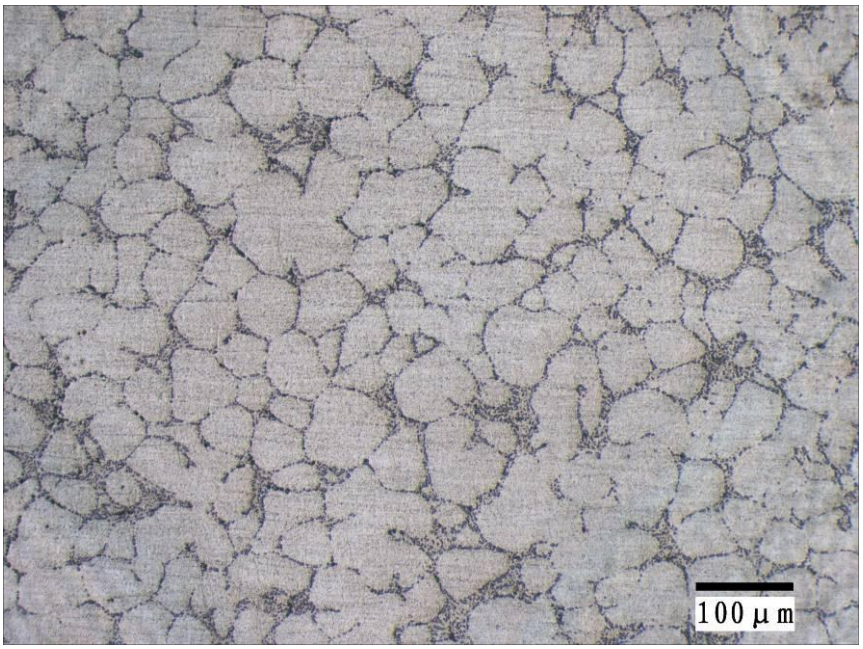

Fig. 1-7 Globular structure of as cast A356 alloy produced by the GISS SSM process.

1.3. Background of T6 heat treatment of aluminum alloys

Heat treatment of metal materials is a group of process for altering physical, mechanical, and sometimes chemical, properties of the materials by controlled heating and cooling without changing the product shape.

The Heat treatment is applicable for both ferrous and nonferrous alloys. However, there are great differences between different alloys so each group of alloys has its own suitable heat treatment principles. The purpose of T6 heat treatment, which concludes two steps, solid solution and artificial aging, is producing maximum strength for aluminum alloys. The principle and strengthening mechanism of T6 heat treatment will be discussed in chapter 2 and the practice of the T6 heat treatment for the A356 alloy will be presented in chapter 3.

1.4. Background of creep

The definition of creep behavior is a sort of time-dependence plasticity of materials under a fixed stress and an elevated temperature, for aluminum alloys are normally above 0.54 T_m, where T_m is absolute melting temperature of the alloys [5]. Suppose that we load a uniaxial constant force on an unnotched tensile specimen at a constant high temperature level, as it is shown in Fig. 1-8, the specimen may creep with a typical elongation-time curve which is shown in Fig. 1-9.

As shown in Fig. 1-9, the creep behavior could easily be observed at a high temperature, this time-deformation phenomenon was first referred to as stretch by Philips [6] and as viscous by Andrade [7]. Generally speaking, most Al-Si based casting alloys was not suitable for high temperature (above 500°F, or 227°C) applications, but nowadays many Al-Si alloys are used or machined on force and high temperature conditions which creep take places, for example diesel and direct fuel injection gasoline engines, for the high value of these applications there are more and more researchers have joined for studying on creep behavior of the Al-Si based alloys and its composites [8].

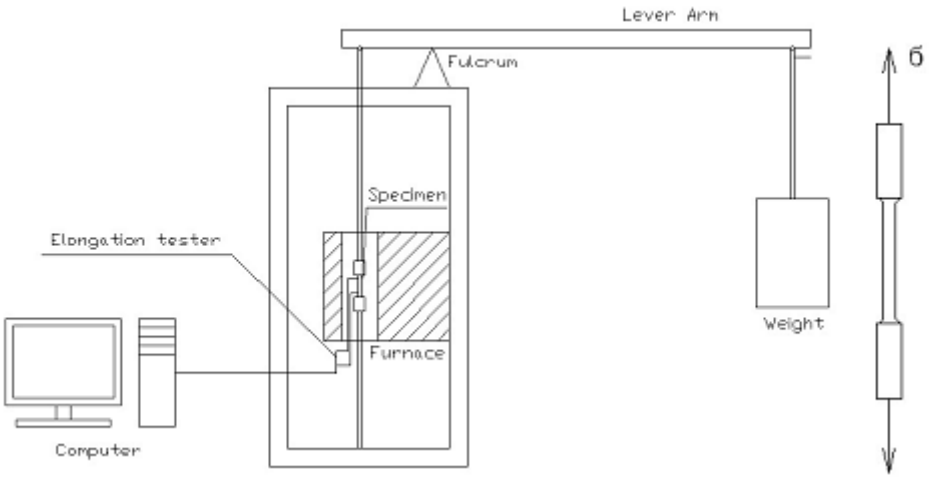

Fig. 1-8 Sketch of a constant load apparatus.

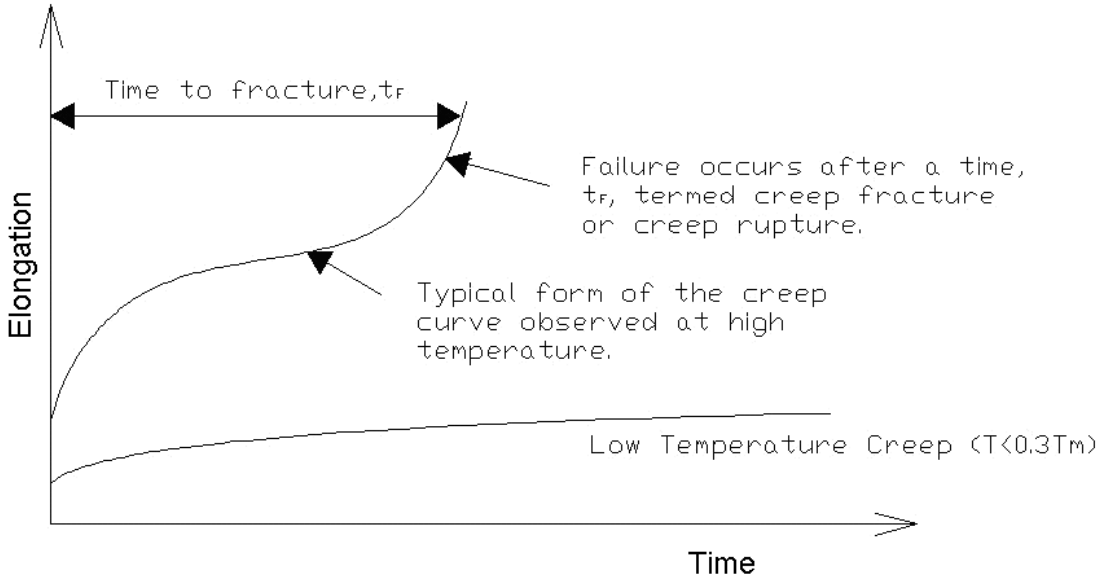

Fig. 1-9 Sketch of a typical creep curve.

1.5. Thai automotive industry

According to a report of Thailand Automotive Institute, automotive industry growths rapidly and seems speeded up in recent years (Fig. 1-10). Engines account 11.14% of exporting market, values about 520,000,000 US dollars, and component parts account 37.89%, 1,768,680,000 US dollars (Fig. 1-11). More and more engines parts and some of the component parts nowadays are made of aluminum alloy to reduce weight of the vehicles, so the future market of aluminum alloy seems good.

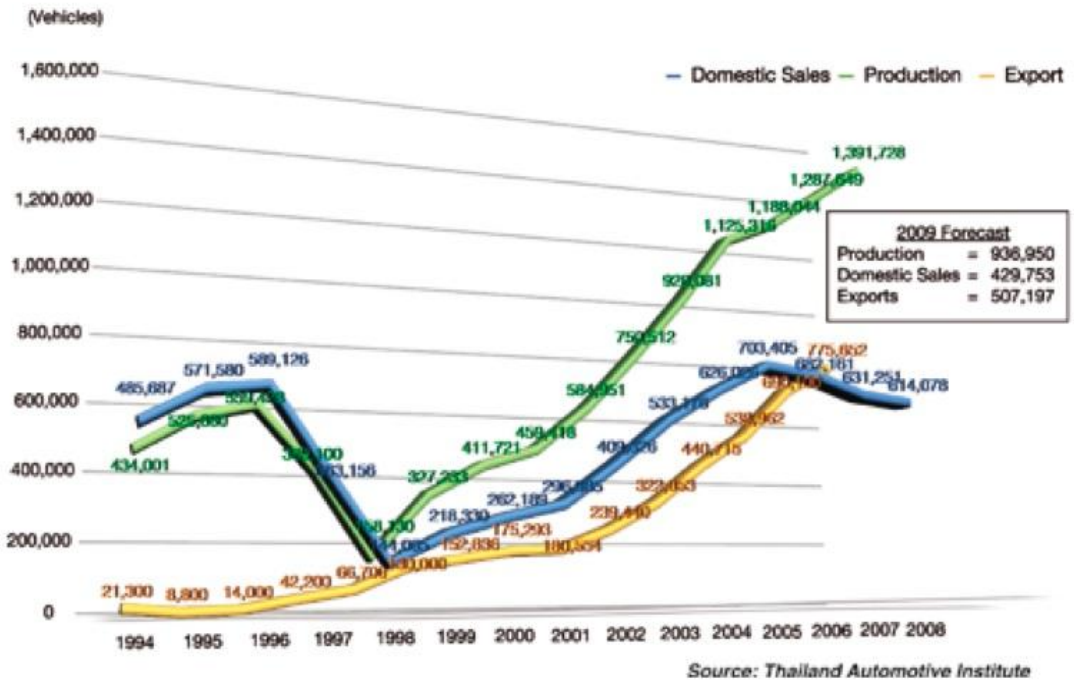

Fig. 1-10 Thailand automotive market capacity changes in the past years. [*http://www.business-in-asia.com/automotive/thailand_automotive.html*]

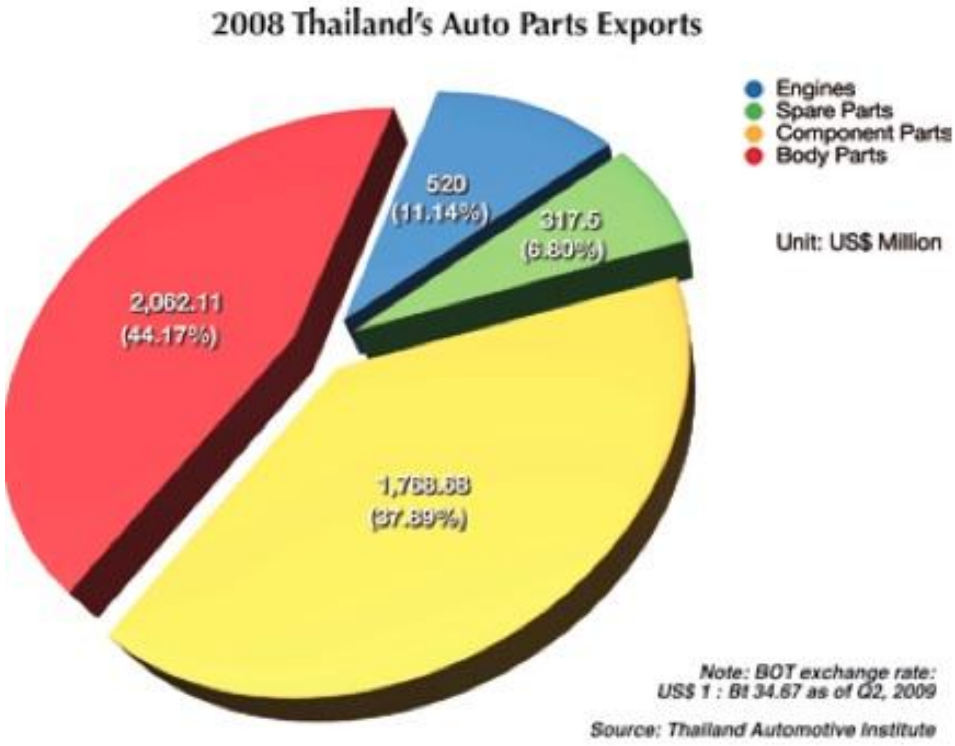

Fig. 1-11 Thailand automotive parts exports.
[*http://www.business-in-asia.com/automotive/thailand_automotive.html*]

1.6. Motivation

Although there are some people who have already studied on the creep behavior of the aluminum alloys, only a few of them work on the heat treatment and precipitation effect on creep properties of the non-ferrite alloy, none of them has well concluded the kinetic constitutive equation of interaction of the precipitations and creep behavior interaction of non-ferrite alloys, and also none of them has studied on the semi-solid cast aluminum alloy. However, as it was mentioned in section 1.1, 1.2, 1.3 and 1.5, both of the GISS semi-solid process and its heat treatment have widespread applications and an expectable future, all these motivated us to study on the creep behavior of the GISS A356 alloy.

1.7. Objectives

1. To investigate room and high temperature tensile properties of the semi-solid A356 alloy produced by the GISS process.

2. To study creep behavior of the semi-solid A356 alloy.

1.8. Scope of thesis

This research program investigated creep behavior of the A356 alloy produced by the GISS semi-solid process, the scope of the full program could be concluded as follows:

1. Design and fabricate two creep test machine.

2. Test run the creep test machine.

3. Practice the Gas-Induced Semi-Solid process and squeeze casting with different parameters for producing A356 aluminum alloy plates.

4. Practice the T6 heat treatment to improve mechanical properties of the SSM a356 aluminum alloy.

5. Investigate the tensile property of both of the SSM A356 alloy and liquid-cast A356 alloy at various temperature levels with a range from room temperature to 250°C.

6. Study on different conditions of artificial aging effect on the creep properties of the SSM A356 alloy.

7. Run creep tests at different temperature and stress levels of the SSM A356 alloy for getting a full map of creep properties of the SSM A356 alloy.

8. Find out a suitable model for describing the creep curves.

9. Study microstructures of the SSM A356 alloy in different conditions by optical, SEM or TEM for learning the mechanism and precipitation of during creep.

Chapter 2. Theory and Literature Review

2.1. Creep test apparatus

Creep test machine is a kind of apparatus could support a long-time force and a harmonious controllable atmosphere at different temperatures on a creep specimen, and could record the deformation of the specimen precisely, normally it includes a environmental chamber or a furnace, a force supporting system and a data acquisition system. There are many sorts of creep test machine in the world such as level arm tensile creep test machine, electronical universal creep and relaxation test machine, hydraulic pressure compression creep test machine, small punch creep test machine and so forth. Our group learned ideas from different kind of creep test apparatus, and then adapted the most suitable type for our research, and the steps of fabrication could be concluded in six steps as follows:

1. Conceptual design
2. Parts Fabrication
3. Machine Assembly
4. Machine Aligning
5. Test-running
6. Modifying for perfection

For overall consideration of the application, property, complexity and cost, we decided to follow the idea in the ASM Metal Handbook [12], which has shown a typical pattern of tensile creep test machine, and we are not only adopted it but also simplified it and modified most parts of it for our situation.

Fig. 2-1 and Fig. 2-2 show a typical creep test machine in ASM Metal Handbook, in the photo we can clearly see a furnace and a level arm system, and Fig. 2-3 shows a rod-and-tube-type extensometer for record the deformation of the specimen. Our research group designed our own tensile creep test machine by following this pattern. By the way, in my opinion the rod-and-tube-type extensometer in Fig. 2-3 is not a good idea, and nowadays people around the world have some better design.

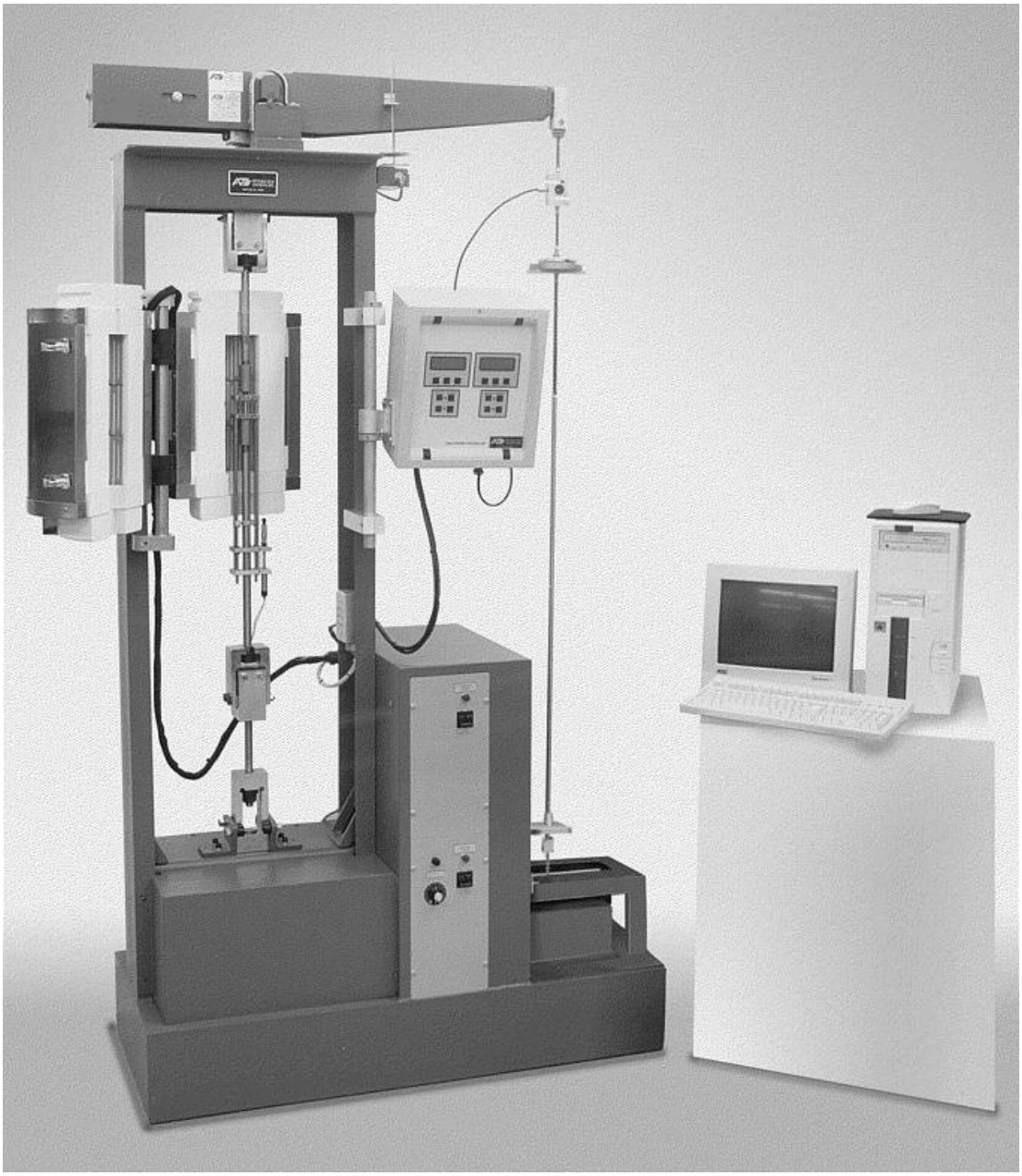

Fig. 2-1 A creep test machine shown in the ASM Metal Handbook. [12]

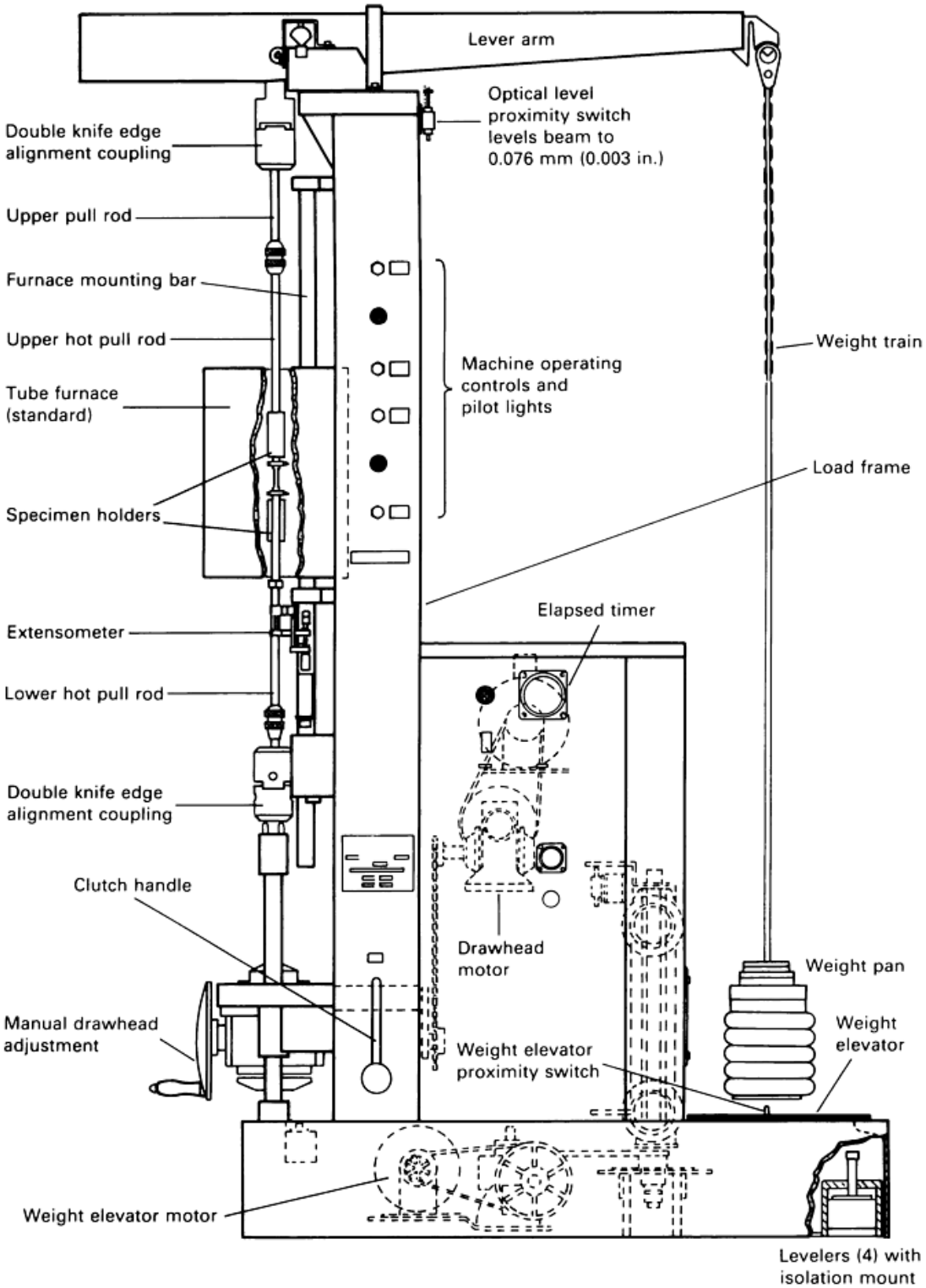

Fig. 2-2 Schematic of a creep test machine shown in the ASM Metal Handbook. [12]

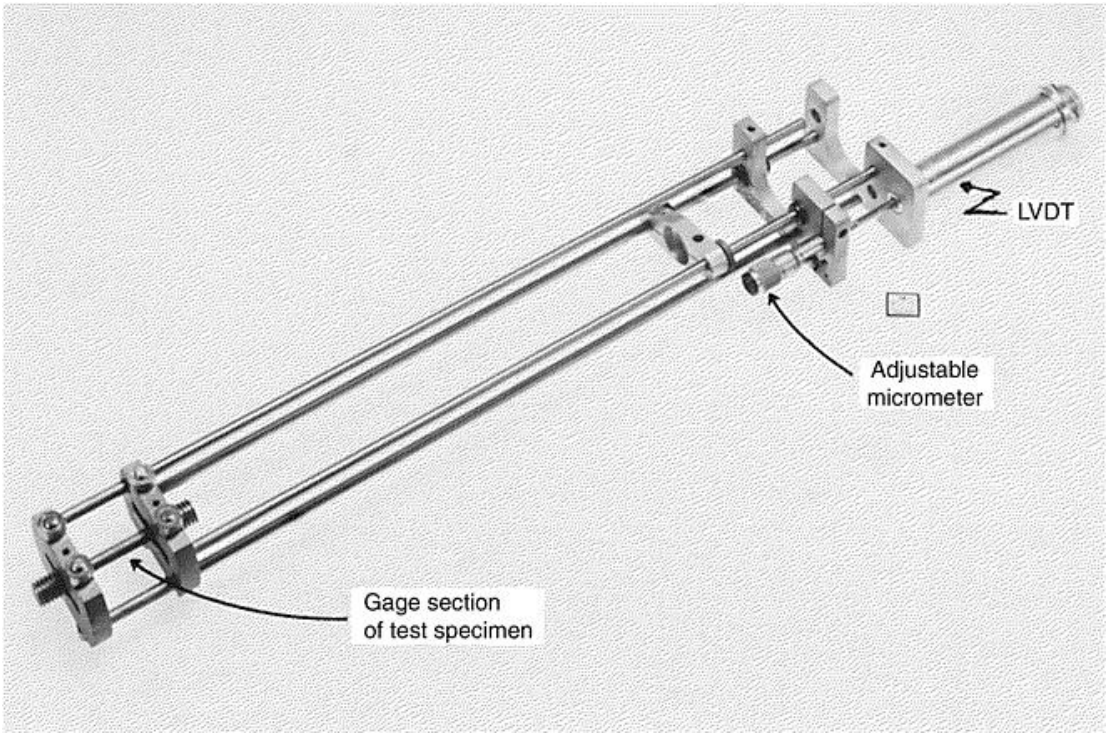

Fig. 2-3 Schematic of a creep test machine shown in the ASM Metal Handbook. [12]

2.2. Semi-solid casting

The mechanism for globular structure growth during semi-solid process is still unclear, a reasonable explanation of this phenomenon is grain multiplication by dendrite fragmentation [10], as shown in Fig. 2-4, dendrites in the metal slurry at the early stage of solidification was broke into small particles, then a large number of small solid grains grow up to mass globular phase, result in a globular structure.

In the GISS, as it was illustrated in Fig. 1-5, fragmentation is achieved by a fine gas bubble flow, many bubbles are induced into the melt through a porous graphite diffuser for infusing vigorous convection in order to impulse grain multiplication and then produce mass fine solid particles.

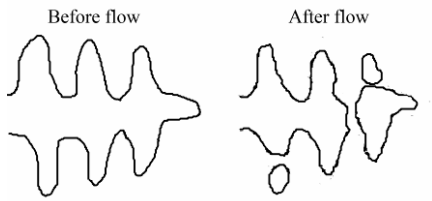

Fig. 2-4 Schematic of Dendrite multiplication model. [10]

2.3. T6 heat treatment

The T6 heat treatment for A356 aluminum alloy follows ASTM standard B 917, it includes a solution treat followed by artificial aging, the suitable temperature and time for solution treat and artificial aging are about 1000°F, 6~12hours and 310°F, 2~5 hours (peak aged), respectively, but it is just a guideline for tempering, people usually tempered with parameters out of this range in practice.

2.3.1 Diffusion

Diffusion in the physical metallurgy field means the movements of atoms within a solution including solid solution [13], and it is the dominant process which governs the rate of structural changes in heat treatment of metals and alloys [14]. There are several different explanations of diffusion mechanism and each of them may takes place in different conditions.

2.3.1.1 Self diffusion

Generally people define the diffusion which is not caused by concentration gradient but lead by atom thermal vibration as self diffusion. There are some conceives of mechanism of atom movement in the lattice, Fig. 2-5, Fig. 2-6 and Fig. 2-7 illustrate three acceptable ones.

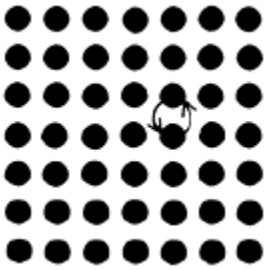

Fig. 2-5 Couple atoms interchange. [13]

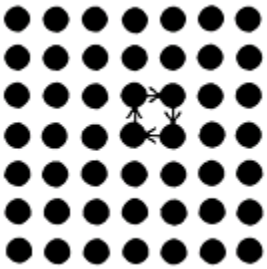

Fig. 2-6 Four atoms rotating. [13]

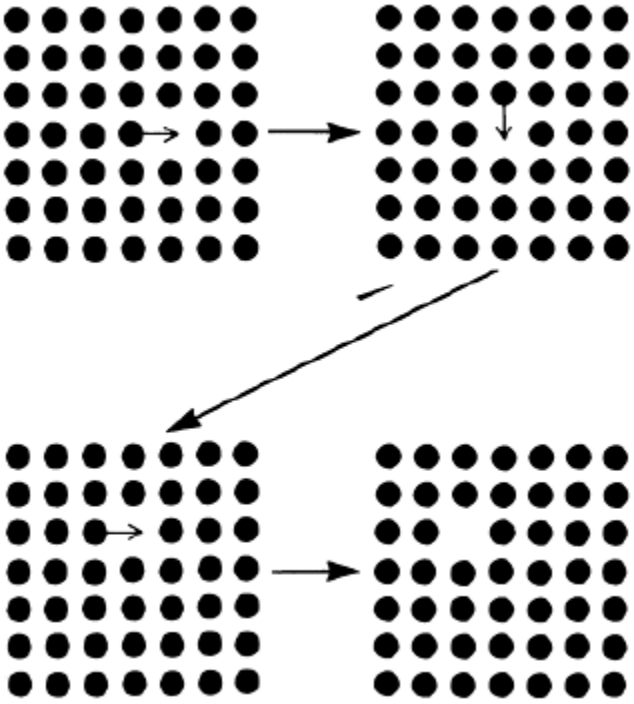

Fig. 2-7 Vacancy movements. [13]

All the three mechanisms have possibility to take place but are normally vacancy movement dominant the self diffusion in most pure metals [13]

because it requires less energy for atom moving when vacancies exist in the lattice.

2.3.1.1 Chemical diffusion

Chemical diffusion usually occurs in alloys because of the electrochemical potential differences between different elements. Fig. 2-5 above describes how do two atoms replacement in the lattice, the process will be easier when there is an electrochemical potential gradient exist between the atoms.

2.3.1.1 Interstitial diffusion

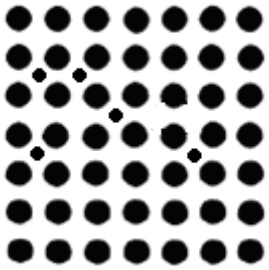

Fig. 2-8 Interstitial movement. [13]

As it is shown in the Fig. 2-8, small atoms sometimes slide into the clearance of larger solvent atoms, this kind of phenomenon was defined as interstitial movement.

2.3.1.1 Grain boundary diffusion

Atoms can diffuse fast along grain boundaries, by crossing cores of dislocations and free surfaces, and this class of diffusion greatly affects the precipitation on the grain boundary of aluminum alloys.

2.3.2 Solution heat treatment

The purpose of solution heat treatment is to solute alloying elements into the solid solution by heat the alloys up to a temperature (t_{SHT}) below solidus line and a period of holding time. Usually there patches of precipitates with a wide range of size distribution and the coarse precipitates always cause brittleness to the alloys, so people use solution heat treatment to dissolve it, Fig. 2-9 illustrates the process of precipitates solution.

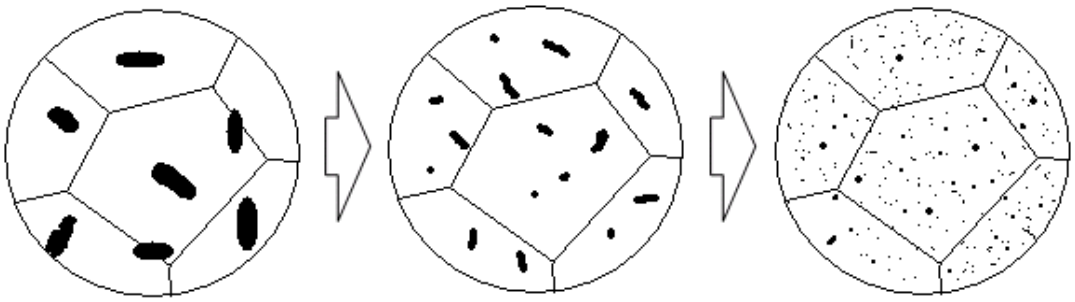

Fig. 2-9 Schematic of microstructure change during solution heat treatment. [13]

2.3.3 Precipitation hardening of the A356 aluminum alloy

As it was mentioned in the paragraph 2.3.2 that the coarse precipitates were dissolved throughout the metal matrix, so it will be a supersaturated solid solution with finely dispersed precipitates if we provide a rapid quench after the solution heating, and ready to precipitate not only below the equilibrium solvus temperature but also below a metastable miscibility gap named Guinier-Preston (GP) zone solvus line [15].

The precipitate often comes out through several stages, for the Al-Si-Mg system it concludes Embryo clusters, needle-shaped GP zones β'', intermediate β' and finally β (Mg_2Si) [16].

Mechanical properties of the A356 alloys is high depends on its β phase because fine and dispersed precipitation could block movement of dislocation moving, as it is illustrated in Fig. 2-10, where *d* is the distance between two particles. Suppose that total volume of precipitation phase *f* is a constant in peak aged alloys, proportion will exist between average precipitation particle radius *r* and average distance of particles *d*, as it is concluded in equation (7). When both *r* and *d* is small, dislocation may get across the precipitates by segmenting of the them when dislocation gliding [31], as it is shown in Fig. 2-11, and when *r* increased to a larger size, Orowan's mechanism may be activated, which is expanding dislocation loops around the precipitates large particles [13] as it is sketched *n* in Fig. 2-12.

$$d = (2\pi / 3f)^{1/2} r \tag{7}$$

In industrial applications it is always realized by artificial aging, which is a class of heat treatment process to hasten precipitation of the alloys.

J. Dunnwald has published his paper of modeling of creep behavior of Al-Cu-Mg 2024 alloy in 1996, a comparison of creep behavior of solution annealed and overaged 2024 alloy was motioned, as it is shown in Fig. 2-13, creep property of as solution annealed 2024 alloy is much better than the overaged 2024 alloy.

The underaging enhanced creep performance of the 2024 aluminum

alloys was presented by R. N. Lumley in 2000 and 2002 [36, 37], these papers reported that the anti-creep property of the underaged 2024 alloy is better than the T6 peakaged ones (Fig. 2-14), because the θ' phase (Al_2Cu) was precipitated in conjunction with the S phase (Al_2CuMg) during creep process of the underaged 2024 alloy and it substantially improved the anti-creep property, though its room temperature properties is lower than the T6 peakaged ones.

A. M. Abd El-Khalek has studied on the aging process effects on the steady state creep and creep recovery behavior of Al-Si alloy and Al-Si-Zr-Ti alloys [38], he aged all of the alloys for 12 hours but with different temperature levels, and found that the lowest aging temperature afforded the lowest steady-stage creep rate as it is presented in Fig. 2-16.

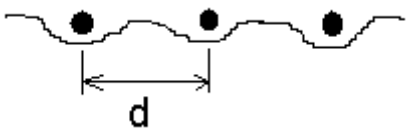

Fig. 2-10 Schematic of precipitation blocking dislocation line moving. [13]

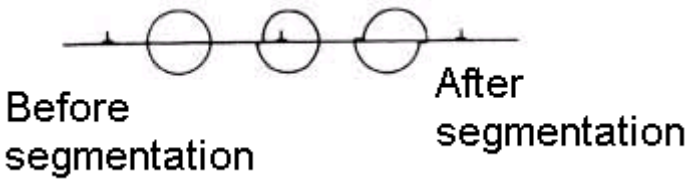

Fig. 2-11 Schematic of precipitation particles segmented by dislocation gliding. [*http://www.usteel.com/plus/view-6688-1.html*]

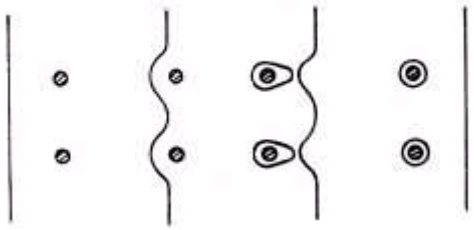

Fig. 2-12 Schematic of precipitation particles surrounded by dislocation loops. [*http://www.usteel.com/plus/view-6688-1.html*]

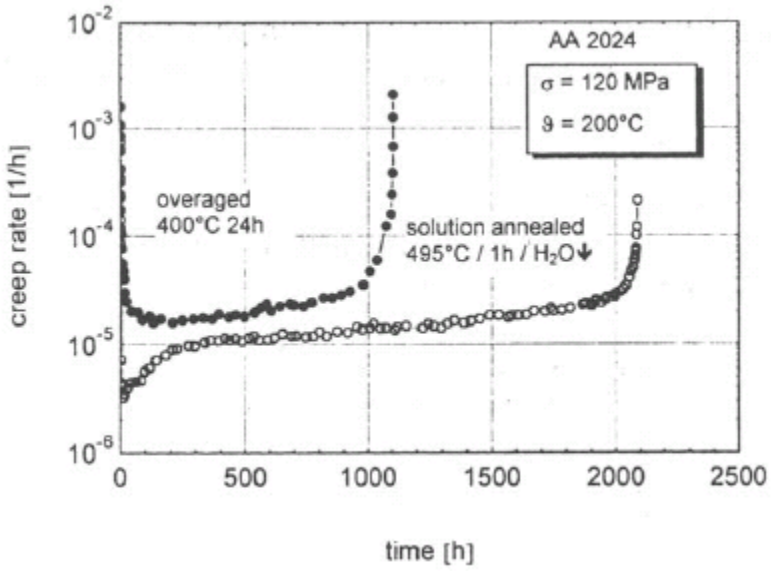

Fig. 2-13 A comparison of creep behavior of solution annealed and overaged 2024 alloys.[35]

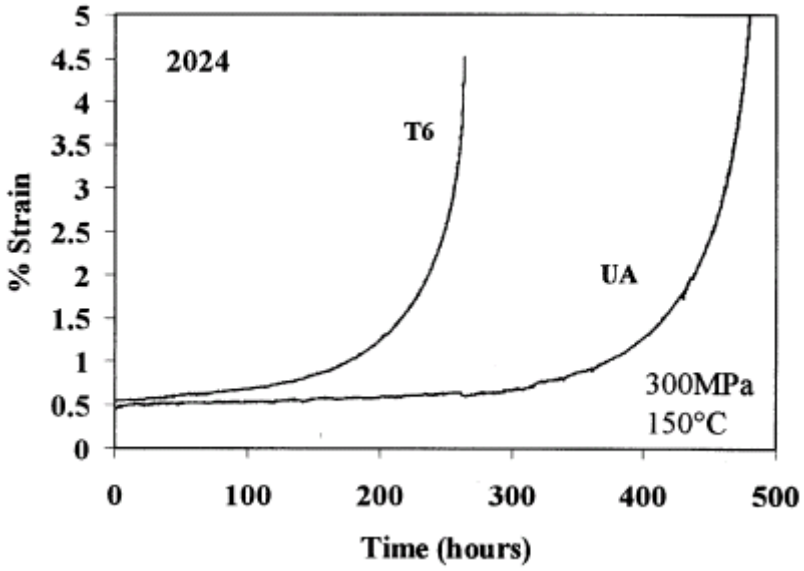

Fig. 2-14 A comparison of creep behavior of underaged and peakaged 2024 alloy.[35]

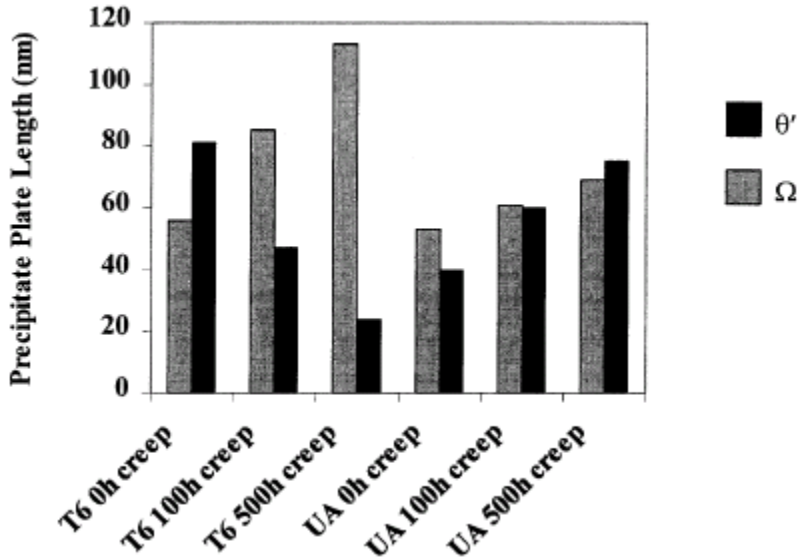

Fig. 2-15 Changes in average precipitate lengths during creep of underaged (UA) and peakaged (T6) 2024 alloys. [37]

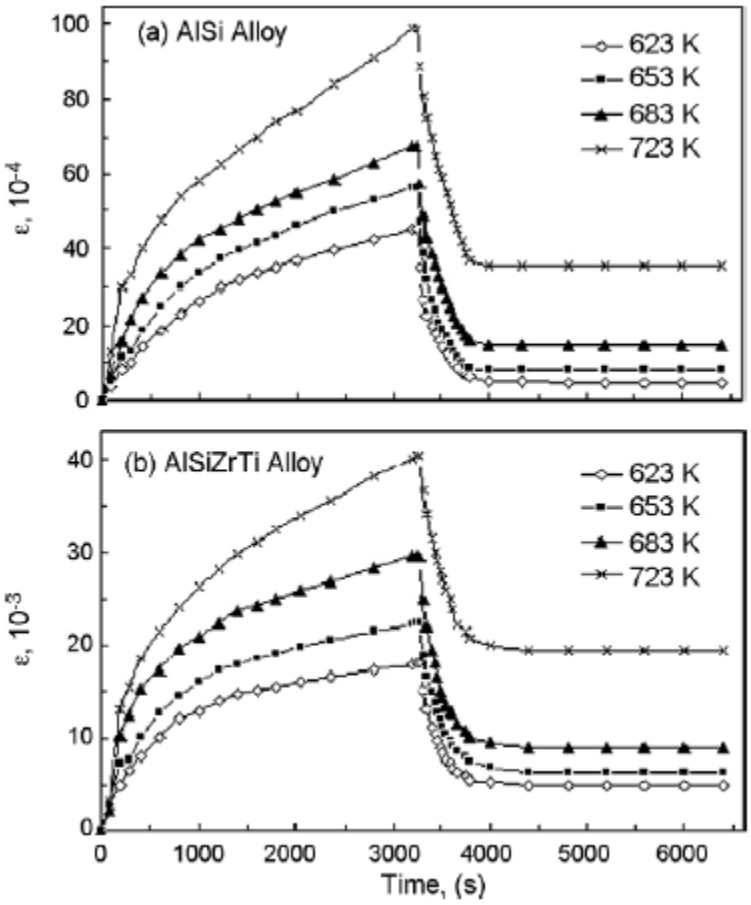

Fig. 2-16 Creep and creep recovery curves of Al-Si and Al-Si-Zr-Ti alloys with different aging temperatures. [38]

2.4. Creep and creep rupture

2.4.1 Uniaxial tensile testing

Uniaxial tensile testing is fundamental mechanical test, by uniaxially tension a sample until failure, by which tensile strength, yield strength, elongation, Young's modulus, Poisson's ratio and strain-hardening of materials could be investigated. Generally a constant displacement or constant load rate will be applied on the sample in a tensile test and the stress and elongation would be recorded to get the force-strain curve, if we load a constant force on the sample instead of the increasing force and record the strain which change with time it will be a creep test. In

this study, we works a lot on the tensile test property of the semi-solid A356 alloy in order to obtain a guide for the creep test.

W. M. van Haaften has studied on the tensile behavior of semi-solid aluminum alloys AA3104 and AA5182 [17], he investigated tensile properties of the semi-solid aluminum alloys at various temperature levels and different strain rates, and then suggested a modified creep law for concluding tensile behavior of these alloys, as it is shown below:

$$\dot{\varepsilon} = A\left(\frac{\sigma}{1-f_{LGB}}\right)^{n} \exp\left(-\frac{Q}{RT}\right) \quad (1)$$

where $\dot{\varepsilon}$ is strain rate, A is a constant, σ is stress, Q is activation energy, R is the universal gas constant, T is absolute temperature, f_{LGB} is fraction of grain boundary area covered with liquid. The reason for the author applied the (1 - f_{LGB}) for modifying the equation is the load carrying area is proportional to (1 - f_{LGB}).

C. Park has investigated the relationship between volume fractions of percentage primary α phase and tensile properties [18], yield strength would be decreased a little bit but ductility could greatly increased with a higher percentage of volume fraction α.

Several researchers like C. D. Lee has concluded micro-porosity effects on tensile properties of the A356 aluminum alloy [22], and it was clearly that the total porosity volume exactly decreased tensile strength of the Alloys.

Tensile properties of a A356 aluminum alloy produced by low-pressure-casting, rheo-casting and casting-forging process were compared by K. Lee [23], the ultimate tensile strength of the A356 reached 321MPa by the casting-forging process and followed by T6 heat treatment.

Recently, relationship between primary phase α morphology and tensile properties was reported by R. Burapa [24], he concluded that a higher shape factor of primary α phase contributes to the tensile properties of a semi-solid Al-Si-Mg-Fe aluminum alloy, as it is shown in Fig. 2-19.

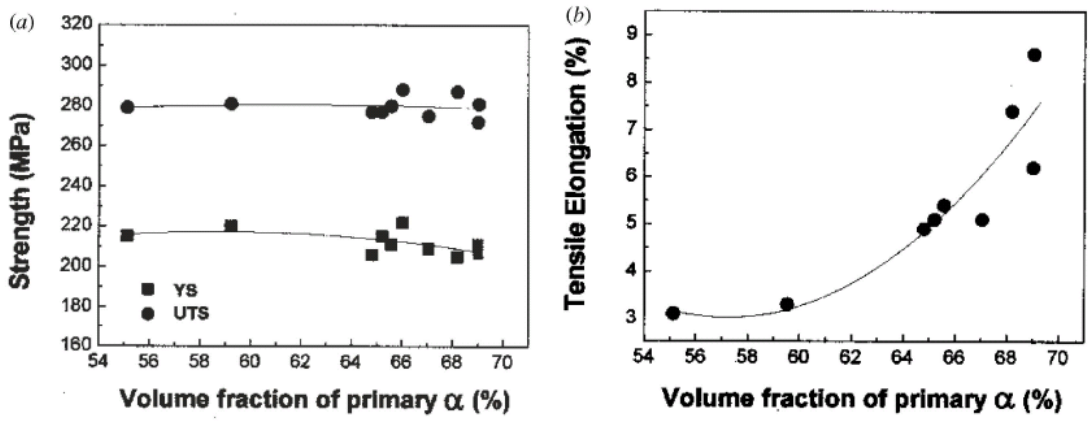

Fig. 2-17 Volume fraction of primary α effects on (a) yield strength and ultimate tensile strength, and (b) tensile elongation. [18]

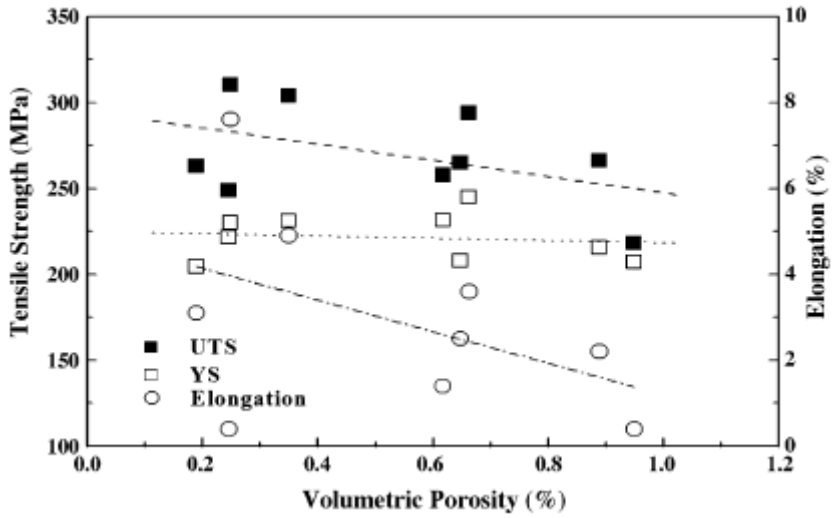

Fig. 2-18 Effects of volumetric porosity on tensile strength of A356 alloy. [22]

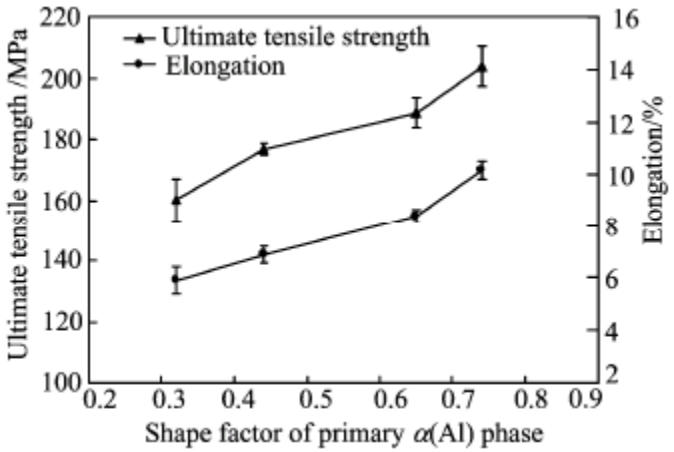

Fig. 2-19 Effect of shape factor of primary α phase on tensile strength of a semi-solid Al-Si-Mg-Fe alloy. [24]

2.4.2 Creep

A typical deformation-time creep was introduced in Section 1.4 above, we could divide the curve into three parts as shown in Fig. 2-20, primary, secondary and tertiary stage. The ε_0 in the graph is elastic strain when we load a force on the material, then it goes to the primary stage, a decelerate stage, we could modeling it as a deflection of creep rate and viscoelastic interactive behavior [25], but in my opinion, for age hardening alloy such as A356 alunimium alloy, it is not only governed by the two mechanisms but also substantially effect by a precipitation process, it will be discussed in chapter 4.

The secondary stage is also called steady stage because creep rate will be low and steady for a period, and then goes to an accelerate stage until ruptured. $\dot{\varepsilon}_{ss}$ in Fig. 2-20 is steady-state creep rate and the stress-sensitively exponent is defined by equation (2) [5], where T and s are features about temperature and substructure, $\dot{\varepsilon}$ could be minimum or steady-stage creep rate and σ is applied stress. The value of n of each group of alloy and temperature level was obtain by plotting minimum creep and applied stress on to log-log scale,

$$n = [\partial \ln \dot{\varepsilon} / \partial \ln \sigma]_{T,s} \tag{2}$$

and the creep constitution modeling and usually described as a power law equation:

$$\dot{\varepsilon}_{ss} = A\sigma^{n}\exp\text{-}(Q_c/RT) \quad (3)$$

where the $\dot{\varepsilon}_{ss}$ is steady-state creep rate, σ is the stress, Q_c is the activation energy, T is the absolute temperature, n is the stress exponent and A is the constant.

The strain-time creep curve could be modeled by a constitutive equation, and it depends on the nature of creep model application. A wide range of creep model equations are in use nowadays to represent the creep behavior of materials, Table. 2-1 shows some equations for classical representation of primary, secondary and tertiary creep.

Fig. 2-21 and Fig. 2-22 are deformation mechanism map of pure aluminum, we can learn the relationship of stress, temperature and mechanism of creep from them.

According to the equation (3), the creep behavior of a pure metal can be divided into three stress regimes [28], as is shown in Fig. 2-23.

1. The high stress regime is not important for creep design because of its high strain rate.

2. The intermediate stress regime characterized by a stress exponent n = 4~5, $Q = Q_0$, Q_0 is activation energy for lattice self-diffusion, in this regime dislocation climbing and gliding controlled the creep.

3. There are two mechanisms may take place in the low stress regime with $n = 1$, diffusion and Nabarro-Herring creep.

Grain boundary sliding mechanism also take place in all of the tree regimes but it is so negligible so normally we can ignore it, except when creep run in a very fine grained materials, for example submicron grain size [28].

Fig. 2-24 illustrates stress exponent in creep of solid solution alloys, unlike pure metal [28]:

The regime I characterized by power law breakdown.

n of regime IIa is 4~5, this regime is governed by climbing.

IIb is controlled by visco-dislocation-gliding and climb is faster than viscous glide in this regime, $n = 3$.

Climb controlled creep governed the regime IIc because the applied stress is big enough to make dislocations gilding easily.

The mechanism of low stress regime is diffusive or Harper-Dorn creep.

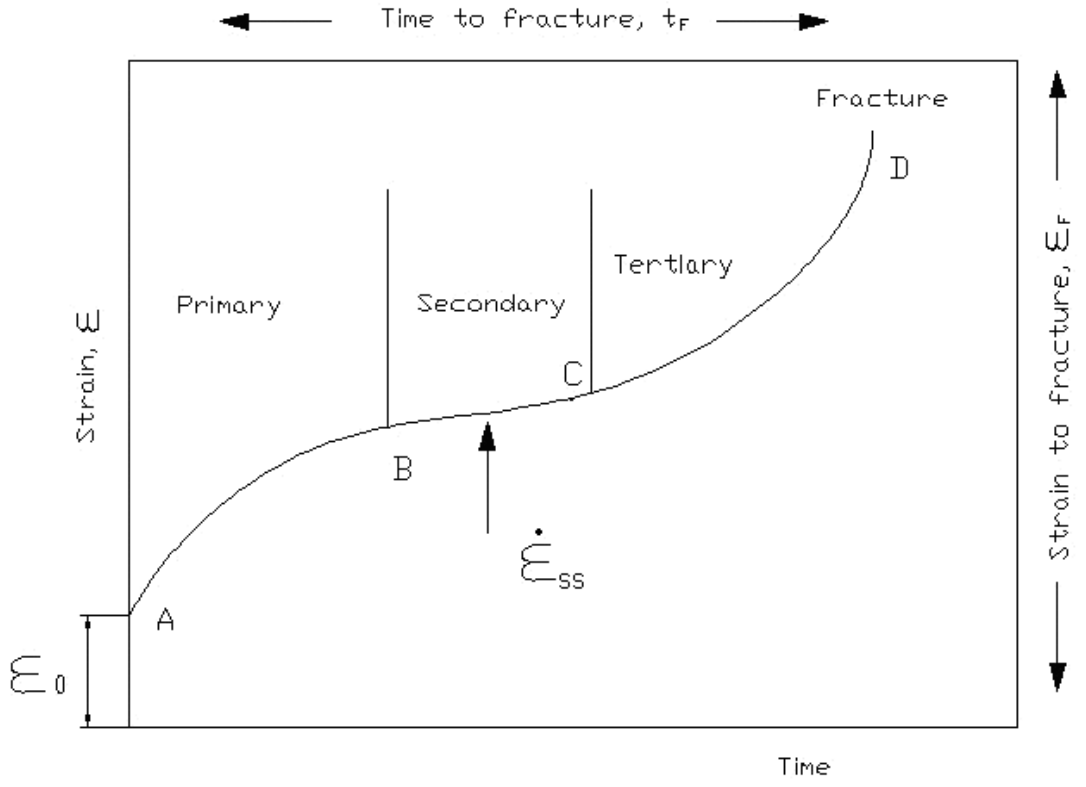

Fig. 2-20 A typical deformation-time creep curve.

Table. 2-1 A survey of creep constitutive equation. [27]

Model reference	Creep equation
Norton, (Norton, 1929)	$\dot{\varepsilon}_{f,min} = d_1 \exp(-Q/RT)\sigma^n$
Modified Norton	$\dot{\varepsilon}_{f,min} = b_1 \exp(-Q_B/RT)\sigma^n + c_1 \exp(Q_C/RT)\sigma^n$
Norton–Bailey	$\varepsilon_f = d_1\sigma^n t^p$
Bartsch	$\varepsilon_f = e_1 \exp(-Q_1/RT)\sigma \exp(-b_1\sigma)t^p$
(Bartsch, 1995)	$+ e_2 \exp(-Q_2/RT)\sigma \exp(b_2\sigma)t$
Garofalo, (Garofalo, 1965)	$\varepsilon_f = \varepsilon_t[1 - \exp(-b_1 t)] + \dot{\varepsilon}_{f,min} t$
Modified Garofalo	$\varepsilon_f = \varepsilon_{f1}[1 - \exp(-g_1(t/t_{12})^u)$
(Granacher, *et al.*, 2001)	$+ \dot{\varepsilon}_{f,min} t + c_{23}(t/t_{23})f]$
BJF	$\varepsilon_f = n_1[1 - \exp(-t)]^\beta + n_2 t$
(Jones and Bagley, 1996)	where $t = (\sigma/A_1)^n \exp(-Q/RT)$
Li–Akulov model	$\varepsilon_f = \frac{\dot{\varepsilon}_{f,min}}{k} \ln\left(1 + \frac{\dot{\varepsilon}_i - \dot{\varepsilon}_{f,min}}{\dot{\varepsilon}_{f,min}}(1 - \exp(-kt))\right) + \dot{\varepsilon}_s t$
(Li, 1963; Akulov, 1964)	$+ \varepsilon_T(\exp(t/t_t) - 1)$
Theta	$\varepsilon_f = \theta_1[1 - \exp(-\theta_2 t)] + \theta_3[\exp(\theta_4 t) - 1]$
(Evans and Wilshire, 1985)	where $\log(\theta_i) = a_i + b_i T + c_i\sigma + d_i\sigma T$
Modified Theta	$\varepsilon_f = \theta_1[1 - \exp(-\theta_2 t)] + \theta_m t + \theta_3[\exp(\theta_4 t) - 1]$
	where $\theta_m = A\sigma^n \exp(-Q/RT)$
Graham–Walles	$\varepsilon_f = at^{1/3} + dt + ft^3$
(Graham and Walles 1955)	
Modified Graham–Walles	$\dot{\varepsilon}_f = e^{(Q_1/T)} 10^{A_1} \left(\frac{\sigma(1+\varepsilon)}{1+\omega}\right)^{n_1} \varepsilon^{m_1}$
	$+ e^{(Q_2/T)} 10^{A_2} \left(\frac{\sigma(1+\varepsilon)}{1+\omega}\right)^{n_2}$
	where $\dot{\omega} = e^{(-QD/T)} 10^{AD} (\sigma(1+\varepsilon))^{nD} \varepsilon^{mD}$
Rabotnov–Kachanov	$\dot{\varepsilon} = \frac{h_1\sigma^n}{(1-\omega)} \dot{\omega} = \frac{k_1\sigma^\nu}{(1-\omega)^\zeta}$
(Kachanov, 1986)	
Dyson and McClean,	$\dot{\varepsilon}_f = \varepsilon_0'(1 + D_d)\exp(-Q/RT)\sinh\left(\frac{\sigma(1-H)}{\sigma_0(1-D_p)(1-\omega)}\right)$
(Dyson and McClean, 1998)	
Baker–Cane model	$\varepsilon_f = At^m + \varepsilon_p + \phi\varepsilon_s + \varepsilon_s(\lambda - \phi)\left[I - \frac{t/t_u - \phi}{1-\phi}\right]^{\frac{1-\phi}{\lambda-\phi}}$
(Baker and O'Donnell, 2003)	where $I = \varepsilon_u/\varepsilon_s$, $\varepsilon_s = \dot{\varepsilon}_m t_u$ and $\phi = t_p/t_u$
Mech. E (CSWP, 1983)	$R_{u/t/T} = (a_1 + b_1/\varepsilon - c_1\varepsilon^2)R_{\varepsilon/t/T} + d_1 + e_1/\varepsilon + f_1/\varepsilon^2 - g_1\varepsilon^2$
Characteristic strain	$\varepsilon_f(\sigma) = \varepsilon(R_{u/t/T}/R_{\varepsilon/t/T} - 1)/(R_{u/t/T}/\sigma - 1)$
model (Bolton, 2005a)	
MHG model, (Grounes, 1969)	$t_\varepsilon = \exp(TF(\varepsilon, \sigma) + C)$ where the $F(\varepsilon,\sigma)$ function is
(Holmström and	freely selected from multilinear combinations of σ
Auerkari, 2004)	and ε with an optimised value of C
Omega, (Prager, 1995)	$\dot{\varepsilon}_f = \dot{\varepsilon}_{f,min}/(1 - \dot{\varepsilon}_{f,min}\Omega t)$
Modified Omega	$\varepsilon_f = \left(\frac{1}{\Omega} - \frac{1}{2C_{tr}}\right)(-\ln(t_u - t) + \ln(t_u))$
(Merckling, 2002)	$+ C_{tr}(1 - \exp(m_{tr}t))$

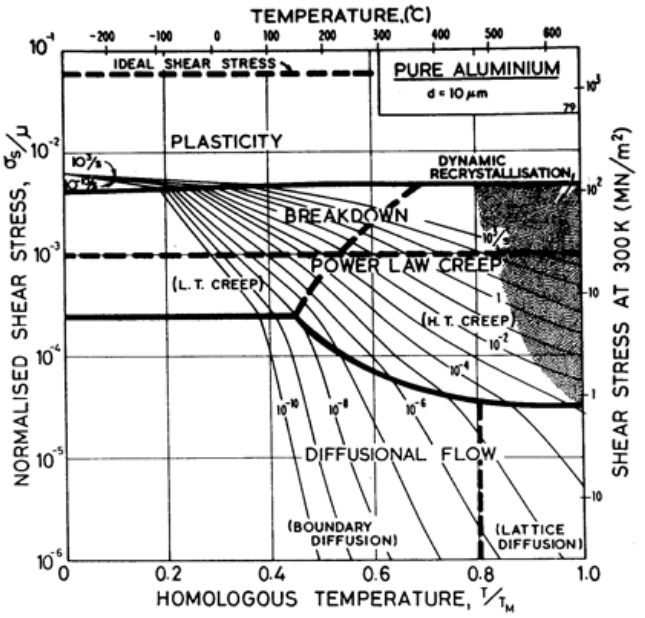

Fig. 2-21 Deformation mechanism map of grain size 10μ pure aluminum.
[*http://engineering.dartmouth.edu/defmech/*]

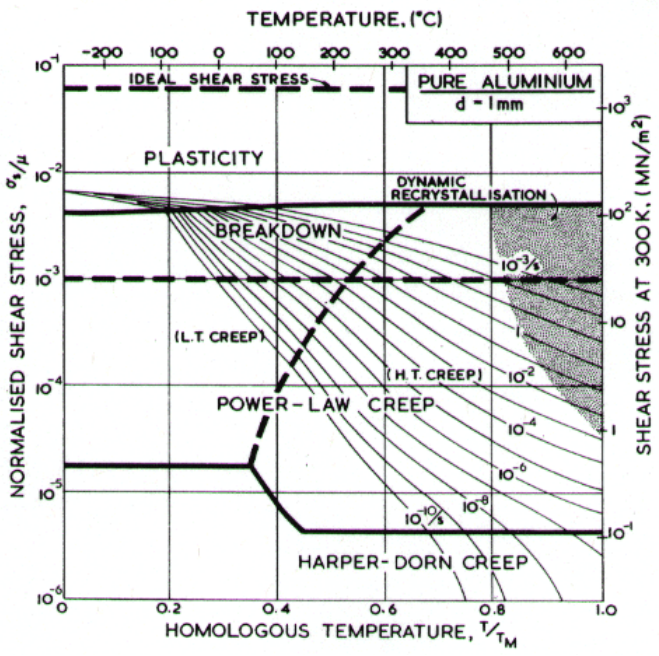

Fig. 2-22 Deformation mechanism map of grain size 1μ pure aluminum.
[*http://engineering.dartmouth.edu/defmech/*]

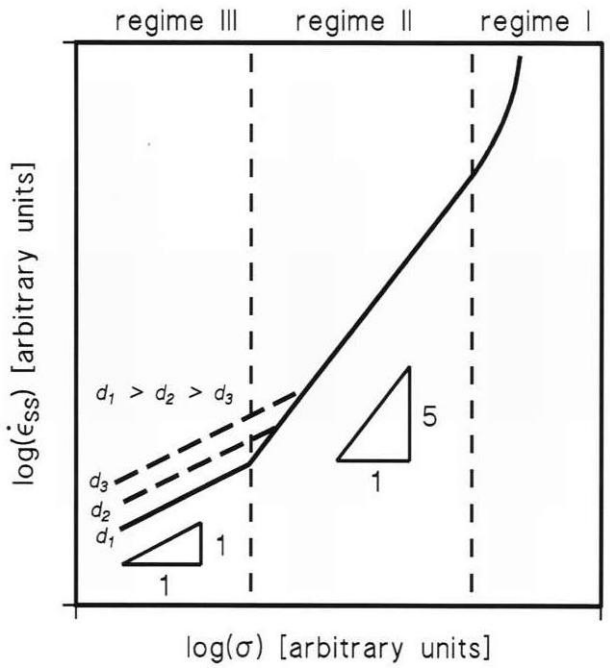

Fig. 2-23 Stress exponent in three regimes. [28]

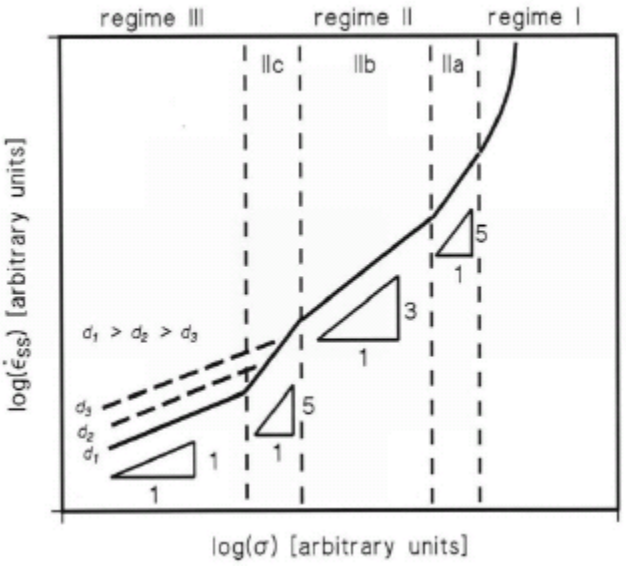

Fig. 2-24 Stress exponent in of solid solution alloys. [28]

2.4.3 Power law fracture

Creep deformation leads to creep facture, some occur with wedge-type cracking (Fig. 2-25) and some with cavitations cleavage (Fig. 2-26) [5].

Equation for creep rupture time prediction had been concluded by the Monkman-Grant relationship and Larson-Miller parameter.

$$\dot{\varepsilon}_{ss}^{m''} t_f = k_{MG} \tag{4}$$

Equation (4) is the Monkman-Grant relationship, it describes the creep fracture controlled by the steady-state creep rate.

$$\mathrm{LM} = T[\log t_r + \mathrm{C_{LM}}] \tag{5}$$

Euqation (5) is the Larson-Miller equation, $\mathrm{C_{LM}}$ is a constant phenomenologically determined as the value describes LM to be the logarithm of the applied stress.

One difficulty still has not been well solved of the steady-state creep rate dependence creep life prediction is the stress component n changes in different creep regimes, though there were many researchers suggested various ways for solving the problem, in my opinion, this difficulty is especially serious in the aluminum alloys because the precipitate phase changes very fast at high temperature, until now no one has found a perfect solution.

T. G. Langdon [30] had reviewed the transitions in creep behavior, included the solid solution alloys. He mentioned the typical equation for describe the steady-stage creep conditions at a temperature above $0.5T_m$,

$$\dot{\varepsilon} = \frac{ADGb}{kT}\left(\frac{b}{d}\right)^p \left(\frac{\sigma}{G}\right)^n \tag{5}$$

where D is the diffusion coefficient ($=D_0 exp(-Q/RT)$), (where D_0 is frequency factor, Q is the activation energy for creep and R is the gas constant), G is the shear modulus of elasticity, b is the Burgers vector, k is Boltzmann's constant, T is the absolute temperature, d is grain size, σ is the applied stress, p and n are the exponent of the inverse grain size and the stress, respectively, and A is a dimensionless constant.

As it is mentioned in the paragraph 2.4.1, a schematic of strain rate versus stress for a typical solid solution alloy shown in Fig. 2-24, this phenomenon has also been discussed by T. G. Langdon in his paper. Furthermore, the author has explained the mechanism of grain boundary sliding in creep and superplasticity.

Grain boundary slides under creep behavior when the grain size of the metal or alloys is large, and superplasticity flow usually occurs with small grain size, Fig. 2-27 illustrates grain boundary sliding in creep and superplasticity. The phenomenon of superplasticity plays important significant in the modern aluminum forming process, in addition, V. Tvergaard has modeled the effect of grain boundary sliding on creep and creep rupture [32, 33].

Data base of Al-Si alloy was further expanded in the last ten years by some researchers for example S. Spigarelli [39], creep properties of an Al-17Si-1Mg-0.7Cu alloy and a 6061-20Al_2O_3 composite were explored and concluded by a fitted equation, as follows:

$$\dot{\varepsilon}_m = A(\frac{\sigma-\sigma_0}{G})^n \exp(\frac{-Q}{RT}) \quad (6)$$

where $\dot{\varepsilon}_m$ is the minimum creep rate, G is the shear modulus and σ_0 is threshold stress. The threshold stress is used for representing the strengthening effects resulted by the interaction between dislocation and finely dispersed particles, and it was achieved by plot the experimental data on linear axes $(\dot{\varepsilon}_m)^{1/n}$ vs. σ, and then to extrapolate the resulting straight line for each temperature, to obtain the value of stress at zero strain rate.

Creep behavior of several grades of hypereutectic Al-Si alloys and Al-Si based composites were presented in 2004, by S. Spigarelli [40] and T. Jaglinski [41].

An interest phenomenon was reported by K. Ishikawa in 2004 [42], as we can learn it from Fig. 2-28 that the initial creep stage curve of A5083 alloy is unlike the typical creep curve of metallic materials, it is called inverse transition type creep, the incubation time t^* is determined by interpolation of the creep curve before and after it.

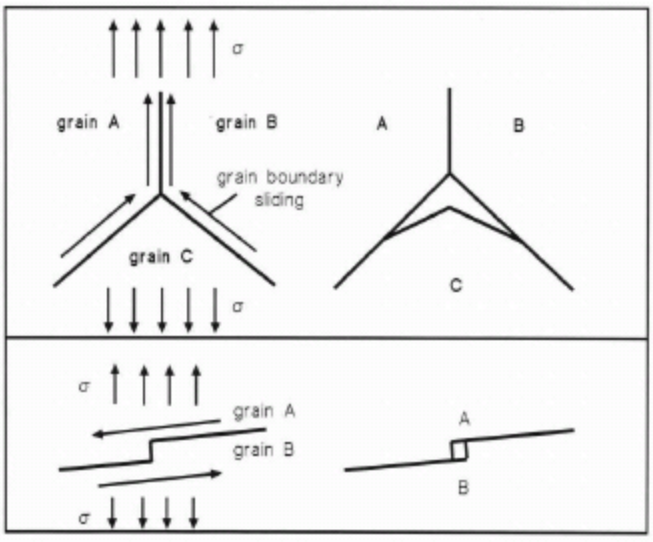

Fig. 2-25 Schematic of wedge-type cracking. [28]

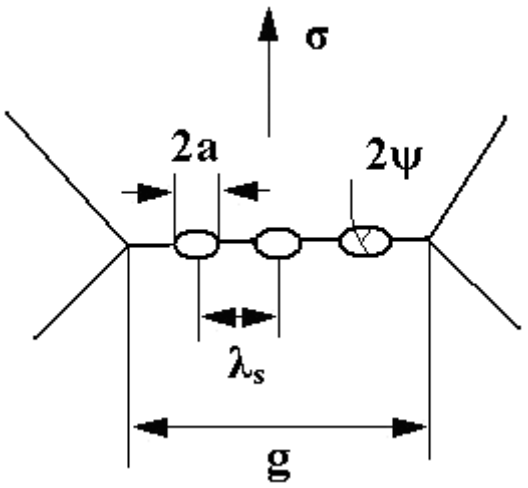

Fig. 2-26 Schematic of cavitations cleavage. [5]

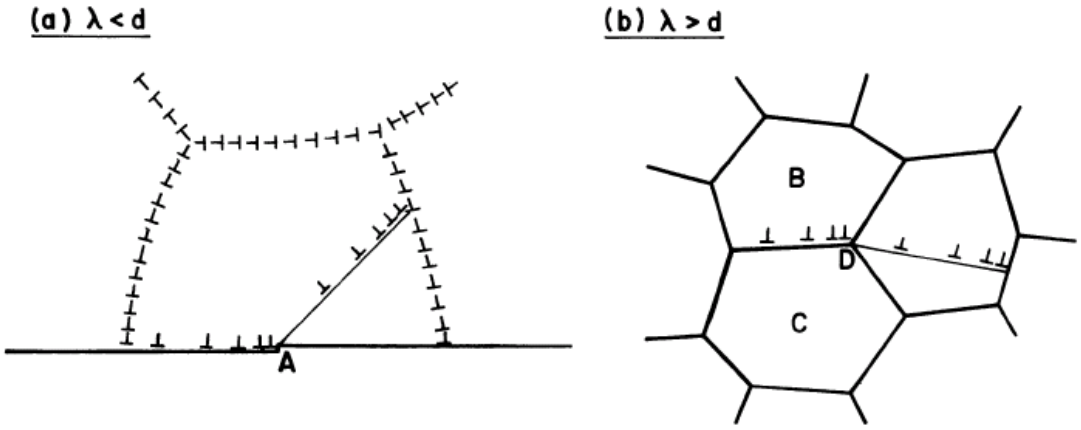

Fig. 2-27 Grain boundary sliding in (a) creep and (b) superplasticity. [30]

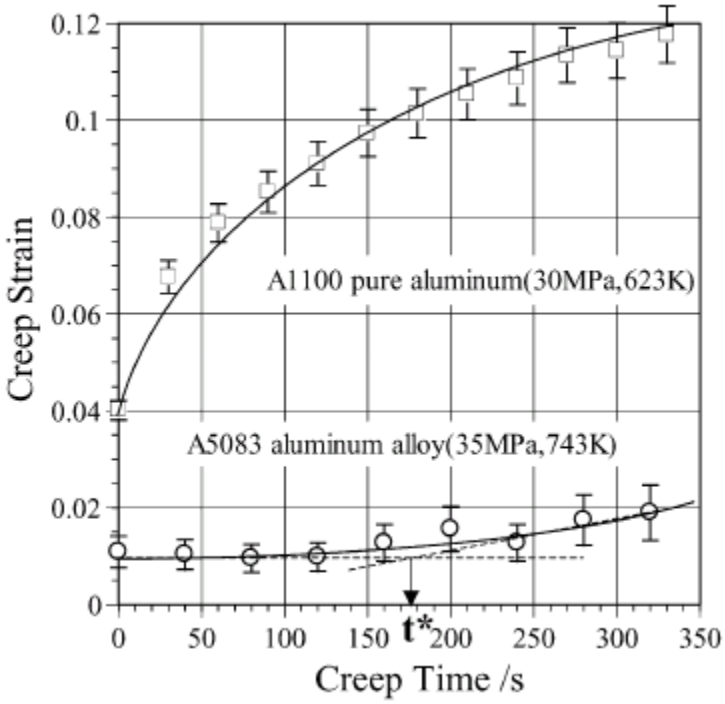

Fig. 2-28 Initial stages of creep for pure aluminum (A1100) and aluminum- magnesium alloy (A5083) at constant applied stress. [42]

2.4.4 Modeling of creep

There are several ideas for modeling of primary stage of creep, but some of them are so complex so that can not be applied on practical field until now. Instead, two simple but high efficient method if widely used in the world, they are time hardening theory and strain hardening theory. The former one assumes a relationship between equivalent creep rate, equivalent stress and time at fixed temperature, and the latter one postulates equivalent creep strain instead of time [57]. Equations (8) and (9) are typical equation used for time hardening modeling and equation (10) is for strain hardening modeling, respectively. Where ε_c is creep strain, which is total strain subtracted elastic strain, $\dot{\varepsilon}_c$ is equivalent creep rate, ε_c is equivalent strain, *A*, *m* and *n* are parameters depends on temperature.

$$\varepsilon_c = A\sigma^n t^m \tag{8}$$

$$\dot{\varepsilon}_c = Am\sigma^n t^{m-1} \tag{9}$$

$$\dot{\varepsilon}_c = A^{1/m} m \sigma^{n/m} \varepsilon_c^{(m-1)/m} \tag{10}$$

Creep damage equations were firstly proposed by L. Kachanov and Rabotnov. Creep damage as an effective loss the materials cross section, due to internal voids. As is defined in equation (11), where A_0 is the initial area of cross section, A_D is area of damages, and ω is damage parameter, and ω = 1 means a piece of virginal material. Equation (12) is a definition of creep damage tolerance proposed by F. A. Leckie, D. R. Hayhurst in 1977s, where ε_f is total strain to rupture and t_f is total time to rupture and $\dot{\varepsilon}_s$ is steady-state creep rate. Finally the constitutive for tertiary creep curve could be concluded as it in equation (13) [58]. In addition, the elastic strain and visco-elastic strain of primary creep stage should be subtracted from the total creep curve and when modeling by the damage theory because the main mechanism of this area is not damage, as it is illustrated in Fig. 2-29, where creep strain has been separated into ε_p and ε_t.

$$\omega = \left(\frac{A_0 - A_D}{A_0}\right) \tag{11}$$

$$\lambda = \frac{\varepsilon_f}{\dot{\varepsilon}_s t_f} \tag{12}$$

$$\varepsilon_c = (\varepsilon_f \quad or \quad \varepsilon_t)\left[1 - \left(1 - \frac{t}{t_r}\right)^{1/\lambda}\right] \tag{13}$$

A θ projection concept was invented by R. W. Evans and B. Wilshire in 1982s. The constitutive equation is obtained by projecting the creep curve and consisted of four θ parameters. The primary stage of creep curve can be described by equation (14), and total curve is described by equation (15), the four of θ are constants relate to the time and stress and they could be concluded by equation (16), where i could be 1, 2, 3 and 4 [59]. The advantage of the θ projection is high precision fitting and extrapolation of creep curve but its disadvantages are such as: (1) It needs many creep data at different stress and temperature levels to get the full map of the four of θ. (2) It is not suitable to analyse complex structures in the industrial applications by this method because the stress distribution of stress at different parts of the structure is inharmonious so that it needs too many experiment to fill the data base for the θ projection.

$$\varepsilon = \theta_1(1 - \exp(-\theta_2 t)) + \dot{\varepsilon}_s t \tag{14}$$

$$\varepsilon = \theta_1(1 - \exp(-\theta_2 t)) + \theta_3(\exp(-\theta_4 t) - 1) \tag{15}$$

$$\log_{10} \theta_i = a_i + b_i T + c_i \sigma + d_i T \sigma \tag{16}$$

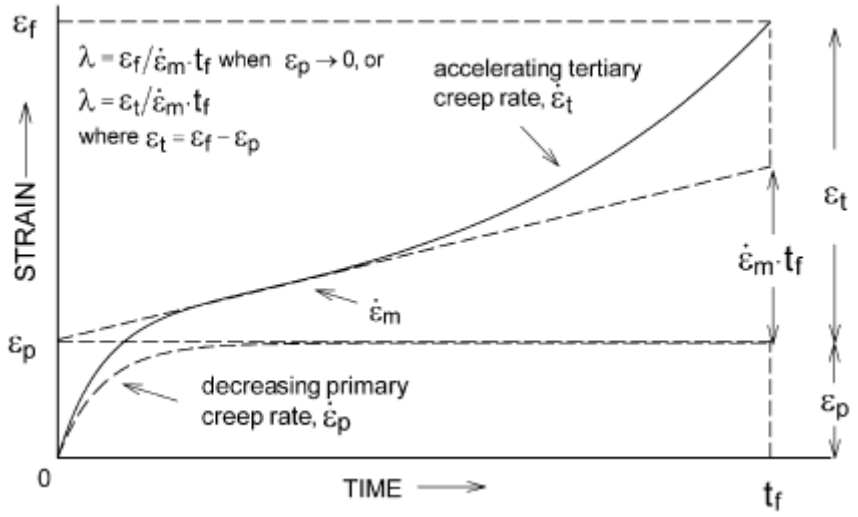

Fig. 2-29 Sketch of damaging strain. [60]

2.4.5 Creep rupture life normalization and prediction

As previously introduced in the previous section, some metallic materials have to service for a long in their creep life, however, laboratory experiments are usually limited to a few weeks, days or even several hours. Therefore, the present technique for predicting long time creep life is called extrapolation, and some of creep life extrapolation methods which are commonly used nowadays will be introduced below.

1) Monkman-Grant relationship, as shown in equation (17) which presumes that the fracture-deforming of materials is controlled by the steady-state creep rate, in which t_f is time to fracture, k_{MG} is sometimes refeered to as the Monkman-Grant constant [61].

$$\dot{\varepsilon}_{ss} t_f = k_{MG} \tag{17}$$

$$M / t_f = A\sigma^n \exp(Q / RT) \tag{18}$$

By combining equations (3) and (17) we can get equation (18) as follow, where M, A and Q are functions of stress and temperature. Moreover, creep and fracture properties of particle-hardened alloys are both temperature and microstructure sensitive, hence, some people normalized the σ through σ_Y or σ_{TS}, as shown in equation (19), where A^* is not At and Qc^* is obtained from constant (σ/σ_{TS}) rather than at constant σ as in the determination of Q_C in equation (3).

$$M / t_f = A^* (\sigma / \sigma_{TS})^n \exp(-Q^*_C / RT) \quad (19)$$

2) Isothermal extrapolation, Equations (20) and (21) are linear and parabola equations for extrapolation, *A*, *B*, *c* and *d* are constants and t_r is creep rupture time. Isothermal extrapolation is a sort of methods which assume that relationship between stress and creep rupture life is linear or parabola distribution, but the nature of most metallic materials is not so, therefore, the limitation of isothermal extrapolation of creep rupture life is less than ten times of the experimental creep rupture life.

$$t_r = A\sigma^B \quad (20)$$

$$\log \sigma = c + d \log^2 t_r \quad (21)$$

3. Time-Temperature parameter extrapolation, such as Larson-Miller parameter (equation (22)), Fisher-Dorn parameter (equation (23)), Dorn parameter (equation (24)), Manson-Haferd parameter (equation (25)), Manson-Succoup parameter (equation (26)), Sud Aviation parameter (equation (27)) and Dorn-Orr-Sherby parameter (equation (28)).

$$P_{LM}(\sigma) = T(C + \log t_r) \quad (22)$$

$$\log t_r - C / T \quad (23)$$

$$t_r = \exp(-\Delta H / RT) \quad (24)$$

$$\frac{T - T_a}{\log t_r - \log t_a} \quad (25)$$

$$\log t_r + CT \quad (26)$$

$$\log t_r + C \log T \quad (27)$$

$$\log t_r - \Delta H / 2.3R \quad (28)$$

According to ASTM Standard E139-06, constant *C* in the equations is 20 for many materials, *T*, *Ta* are constant, ΔH is activation energy. The Dorn-Orr-Sherby parameter has best physical basis but Larson-Miller is the most popular in practical area.

2.5. Conclusions

This chapter reviewed current status of research on tensile and creep behavior of the solid solution Al-Si based alloys. Though there are many researchers have reported on this area, none of them has studied on the creep behavior of the globular α phase Al-Si based alloy produced by the semi-solid process.

Chapter 3. Experiment

3.1. Creep test machine fabrication

The procedure of creep test machine fabrication is as follows:

1. Design,
2. Frame building,
3. Accessories making and assembling,
4. Alignment and running,
5. Modifying for perfect.

Main frame of the creep test machine (Fig. 3-1) was designed by Mr. Suchart Chanratamanee, an extensometer and some accessories were designed by the author (Fig. 3-2, Fig. 3-3). Most parts of the machine are fabricated in by workshops and assembled by our group.

As it is introduced in chapter 2, main idea of the creep test machine was learned from the ASM metal handbook, but our research group had also consulted several different ideas such as the ones shown in Fig. 3-4, Fig. 3-5 and Fig. 3-6. By synthetically considerate of application, capability, precision, cost and building difficulty, we finally designed the suitable one for our own situations. As it is shown in the paragraph above, it is a kind of simple level arm driving force creep test machine because it is easy making with high precision. Fig. 3-7 illustrates the method of estimation of error caused by level arm moment changes during creep test, and it figures out an error smaller than 0.2%.

Real tension of the machine was calibrated by a load cell (Fig. 3-8) with precision ±0.01kg of 0-99kg and ±0.1kg of 100-999kg, and relationship between load weight and true force is illustrated in Fig. 3-9.

Deformation of the creep specimen is recorded by a data acquisition system (DAQ) based on a LVDT produced by National Instruments Corporation as it is shown in Fig. 3-10.

Many parts of the creep test machine were modified after long time running in order for perfection.

The capability of the creep test machine is listed in Table. 3-1.

Table. 3-1 Capability of the creep test machine.

Tension	15-1000Kg, ±0.4Kg.
Temperature	70-270°C, ±1°C; 350-400°C, ±1.5°C; 400-1050°C, ±1°C. (With different furnaces adapted.)
Total elongation of specimen	13mm (Could be extended by decreasing precision).
Data recording velocity	$>10s^{-1}$.
Max. testing period	70-270°C, unlimited; 350-1050°C, 99hours.

Fig. 3-1 Creep test machine with high (left) and low (right) temperature furnaces.

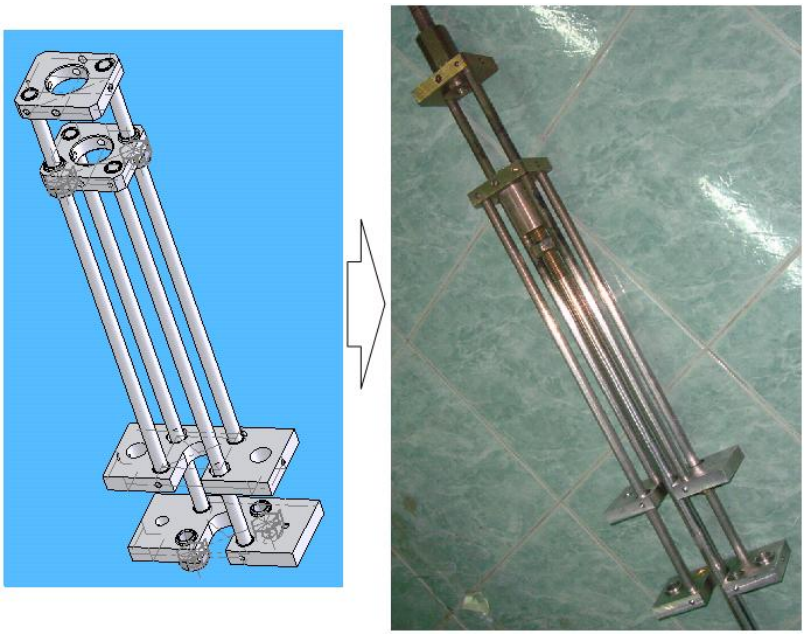

Fig. 3-2 An extensometer from design to the product.

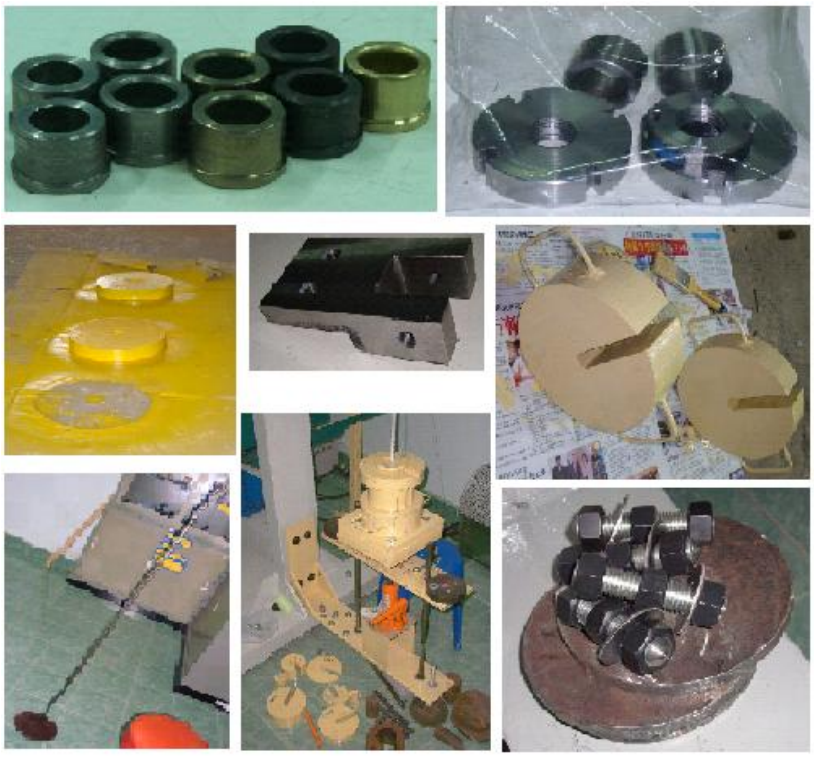

Fig. 3-3 Some accessories of the creep test machine.

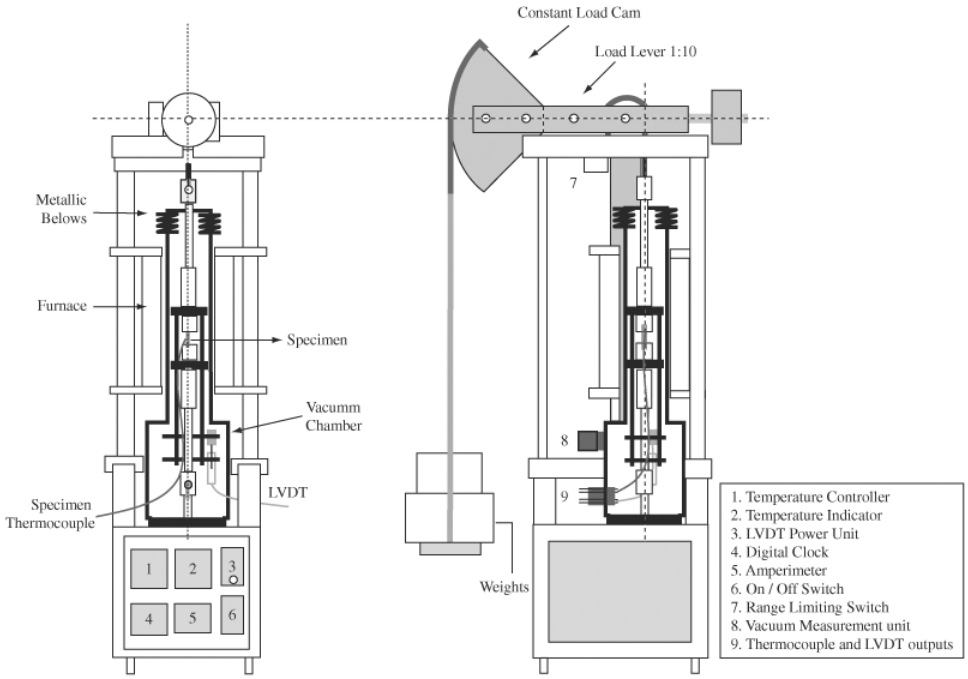

Figure 1. Schematic drawing of main components of creep machine and vacuum chamber.

Fig. 3-4 A constant load creep test machine.
[*http://www.scielo.br/scielo.php?script=sci_arttext&pid=S1516-14392005000400008*]

Fig. 3-5 A mini creep test machine.
[*http://www.tecquipment.com/Materials-Testing/Creep/SM1006.aspx*]

Fig. 3-6 A electronical creep test machine.
[*http://www.sunstest.com/productshow_eng.asp?id=120*]

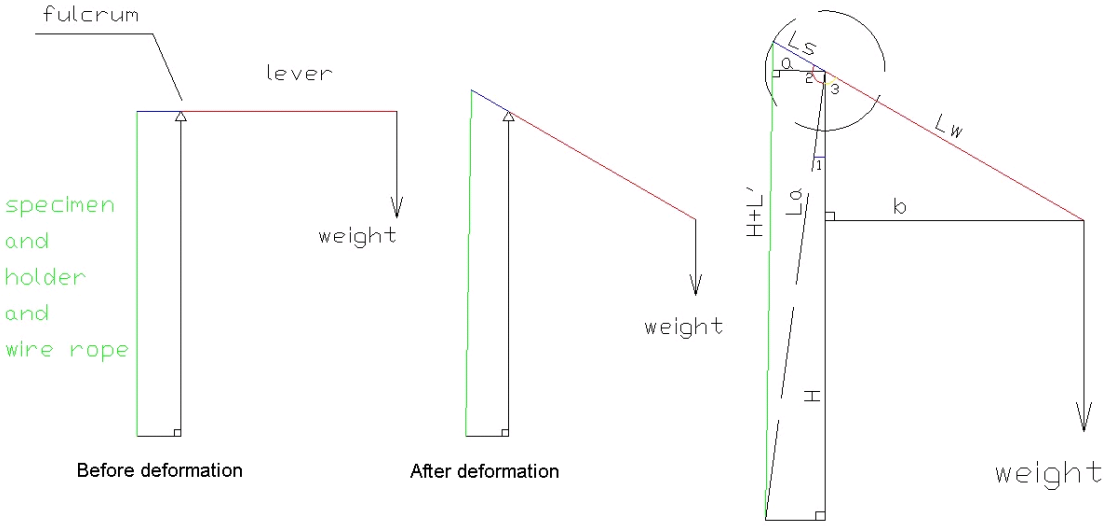

Fig. 3-7 Calculation of error caused by the moment changes during creep test.

Fig. 3-8 Load cell.

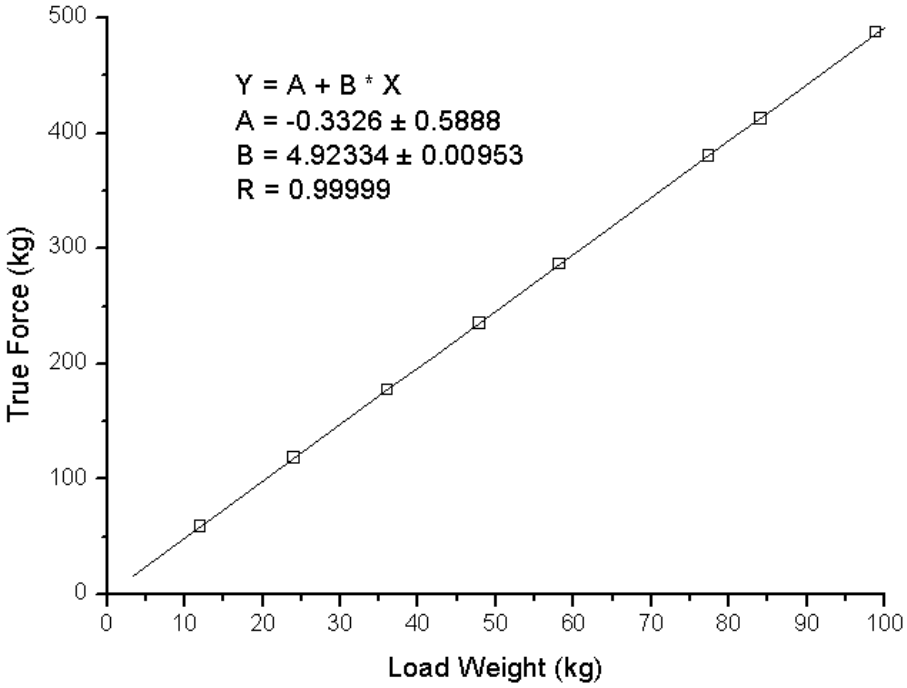

Fig. 3-9 Relationship between load weight and true force of the creep test machine.

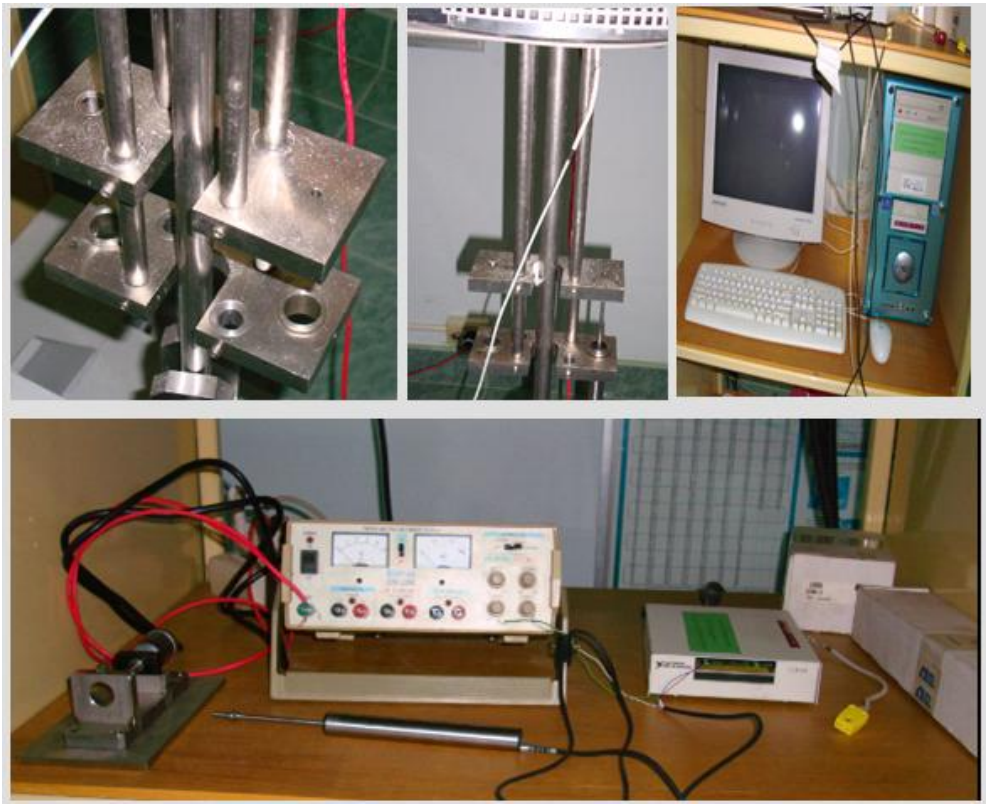

Fig. 3-10 Data acquisition system (DAQ).

3.2. Casting

Primary A356 aluminum alloy was used in this study. The chemical composition of the raw material was checked by optical emission spectrometer (OES) and the result is shown in Table. 3-2. Ten different groups of alloys was cast in this study, parameters of them are listed in Table. 3-3, the group 1 was the first batch, group 2~9 were cast after squeeze apparatus was improved. The A356 alloy pates are shown in Fig. 3-11. Each plate was cut to five or six bars for tensile or creep test and several small pieces for microstructure and hardness exam, as it is illustrated in Fig. 3-12, bar E, M and C would be machined to specimens of tensile and creep test, and another small bar will be used for hardness and microstructure test.

Table. 3-2 Chemical composition of the A356 alloy ingot.

Sample	Concentration (%)				
A356	Al	Si	Fe	Cu	Mn
	Bal.	7.4300	0.0949	0.0246	0.0063
Standard Deviation	-	0.5843	0.0074	0.0098	0.0004
A356		Mg	Ti	Ni	Sr
		0.3146	0.0966	0.0057	0.0068
Standard Deviation		0.0186	0.0068	0.0007	0.0006

Table. 3-3 Parameters of casting.

Group	Weight of one piece (kg)	Melting Temp. (°C)	Gas induce or casting Temp. (°C)	Gas flow (L/min)	Gas induce time (s)
1	≈1.25	720	620	4	15
2	≈0.4	720	680	0	0
3	≈0.4	720	640	0	0
4	≈0.4	720	620	4	5
5	≈0.4	720	620	4	10
6	≈0.4	720	620	4	15
7	≈0.4	720	620	4	10
8	≈0.4	720	680	4	10
9	≈0.4	720	620	4	10

Group	Plus holding time (s)	Mold Temp. (°C)	Squeeze pressure (MPa)	Solid fraction before casting (%)	Geometry size (mm).
1	0	300~350	22	≈10	r100*15
2	0	300~350	69	0	100*100*15
3	0	300~350	69	<10	100*100*15
4	0	300~350	69	≈10	100*100*15
5	0	300~350	69	>10	100*100*15
6	0	300~350	69	>10	100*100*15
7	10	300~350	69	>10	100*100*15
8	20	300~350	69	>10	100*100*15
9	70	300~350	69	≈25	100*100*15

Fig. 3-11 As cast A356 alloy plate of group 1 (left) and group 2~9(right).

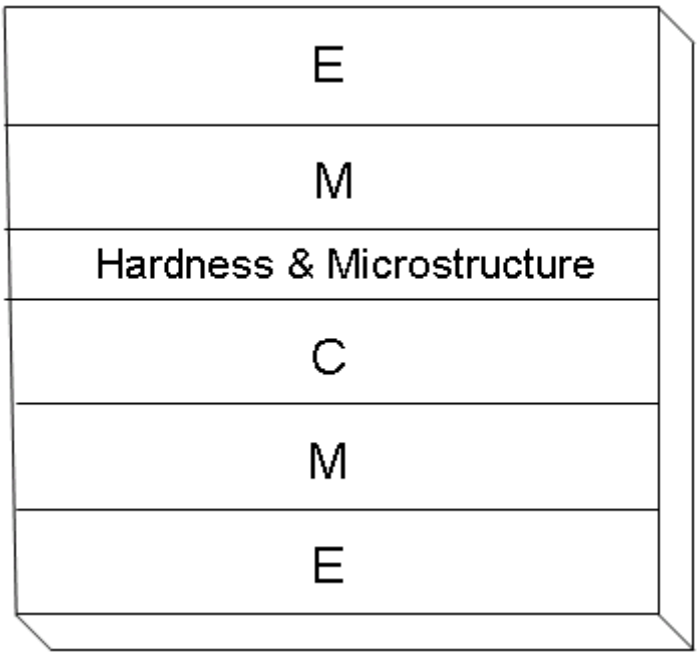

Fig. 3-12 Schematic of pate cutting.

3.3. Heat Treatment

As it was mentioned before the T6 heat treatment of A356 aluminum alloys in this study is followed by ASTM B 917 Standard, and the parameters of application process is learned from Heat Treatment Group of the Department of Mining and Materials Engineering, Faculty of Engineering, Prince of Songkla University. By following their suggestion, the temperature of solution heat treatment in this study was 540°C and holding for 8 hours, then rapid quench in water which was kept at room temperature (approximately 27°C) for several days. The quench-ability of long time storage water is better than the fresh tap water, because small bubbles in the water would be gone during long time storage and these bubbles were bad for quenching.

Four kind of artificial aging processes were applied in this study in order to investigate effect of aging on tensile and creep properties, they are under aging, peak aging and over aging, and the parameters are listed in Table. 3-4, and it was designed by referring the database of Heat Treatment Group of Department of Mining and Materials Engineering, Faculty of Engineering, Prince of Songkla University, as is shown in Fig. 3-13.

Table. 3-4 Parameters of artificial aging.

Groups of heat treatment process	Solution Temp. (°C)	Time (hour)	Artificial Aging Temp. (°C)	Time (hour)	Quenching media
1. Under aging	540	4	135	12	Water(27°C)
2. Under aging	540	8	165	2	Water(27°C)
3. Peak aging	540	8	165	12	Water(27°C)
4. Over aging	540	8	165	72	Water(27°C)

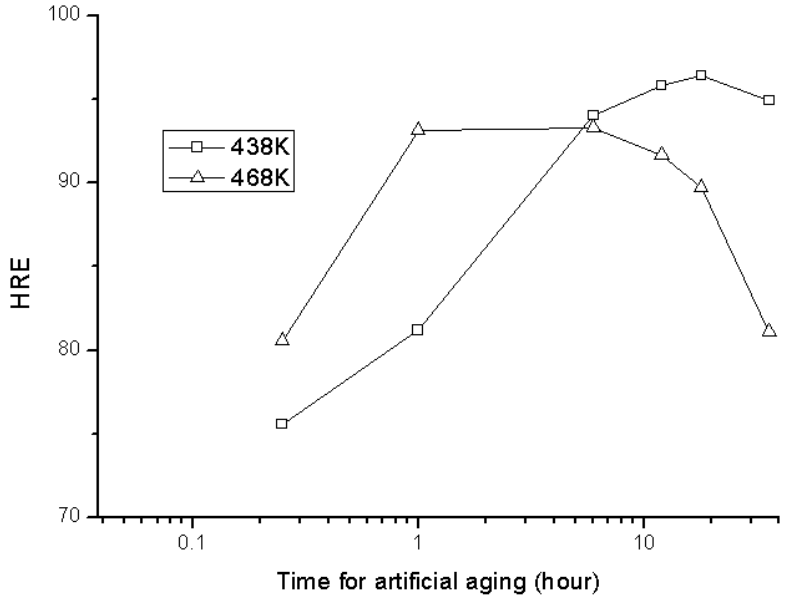

Fig. 3-13 Effect of artificial aging on hardness of the SSM A356 alloy.

3.4. Microstructure and hardness test

As it was mentioned in the section 3.2, a cuboidal bar from centre of the casting plate was cut for microstructure and hardness test. As it is illustrated in Fig. 3-14, nine positions from centre to edge of the casting plates were investigated in order to learn micro morphology distribution of the plates.

Hardness test of the alloy was performed with a Rockwell B-Scale Hardness test machine, and followed ASTM E18-03 standard [48]. Micrographs were shot by an optical microscope with a CCD camera.

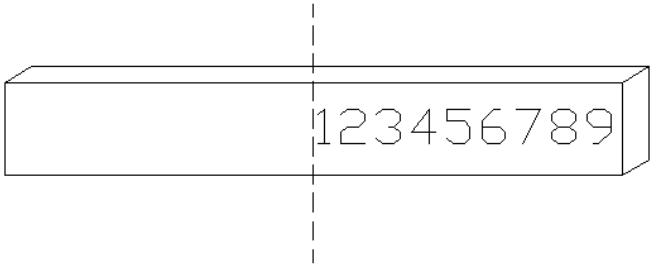

Fig. 3-14 Schematic of the bar for microstructure and hardness test.

3.5. Tensile test

The alloys were machined to dog-bone shape specimens by following ASTM E8-08 standard [50] for tensile and creep test, with dimensions shown in Fig. 3-15. The tensile test were performed by using a Hounsfield UTM equipped with a controlled temperature electric furnace with maximum operating temperature of 270°C±1°C. Tensile test of all the nine groups of alloys with T6 heat treatment were performed at 25°C and of strain rate $0.001s^{-1}$, and group 1 alloy with both T6 peak aged and under aged (135°C, 12hrs.) were extra performed at 100, 150, 200 and 250°C.

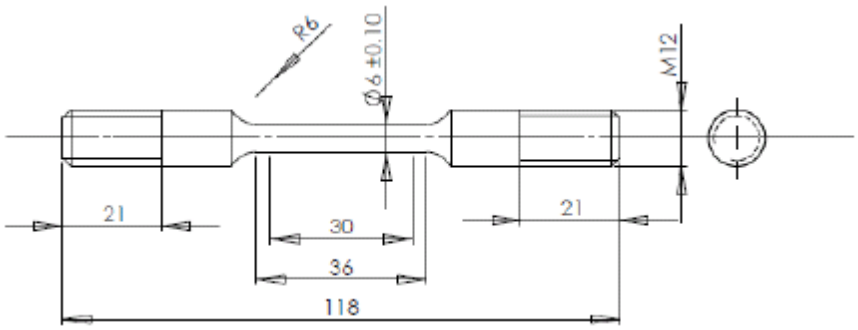

Fig. 3-15 Geometry of tensile test specimen.

3.6. Creep test

Group 3, 5 and 7 of the A356 alloys were chosen for creep test, each group was investigated at 225±1°C with different constant stress levels, and group 7 was extra performed at 175, 200, and 250°C to learn a full map of creep behavior of the SSM A356 alloy. All the specimens were preheated from room termperature by 30min, then kept at constant temperature for another 30min, for achieving a homogeneous temperature before loading.

Chapter 4. Results and discussion

4.1. Effect of casting and heat treatment on microstructure and Tensile properties of the alloys

Table. 4-1, Fig. 4-1, Fig. 4-2, Fig. 4-3 and Fig. 4-4 present tensile properties and morphology of microstructures of the A356 Alloys of group 2~9, Fig. 4-5 makes a comparison of as cast and T6 peak aged A356 alloys of group 2~6, and typical microstructure of the A356-T6 alloys are shown in Fig. 4-6. The average grain size statistics followed ASTM Standard E112-96 [49]. From the data it is learned that:

1. Satisfactory tensile strength (331.6±2.7MPa, strain rate 0.001/s) was obtained by the GISS process with appropriated gas-induced time. It is comparable with other researchers' results who study on the same alloy produced with other costly advanced processed, which are at a range of 288~332MPa, and some of them are listed in Table. 4-2 [18, 21].

2. Higher strength was obtained by higher squeeze pressure.

3. A proper GISS time (5s) is helpful for α grain refining and a longer GISS time (10s) receives a higher shape factor. Another way for obtaining high shape factor is plus a holding period after the GISS process, which also provides higher total volume fraction of α phase and larger α grains.

4. There is not any obvious relationship between total volume of α phase and tensile properties, unlike the results reported by C. Park *et al.* [18] in 2004 that higher total volume fraction of α phase does not affect on tensile/yield strength but great improved the tensile elongation of the A357-T5 Al-Si-Mg cast alloy. It might because other factor replaced the key factor of the total volume fraction of α phase in the GISS A356-T6 squeeze cast alloy and some evidences was given by Fig. 4-2, it is learned from the graph that average α grain size plays a key factor on the tensile/yield strength and elongation of the GISS A356-T6 squeeze cast alloy, as it is widely exist in many sorts of metallic materials.

5. As reported by Burapa *et al.* [24] that more round α alpha grain provides higher tensile/yield strength of the GISS SSM A356-as-cast alloy, however such results can not be found in this study, it might because as it is compared in Fig. 4-7 that the most of the eutectic phases of the as cast A356 alloy was dissolved after T6 heat treated, and left many silicon particles dispersed alone in the old eutectic area, finally made the microstructure more like a kind of Si particle strengthened Al alloy, instead of the as cast α-eutectic binary alloy and then impaired effects of shape factor on tensile/yield strength. Though these Si particles are too spare to pin the dislocations effectively according to the equation (29) [45, 47], where σ is stress which bends a dislocation, b is burgers vector, d is distance between two particles and r is radius of the particles. Moreover, substantial contribution from shape factor to tensile elongation can be found in [13].

$$\sigma = (\frac{1.13}{2\pi})(\frac{b}{d})\ln(\frac{r}{2b}) \quad (29)$$

6. Average size of silicon particle of the A356 alloys group 2~8 are almost the same, 2.42±0.04μm, and density of silicon particle of different group of alloys is shown in Fig. 4-4. It is learned that high density of silicon particle might be an important factor contribute to tensile strength.

7. T6 heat treatment with peak aging great improve ultimate tensile strength of the alloys because though the coarse precipitates was dissolved by the solution treatment of T6 process, and fine precipitates, which were created in the peak aged process, obstruct dislocation moving during tensile test. Similar mechanism will be discussed in the next section.

Table. 4-1 Morphology of microstructure and tensile properties of the A356 alloy with T6 heat treatment.

Group of alloys	Main feature of α phase	Total volume fraction of α phase (%)	Average diameter of α grain (μm)	Shape factor	Ultimate tensile strength (MPa)	0.2% yield strength (MPa)	Total elongation at failure (%)
2	Dendritic & Petaloid	91.3	-	-	310.6±11.3	260.1±3.1	5.7±1.4
3	Petaloid & Polygonal	90.3	53.4	0.52	326.3±1.1	265.5±10.5	10.6±5.5
4	Polygonal & Globular	90.8	49.8	0.67	331.6±2.7	266.0±13.4	13.4±1.0
5	Polygonal & Globular	90.8	56.6	0.79	324.3±2.1	260.4±13.8	13.8±0.43
6	Polygonal & Globular	91.5	55.6	0.70	318.3±4.9	253.9±12.4	12.4±0.5
7	Polygonal & Globular	94.2	63.4	0.79	325.9±4.0	263.4±13.1	13.1±0.45
8	Polygonal & Globular	94.1	68.4	0.80	304.7±5.8	237.2±13.3	13.3±2.8
9	Failed because of unharmonious microstructure						

Table. 4-2 A comparison of tensile properties.

Reference	Material	Process	Ultimate tensile strength (MPa)	Strain rate (s^{-1})	Elongation (%)
Y. Zhou (This study)	A356	GISS + 70MPa squeeze casting + T6	331.6±2.7	0.001	13.4±1.0
Y. B. Yu, 1999	A356	SSM + 100MPa die casting + post heat treatment	329	0.0005	-
H. M. Guo, 2009	A356	SSM + 120MPa die casting + T6	330	-	13
H. Moller, 2009	A356	SSM + high pressure die casting + T6	332±4.4	-	7.9±1.5
C. D. Lee, 2007	A356	Low pressure die casting + T6	310	0.00027~0.0027	8

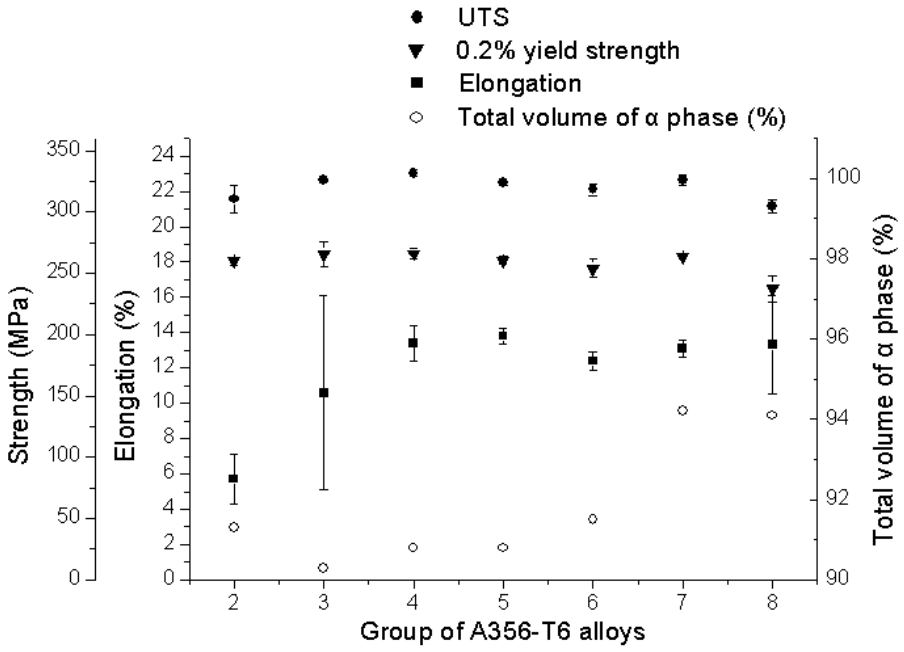

Fig. 4-1 Tensile properties and total volume of α phase of A356-T6 alloy of group 2~8.

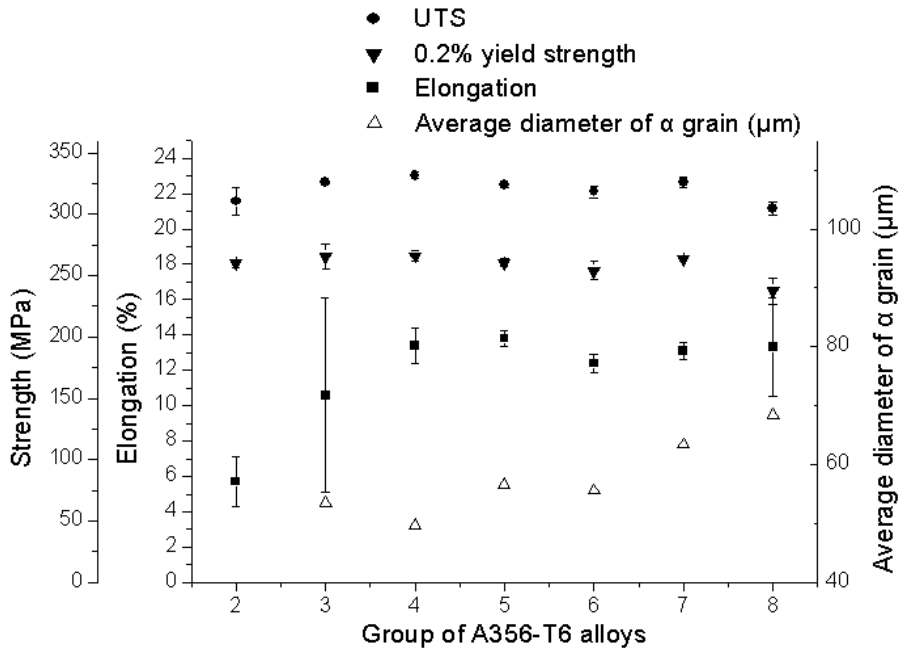

Fig. 4-2 Tensile properties and α grain size of A356-T6 alloy of group 2~8.

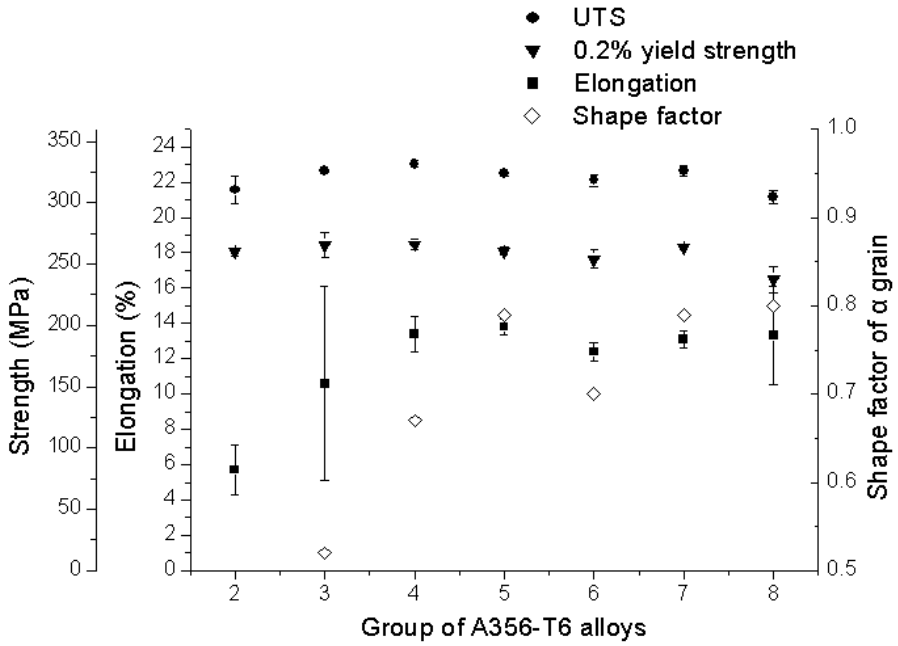

Fig. 4-3 Tensile properties and shape factor of A356-T6 alloy of group 2~8.

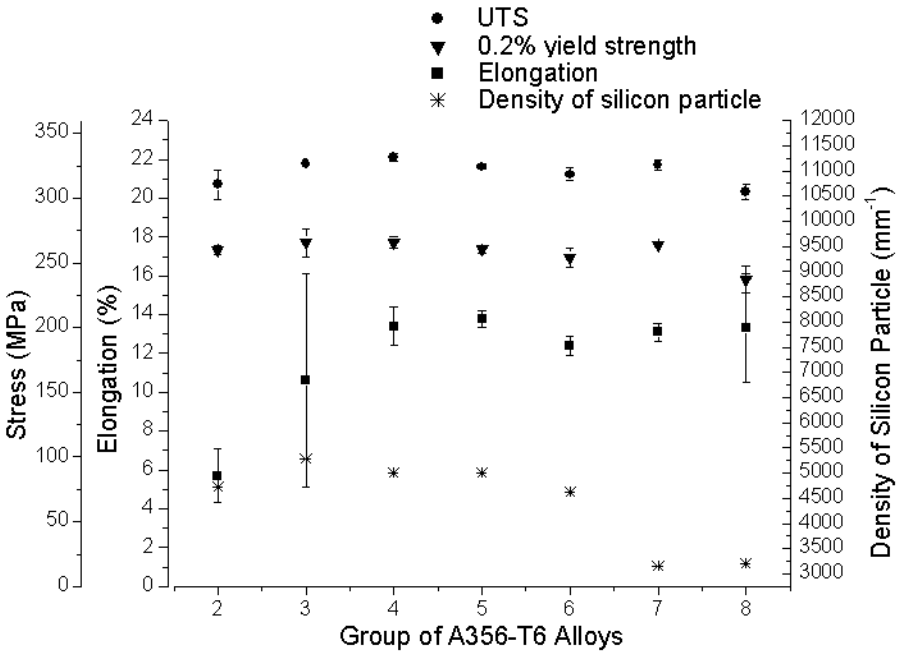

Fig. 4-4 Tensile properties and density of silicon particle of A356-T6 alloy of group 2~8.

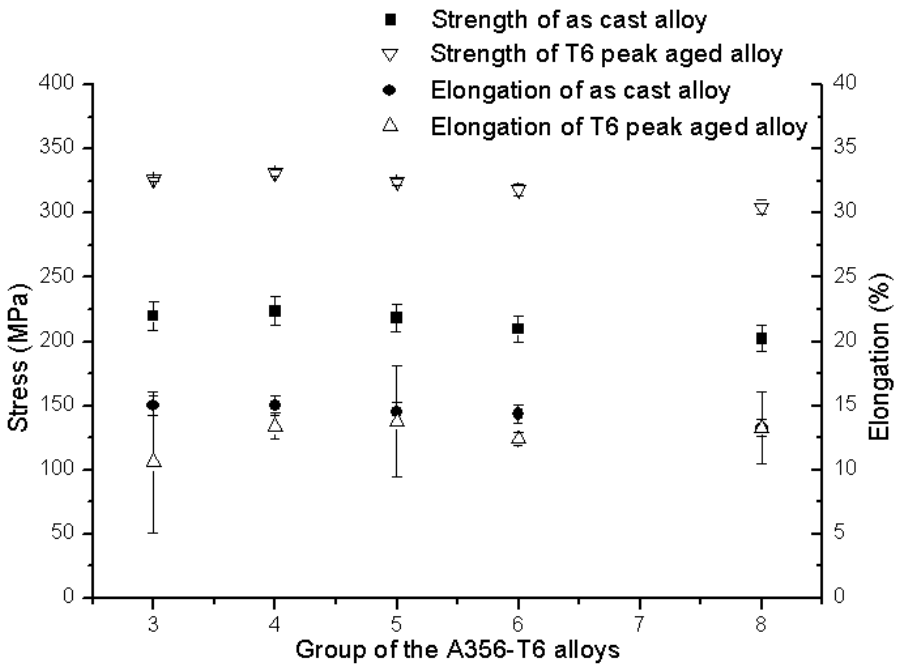

Fig. 4-5 Effect of T6 heat treatment on tensile properties of group 3, 4, 5, 6 and 8 alloys.

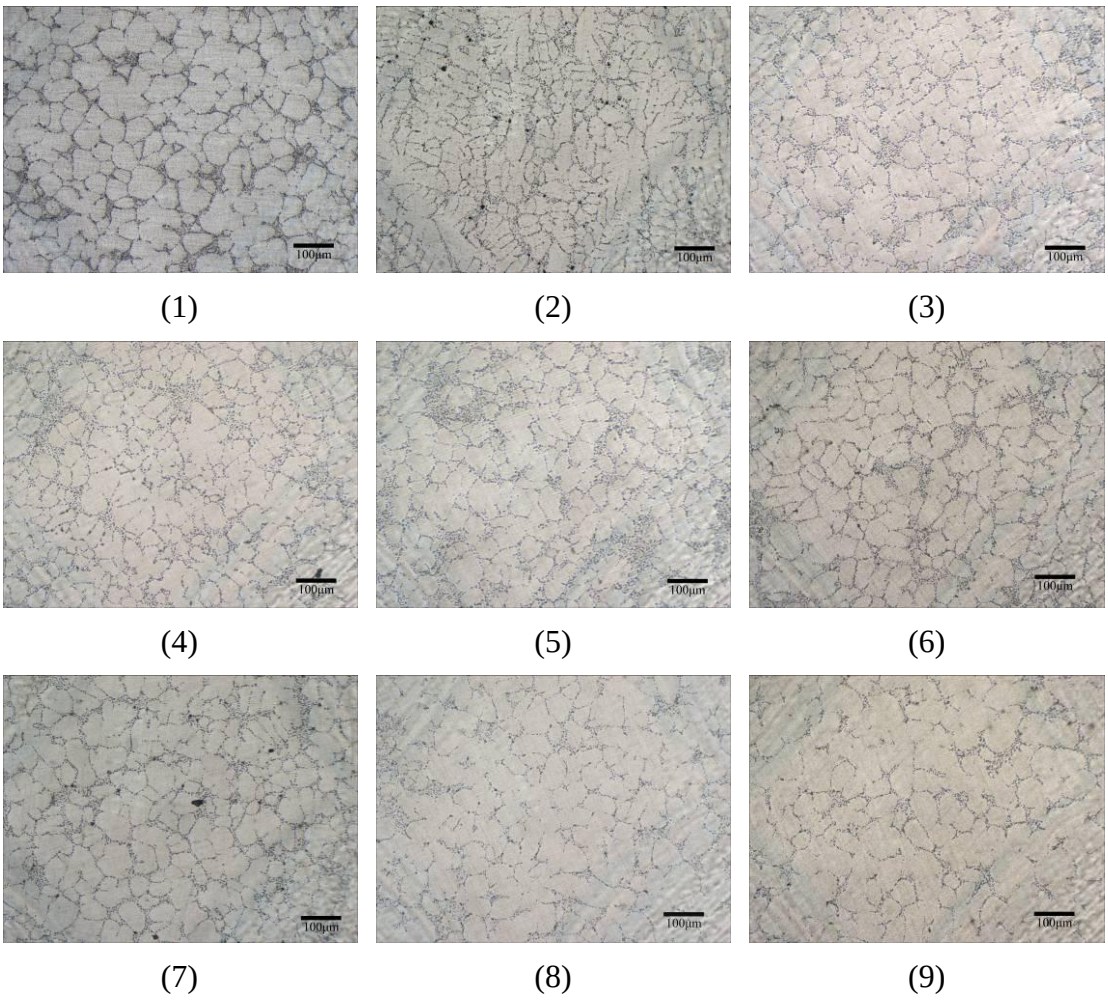

Fig. 4-6 Typical microstructures of the A356-T6 alloys group 1~9.

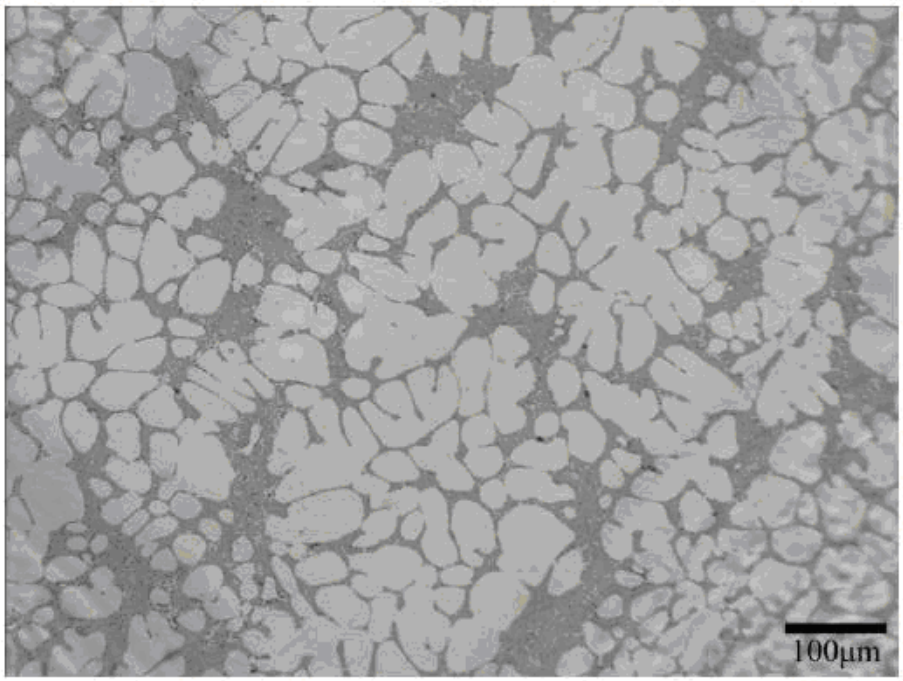

(A)

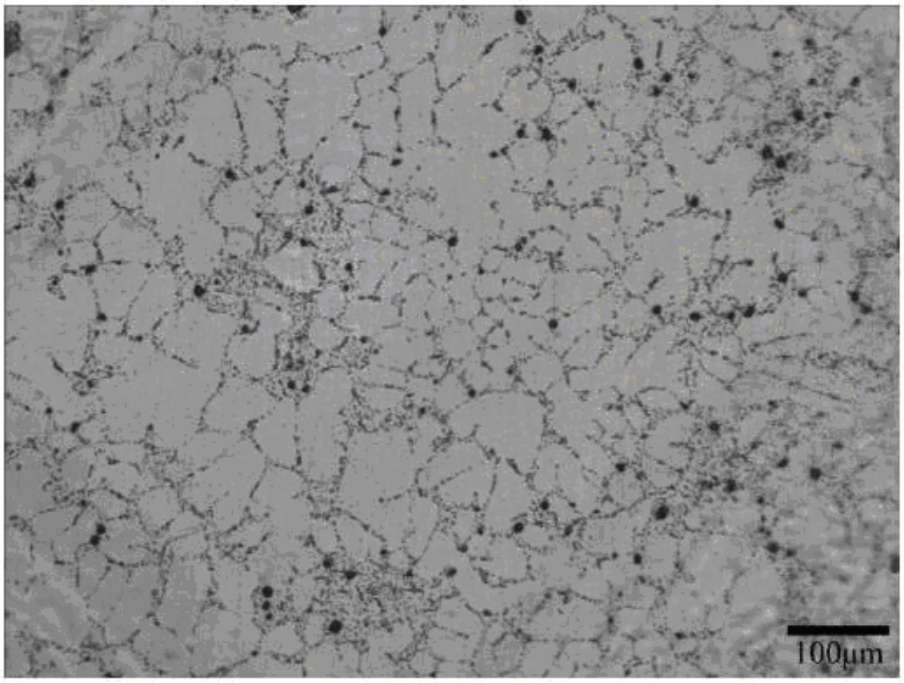

(B)

Fig. 4-7 Microstructures of the SSM A356 alloy group 5 before (A) and after (B) T6 heat treatment.

4.2. High temperature tensile properties of the SSM A356 alloy

High temperature tensile properties of the semi-solid A356 alloy group 1 with T6 under aged and peak aged listed in Table. 4-3 and Table. 4-4. Tensile stress strain curve are shown in Fig. 4-8 and Fig. 4-9. A comparison between microstructures of SSM A356 alloy after tensile test at 25°C and 200°C are shown in Fig. 4-10 and Fig. 4-11. Comparisons of ultimate strength and 0.2% yield strength between the GISS SSM A356-T6 peak aged alloy from the present work and the data of A356 alloy from ASM handbook [51] are presented in Fig. 4-12 and Fig. 4-13. It was learned that:

1. Peak aging provides higher tensile strength and lower tensile ductility compared to the under aging, it might because the peak aging provides more precipitates and the precipitates effectively obstruct dislocation moving and sequentially reduced ductility during tensile test.

2. Ultimate tensile strength of the alloy decreased with increasing test temperature (Fig. 4-12), but 0.2% yield strength of them are not sensitive with temperature (Fig. 4-13). It is because the Al-Si based alloy is a sort of fcc alloy which is featured by larger dislocation width and lower peierls stress [53].

3. High temperature ductility lost occurred on both of the two groups of alloys (Fig. 4-8, Fig. 4-9), which might be resulted from the effect of porosity shrinkage. And the reason of tensile ductility of the peak aged alloy increased again above 200°C might be the effect of micro void coalescence.

4. Work softening took place of work hardening at 250°C so that it is not suitable to use the A356 alloy for application at and above 250°C. The mechanism of work softening would be recovery and recrystallization.

5. Initial cracks start at eutectic phase and the alloy ruptured along the brittle eutectic phase. The Al alpha phase was obviously deformed after tensile test (Fig. 4-10).

Table. 4-3 Tensile properties of A356 alloy of group 1 with heat treatment group 1, under aged.

Temperature (°C)	Ultimate Strength (MPa) ±S.D.	0.2% Yield Strength (MPa) ±S.D.	True Elongation (%) ±S.D.
25	252.2±6.5	142.5±6.5	23.9±0.4
100	203.0±2.5	130.3±2.5	21.7±2.5
150	178.5±3.1	130.3±3.1	22.2±1.9
200	165.8±0.7	130.2±0.7	17.8±1.3
250	139.4±1.1	137.8±1.1	15.1±1.3

Table. 4-4 Tensile properties of A356 alloy of group 1 with heat treatment group 3, peak aged.

Temperature (°C)	Ultimate Strength (MPa) ±S.D.	0.2% Yield Strength (MPa)	True Elongation (%) ±S.D.
25	291.5±3.6	233.7±3.9	11.0±4.9
100	262.6±3.4	222.8±3.6	10.3±0.7
150	228.2±1.5	198.6±2.9	7.9±1.6
200	190.6±4.2	170.7±4.0	9.7±1.6
250	148.9±3.9	145.6±2.9	10.8±2.0

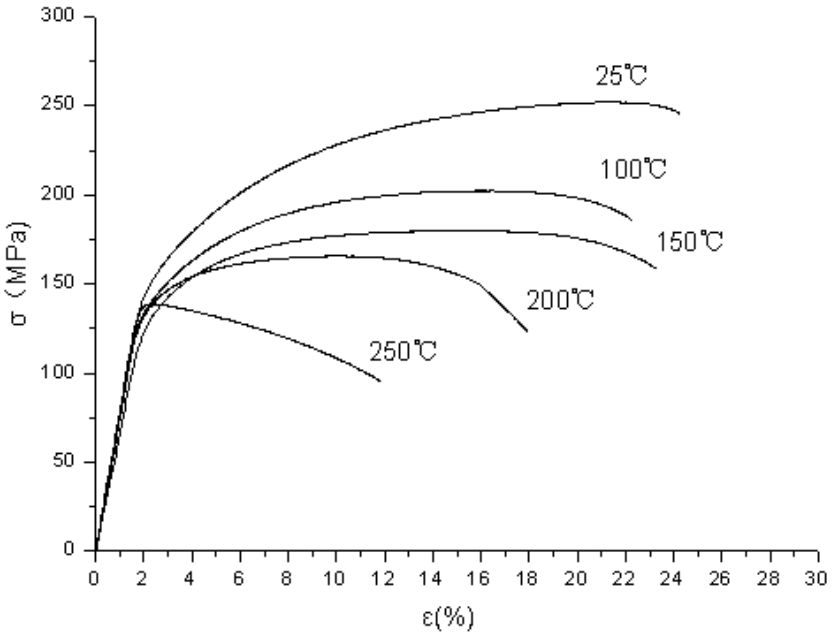

Fig. 4-8 Stress-strain curves of A356 alloy of group 1 with heat treatment group 1, under aged.

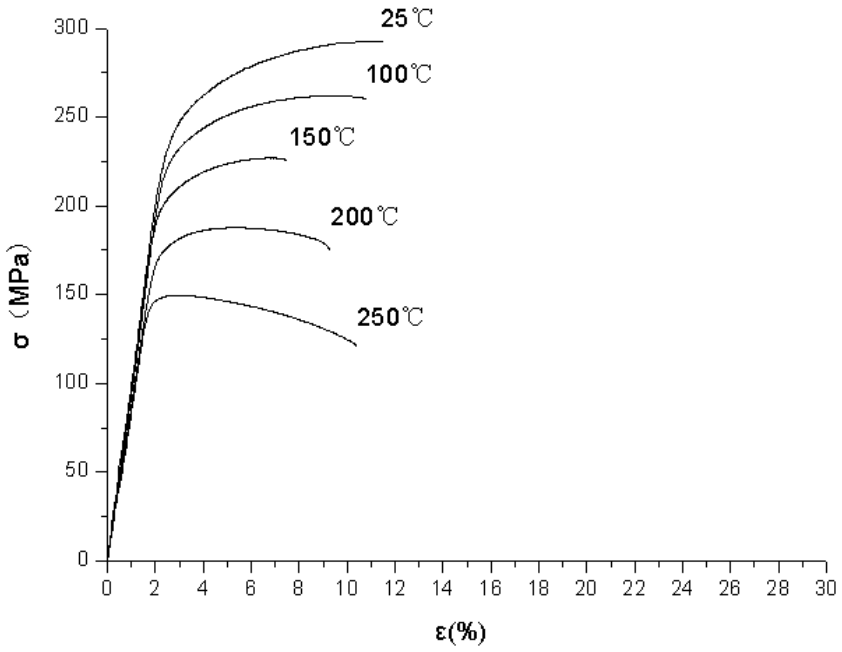

Fig. 4-9 Stress-strain curves of A356 alloy of group 1 with heat treatment group 3, peak aged.

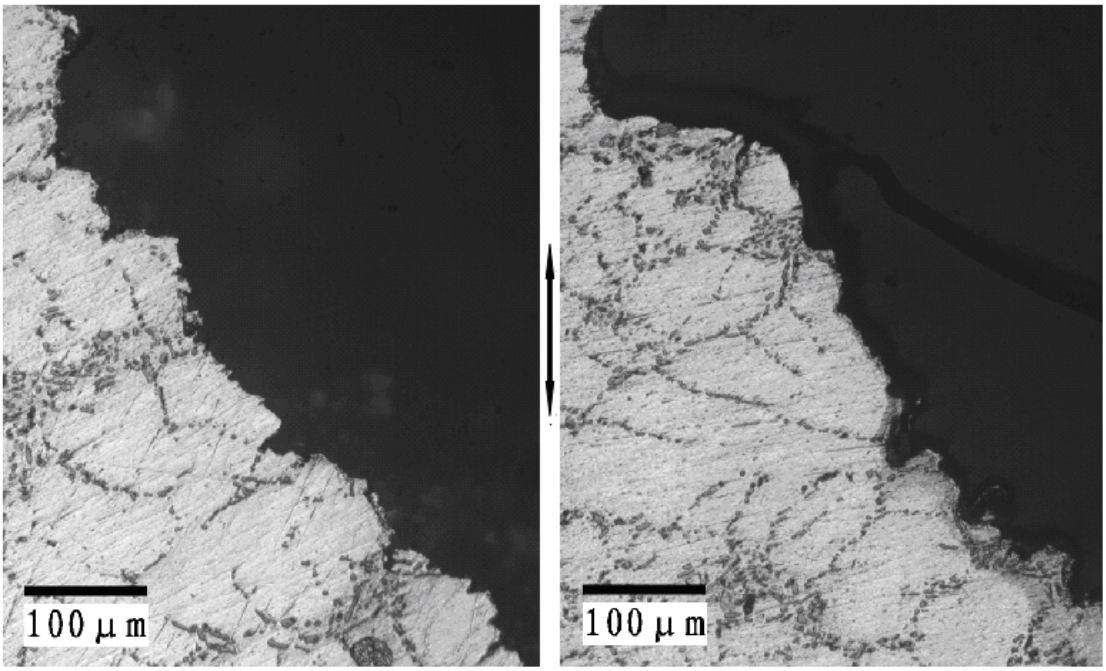

Fig. 4-10 Optical micrographs of SSM A356 alloy group 1 with T6 peak aged after tensile test at 25°C (left) and 200°C (right); the arrow denotes stress direction.

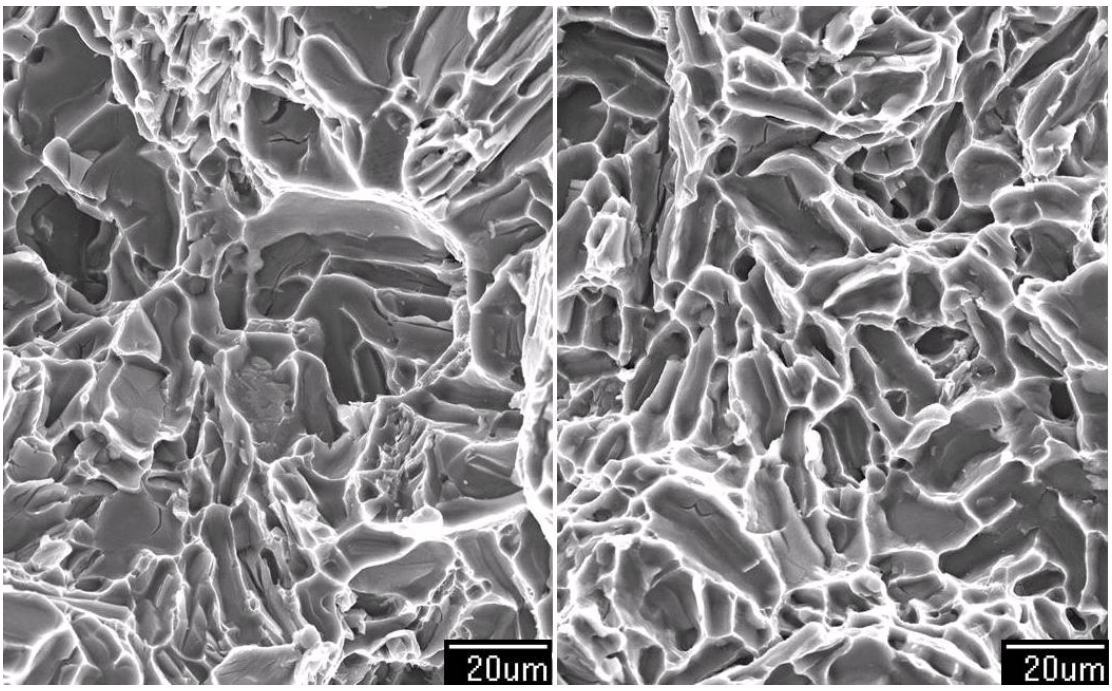

Fig. 4-11 Fracture surface of SSM A356 alloy group 1 with T6 peak aged after tensile test at 25°C (left) and 200°C (right) observed by scanning electron microscope.

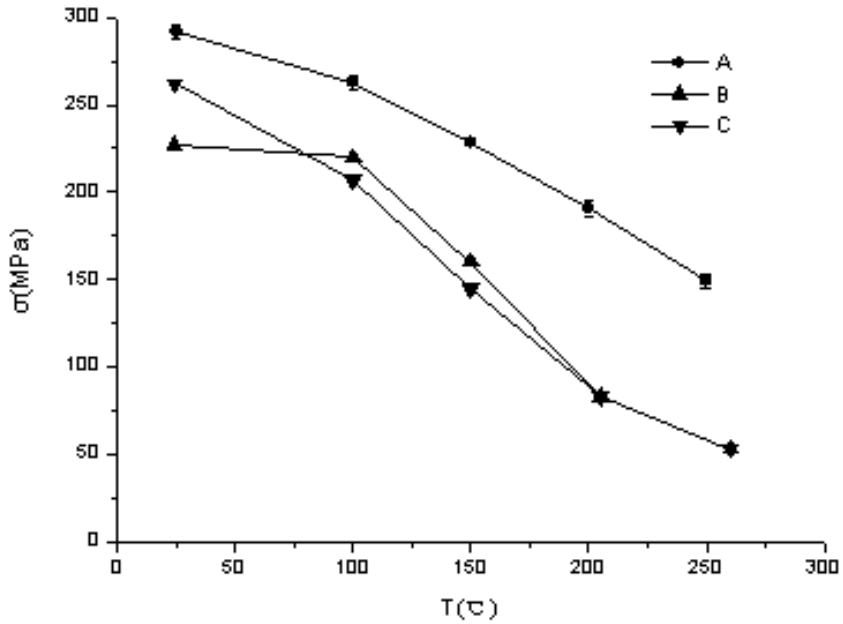

Fig. 4-12 The UTS at different test temperatures, A is the SSM A356-T6 data from the present work, B and C are the sand cast and permanent mold cast A356 data from the ASM handbook. [52]

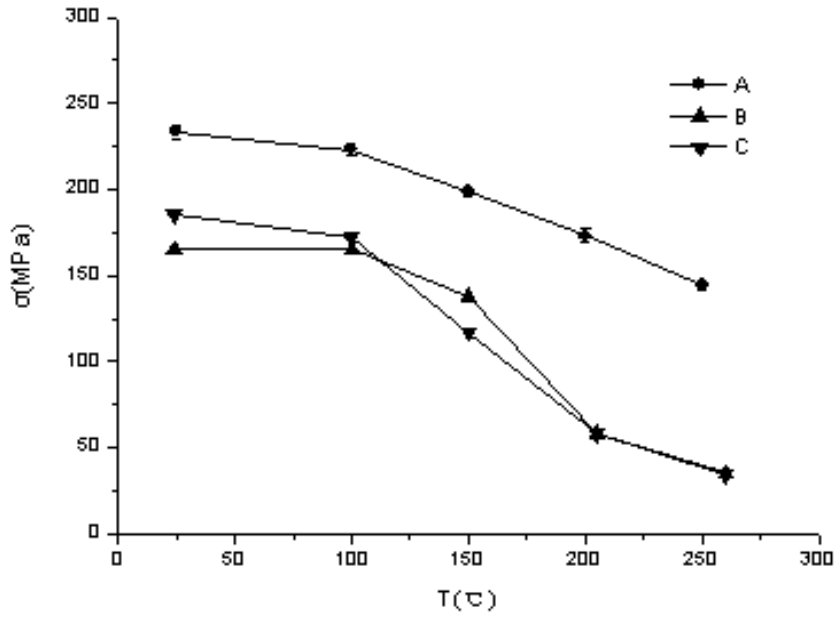

Fig. 4-13 The 0.2% yield strength at different test temperatures, A is the SSM A356-T6 data from the present work, B and C are the sand cast and permanent mold cast A356 data from the ASM handbook. [52]

4.3. Creep behavior of the group 2, 5 and 7 alloys

As it was mentioned in chapter 2 the ten groups of A356 alloy cast with different processes, and group 2, 5 and 7 were selected as representatives of the A356-T6 alloy produced by conventional liquid casting (CLC), GISS and GISS + holding (G+H) processes, respectively, for investigating the effects of different processes and microstructural features on creep behavior. Three typical creep curves are shown in Fig. 4-15, for making a comparison of creep properties between the CLC, GISS and G+H alloys. Minimum creep rate and time to creep rupture of the three groups of alloys are listed in Table. 4-5 and comparison with other researchers results are listed in Table. 4-6 [17, 29, 39, 40, 41]. From the experimental results it is learned that all of the three groups of alloys can be classified into "Class-M alloy" [54], which is featured by a normal or large primary creep stage with taylor hardening [55], a dependence on the stacking-fault energy [56], creep with polygonization and an area of five power-law creep between power-law breakdown and Nabarro-Herring creep, Coble creep or Harper-Dorn creep.

Activation energy *Qc* for creep could be defined by equation (30),

$$Qc = -R[\delta(\ln \dot{\varepsilon}) / \delta(1/T)] \tag{30}$$

and $[\delta(\ln\dot{\varepsilon})/\delta(1/T)]$ of each group of alloy is achieved by plotting $\ln\dot{\varepsilon}$ and (1/T) in the x-y coordinate system as shown in Table. 4-6 and on Fig. 4-19, Fig. 4-20 and Fig. 4-21. Average value of activation energy of creep of the CLC, GISS and G+H alloys are 160 kJ/mol, 163 kJ/mol and 159 kJ/mol, respectively, and those are a little higher to the lattice self-diffusion energy of pure aluminum (142 kJ/mol) [57].

Effect of artificial aging on creep properties of SSM A356 alloy is shown in Fig. 4-14, all the four alloys were performed at constant temperature of 200°C (473K) and constant load of 150MPa, and repeated at least one time. From the graph we can learn that under aged SSM A356 alloy has best anticreep property, it might be because of the hardening phase precipitating at preheating stage and primary creep stage. Over aged SSM A356 alloy performed shortest creep life and smallest total elongation, it might be because the precipitates congregated and grew up to coarse particle which lead to brittleness and could not efficiently obstruct the dislocation moving. There is a big and clear tensile elongation after loading but before primary creep stage of the as-solutioned SSM A356 alloy, moreover, the creep rate of steady stage of the SSM A356 alloy is similar to the alloys with other heat treatment conditions. Mechanism of this phenomenon is still not clear, and a reasonable conjecture is a kind of rapid work hardening due to dislocation rapidly accumulating. Morphology of creep rupture surface with different heat treatment conditions are shown in Fig. 4-22, from which it is observed that rupture line grew across the eutectic phases of all the four conditions.

A comparison of creep properties of the A356-T6 alloys is shown in Table. 4-5. It is learned from tensile results that the CLC alloy has worst tensile properties at room temperature when compare to the GISS and G+H alloy. And room temperature tensile strength of the GISS alloy and G+H alloy are almost the same but its creep life of both GISS alloy and CLC alloy are longer than that of the G+H alloy. This phenomenon might indicate that there is not much effect of shape factor of α grain on high temperature creep properties, instead, total volume fraction of α phase took a more important place because the lower volume fraction of α phase the higher density of silicon particles of the alloy, which can not only obstruct dislocation climbing or sliding but also reduce the rate of recovery more efficiency [47, 65].

Optical microscopy (OM) images of creep ruptured specimens are shown in Fig. 4-23, it is found that crack always initialized and grows along the boundaries between α phases and silicon particles, and some times occurred inside and dissevered the silicon particles. Cavity nucleation and accumulation phenomenon can be clearly observed in the Fig. 2-21. Fracture surfaces were observed by SEM and shown in Fig. 4-25~Fig. 4-29. It is learned that the flowability of α phase of both of the GISS and G+H alloys are higher than the CLC alloy. In addition, the dimples of rupture surface of G+H alloy after creep at 225°C, 110MPa are deeper than those at 200°C, 110MPa because higher temperature provides higher ductility. Some cracked silicon particles can be obviously found in SEM image with high magnifications such as in Fig. 4-29, the mechanism of silicon particle dissevering might be dislocation line cutting.

Table. 4-5 Minimum creep rate and time to rupture of SSM A356-T6 alloys.

Stress	Temperature (K)	Average minimum creep rate $\dot{\varepsilon}_{min}$ (s^{-1})			Average time to rupture (hour)		
		CLC	GISS	G+H	CLC	GISS	G+H
210	473	-	-	3.19E-3	-	-	0.01
190	473	-	-	4.91E-5	-	-	0.93
190	448	-	-	6.00E-7	-	-	7.2
170	498	-	-	2.10E-5	-	-	0.19
170	473	-	-	1.84E-6	-	-	1.8
170	448	-	-	1.05E-7	-	-	21
150	523	-	-	9.22E-6	-	-	0.12
150	498	-	-	2.66E-6	-	-	0.93
150	473	2.15E-7	3.13E-7	2.65E-7	7.3	6.3	6.6
150	448	-	-	4.28E-8	-	-	-
130	523	3.76E-6	5.26E-6	3.66E-6	0.35	0.29	0.29
130	498	8.82E-7	9.53E-7	1.11E-6	2.0	2.0	1.8
130	473	1.08E-7	1.48E-7	1.34E-7	14	15	13
130	448	-	-	2.23E-8	-	-	-
120	473	-	-	7.13E-8	-	-	19
110	523	2.10E-6	2.29E-6	2.24E-6	0.78	0.81	0.87
110	498	3.20E-7	4.38E-7	4.30E-7	4.8	4.8	4.1
110	473	4.99E-8	5.39E-8	4.66E-8	-	-	-
110	450	-	-	6.73E-8	-	-	-
110	448	-	-	1.26E-8	-	-	-
100	473	-	-	3.63E-8	-	-	-
90	523	9.99E-7	1.14E-6	7.58E-7	-	-	-
90	498	1.39E-7	1.44E-7	1.72E-7	-	-	-
90	473	1.88E-8	1.95E-8	2.03E-8	-	-	-
90	450	-	-	8.82E-9	-	-	-
90	448	-	-	5.23E-9	-	-	-
80	473	-	-	1.54E-8	-	-	-
70	523	3.56E-7	3.80E-7	3.54E-7	-	-	-
70	498	4.87E-8	4.56E-8	5.75E-8	-	-	-
70	473	-	-	8.86E-9	-	-	-
60	473	-	-	8.50E-9	-	-	-
50	498	-	-	1.31E-8	-	-	-
50	473	-	-	6.38E-9	-	-	-
30	498	-	-	4.48E-9	-	-	-

Table. 4-6 Stress exponential and activation energy of creep.

Reference	Material	Process	Power law stress exponent *n*	Activation energy of creep *Qc* (kJ/mol)
Y. Zhou (This Study)	A356	CLC + T6	3.8-4.8	146.4-175.9
	A356	GISS + T6	4.2-5.5	146.9-183.7
	A356	G+H + T6	4.2-5.1	138.6-151.6
W. M. V. Haaften, 2002	AA3104	SSM + direct chill casting	5.7	174
	AA5182		3.3	120
S. Spigarelli, 2002	Al-17Si -1Mg-0.7Cu	-	3-5	130
T. Jaglinski, 2004	Al-Si based	Die-casting		163-261
S. Spigarelli, 2004	Al-17Si-4Cu -0.55Mg	Thixoforming	4.4	210
J. C. Dandrea, 2009	M4032-2	High pressure die-cast	-	190-272
	332	Permanent mold	-	173-284
	332RR	Permanent mold	-	122-137
	333	Permanent mold	-	125-356

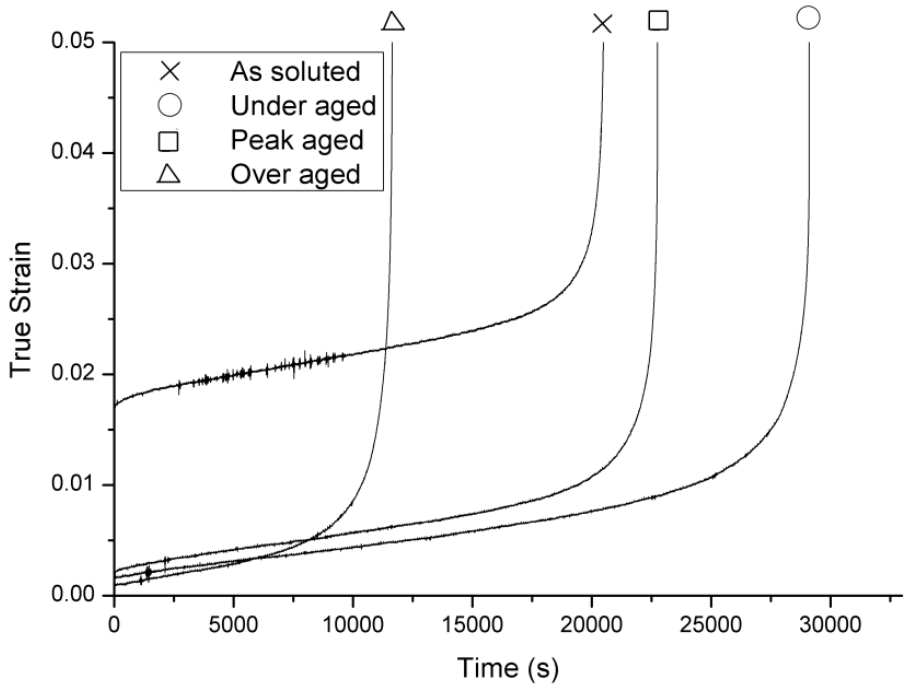

Fig. 4-14 Typical creep curve of as-solutioned, under aged, peak aged and over aged A356 alloy at constant temperature of 473K (200°C) and constant load of 150MPa.

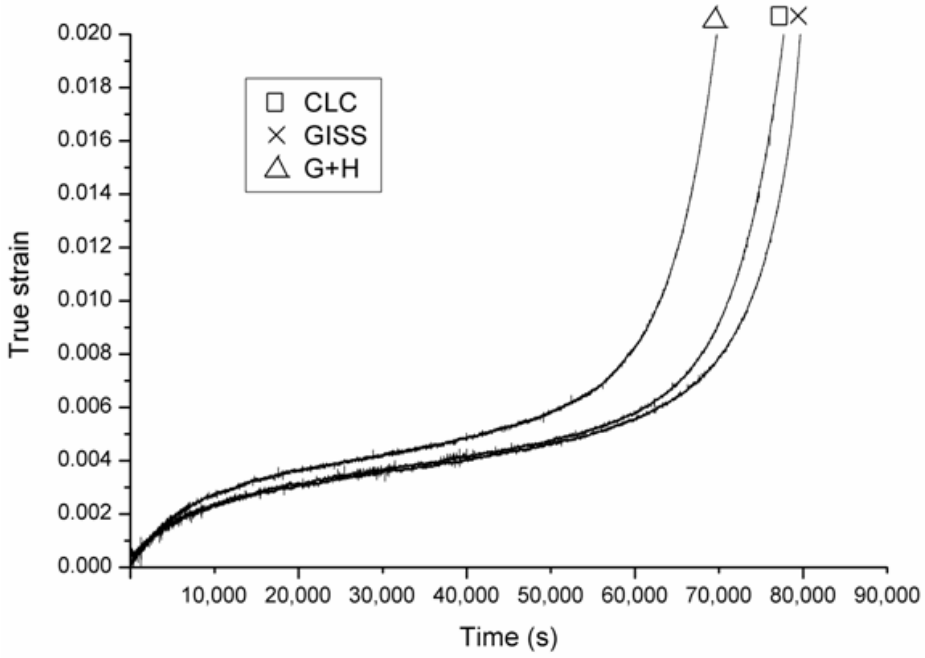

Fig. 4-15 Creep curves of CLC, GISS and G+H alloys of creep tested at 498K (225°C) and constant load of 70MPa.

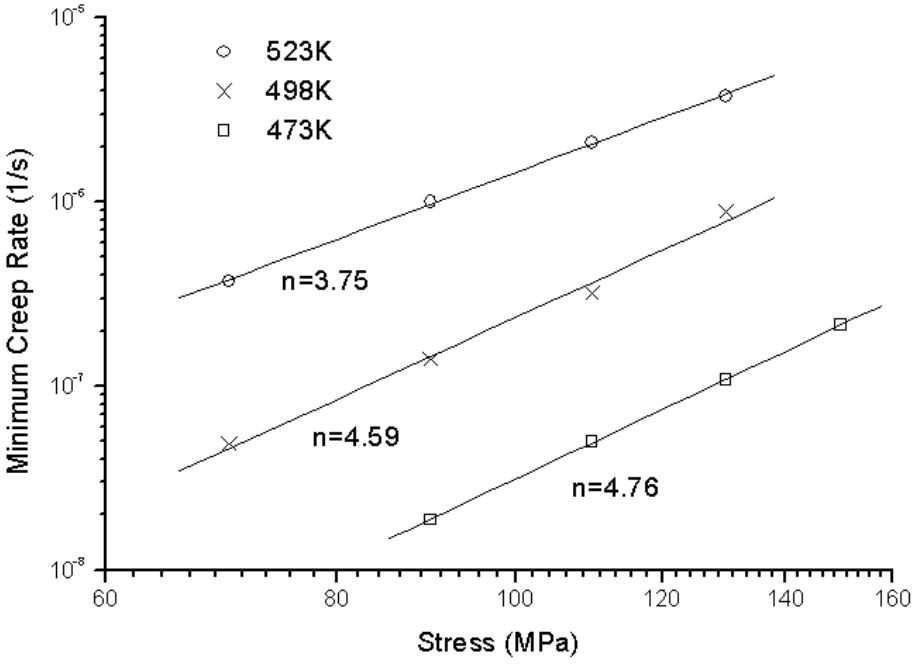

Fig. 4-16 Stress exponent *n* of CLC A356-T6 alloy.

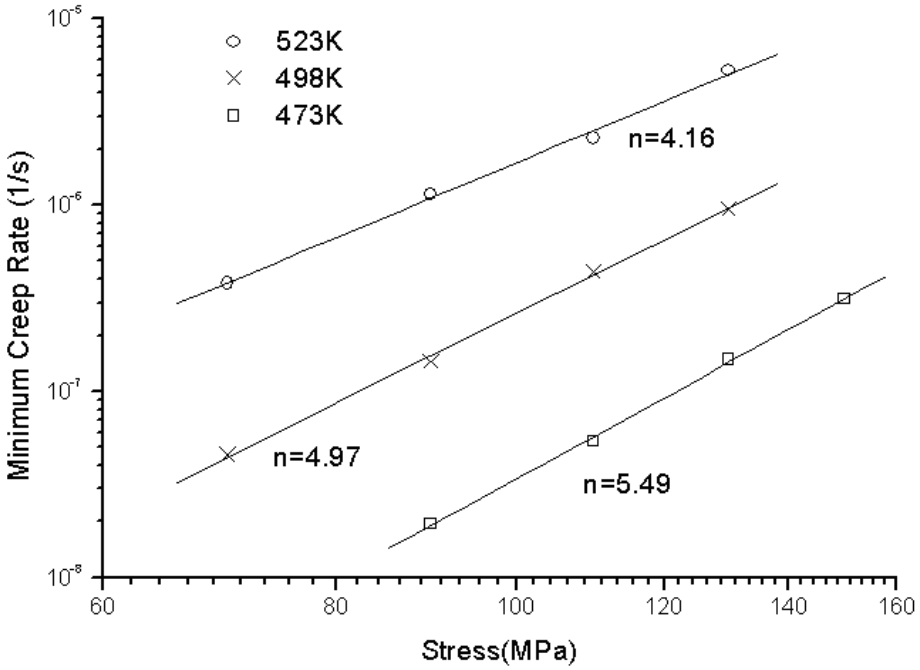

Fig. 4-17 Stress exponent *n* of GISS A356-T6 alloy.

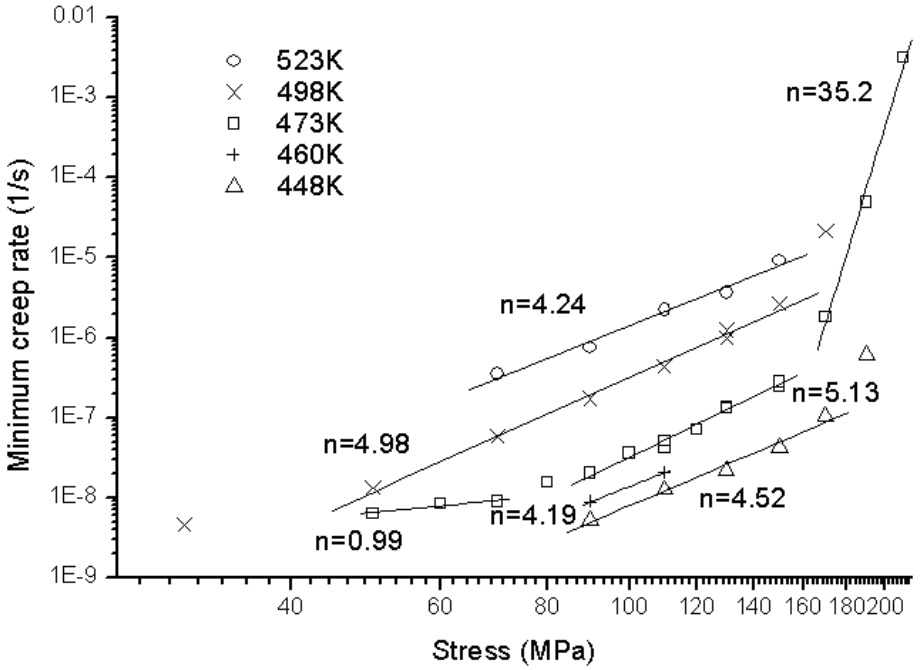

Fig. 4-18 Stress exponent *n* of G+H A356-T6 alloy.

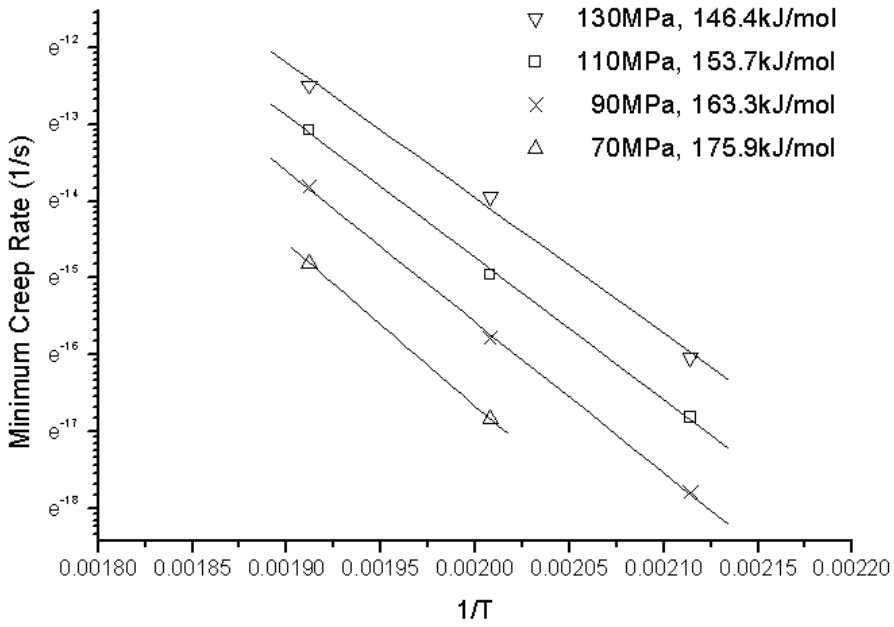

Fig. 4-19 Activation energy of creep of the CLC A356-T6 alloy.

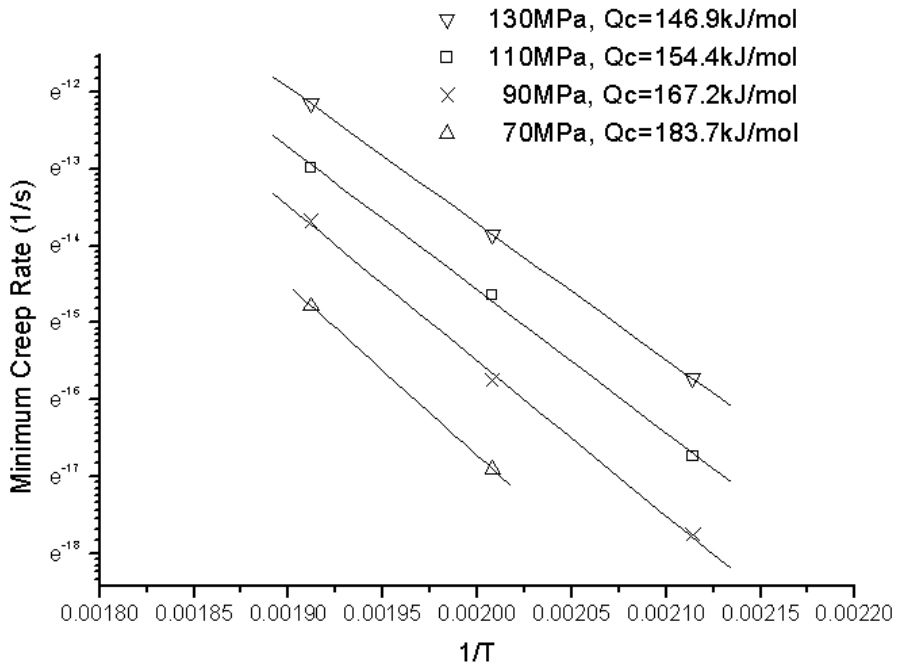

Fig. 4-20 Activation energy of creep of the GISS A356-T6 alloy.

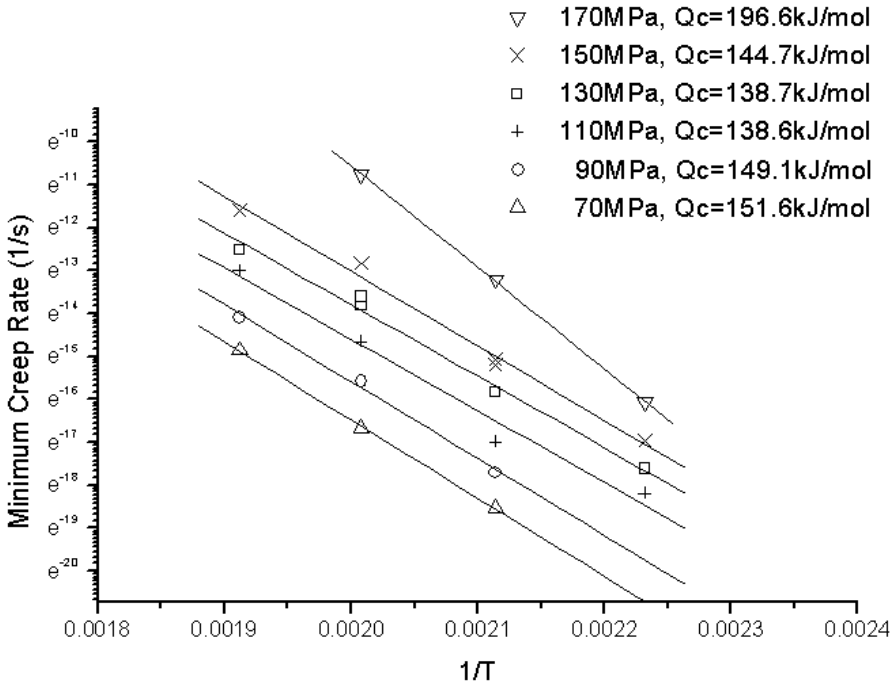

Fig. 4-21 Activation energy of creep of the G+H A356-T6 alloy.

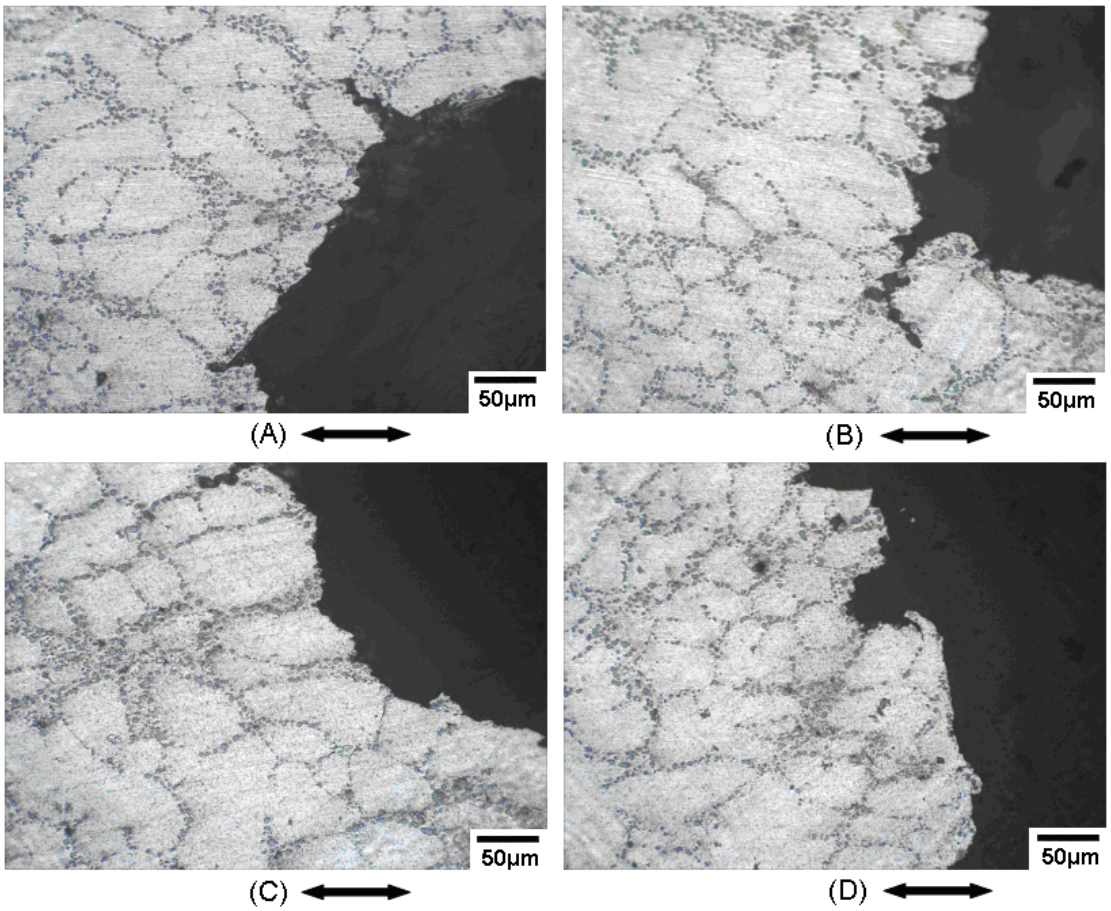

Fig. 4-22 Optical micrographs of longitudinal section of SSM A356 alloy group 9 with (A) as-solution, (B) Under aged, (C) Peak aged and (D) Over aged, and the arrows denote stress direction.

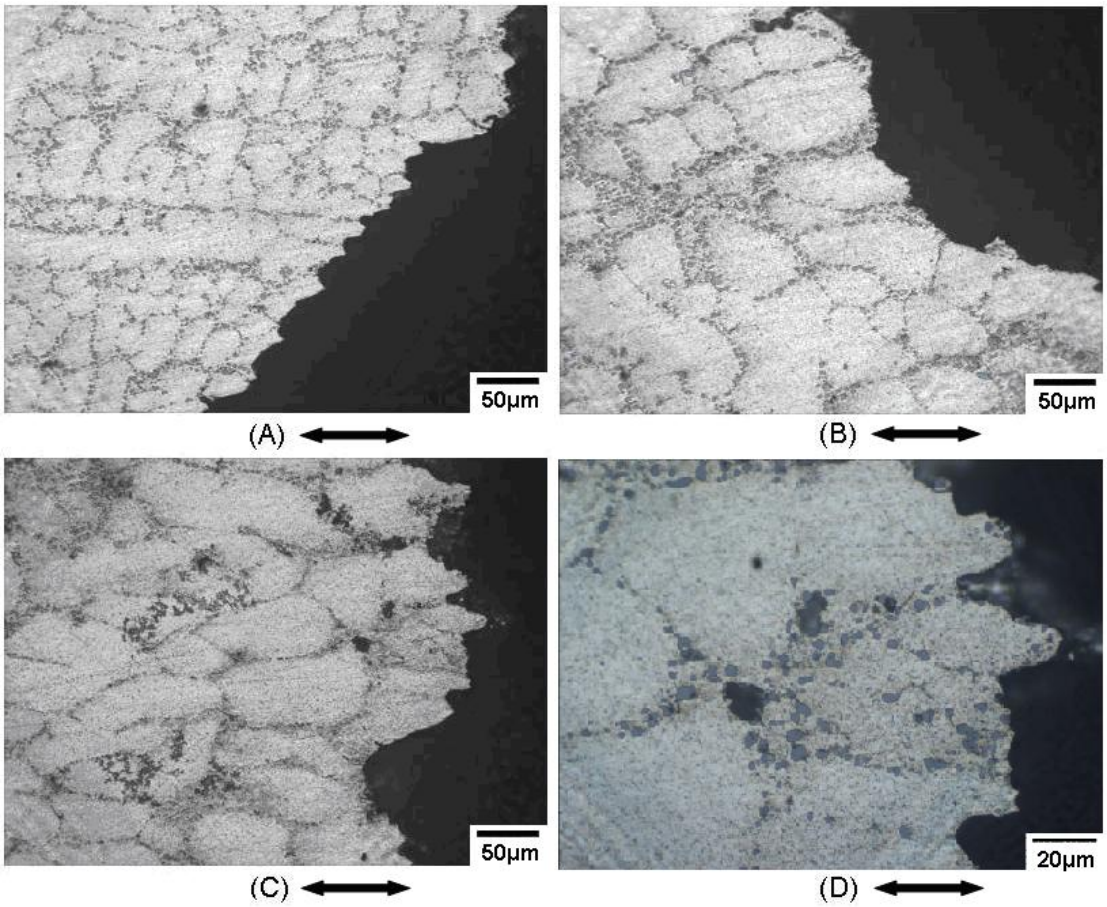

Fig. 4-23 Optical micrographs of longitudinal section of SSM A356-T alloy (A) CLC, (B) GISS, (C) G+H and (D) G+H with higher magnification, and the arrows denote stress direction.

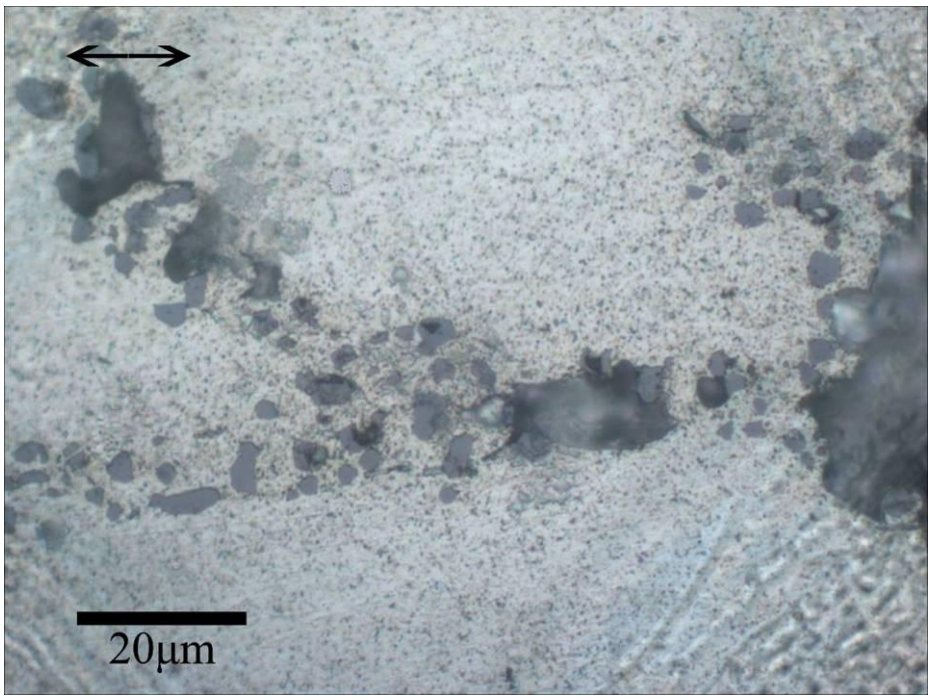

Fig. 4-24 Optical micrograph of longitudinal section of SSM A356-T6 alloy G+H and the arrows denote stress direction.

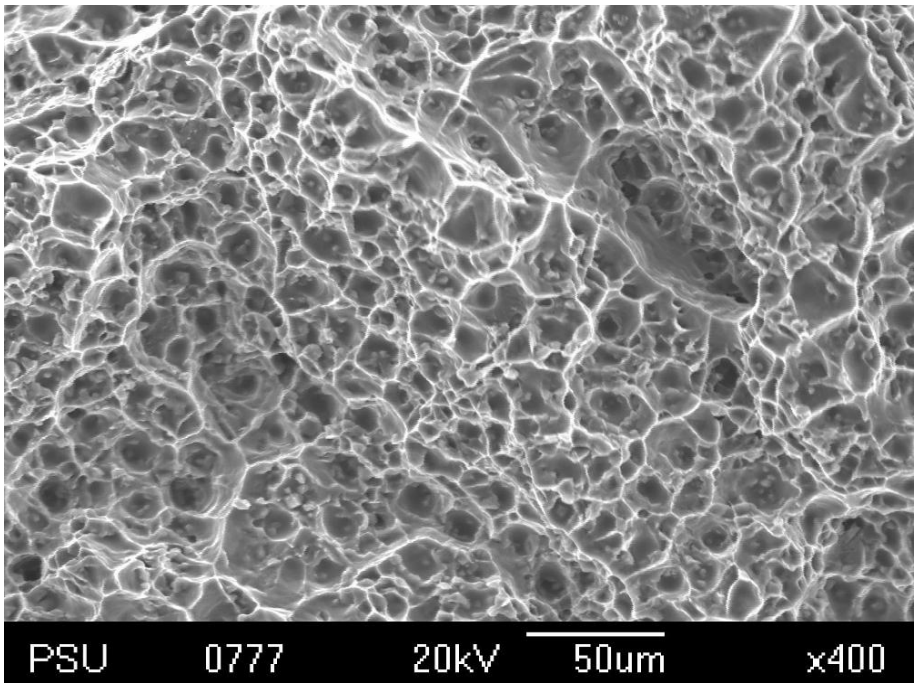

Fig. 4-25 SEM fractograph of SSM A356-T6 alloy CLC after creep test at 200°C, 110MPa.

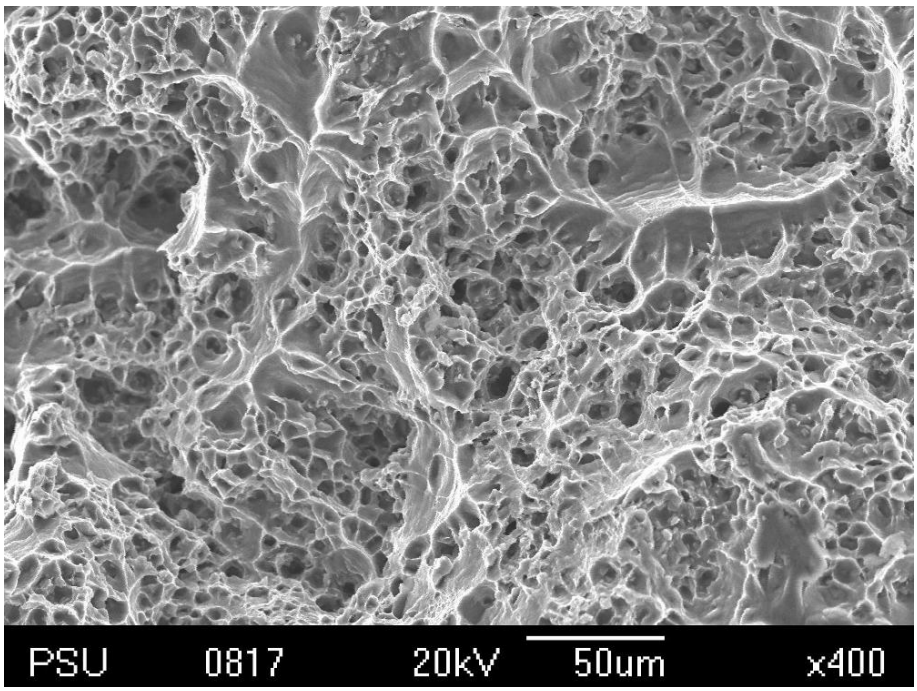

Fig. 4-26 SEM fractograph of SSM A356-T6 alloy GISS after creep test at 200°C, 110MPa

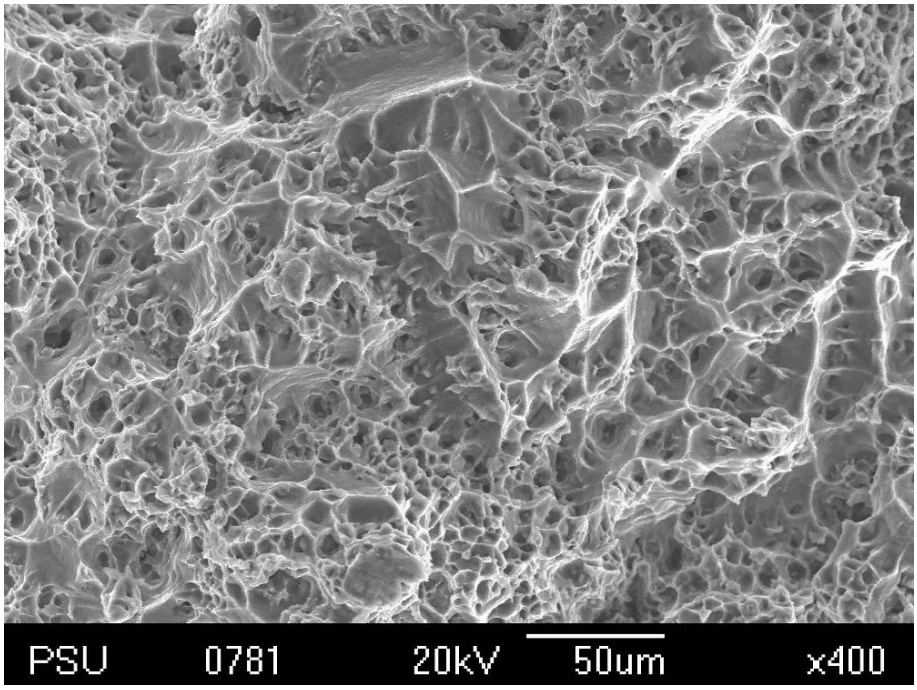

Fig. 4-27 SEM fractograph of SSM A356-T6 alloy G+H after creep test at 200°C, 110MPa.

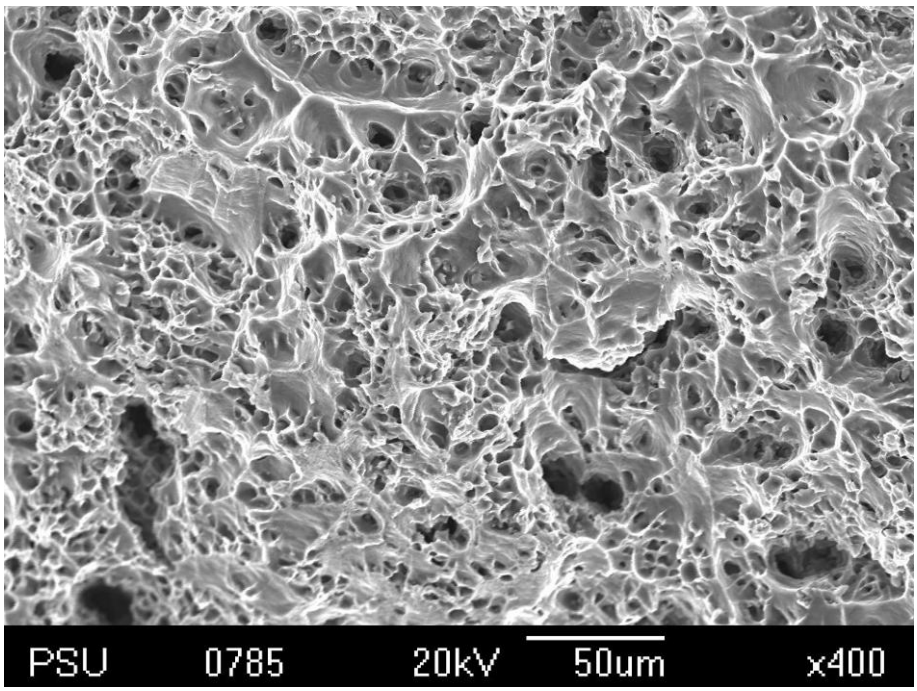

Fig. 4-28 SEM fractograph of SSM A356-T6 alloy G+H after creep test at 225°C, 110MPa.

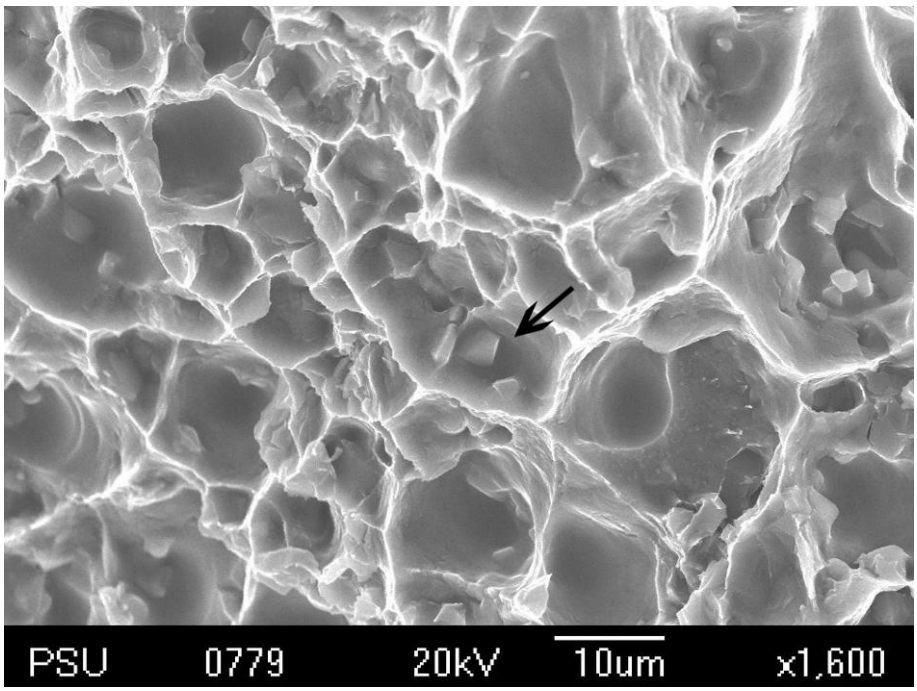

(A)

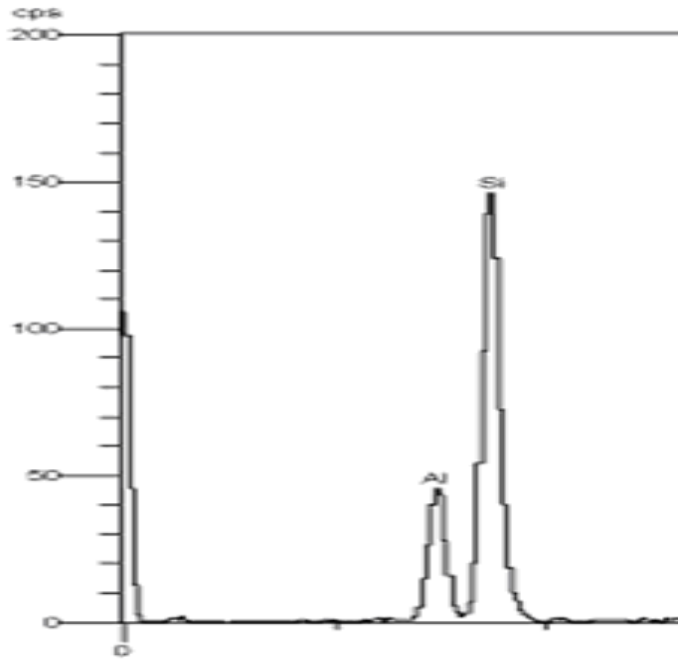

(B)

Fig. 4-29 (A) SEM fractograph of SSM A356-T6 alloy G+H after creep test at 200°C, 110MPa. (B) The corresponding EDS of the silicon particle at arrow tip.

4.4. Primary stage of the creep curves

Unlike some researchers' report previously introduced in the Chapter 1 and 2, in this study, very long time primary stages were observed on the creep curves especially those at 175-200°C (448-473K) with low applied stress and most of them seems have a very slow decelerating stage after the short fast decelerating stage, which is so slow that some times it could be approximately considered as a linear stage (Fig. 4-30). However, this kind of phenomenon could not be clearly observed at higher temperature (225-250°C, or 498-523K) or high stress conditions (175-200°C, or 448-473K with σ>0.8UTS) (Fig. 4-31). Consider of the stress-strain curves of various temperature tensile tests, it means this stage appears at the temperature range of work hardening process only, thus it is reasonable to assume that it is a sort of dislocation or maybe also precipitates hardening process, and we would like to name it as linear hardening stage. Fig. 4-30 demonstrated a typical four stage creep curve of the A356-T6 alloy at 200°C (473K), moreover the linear hardening stage will be more clear if we minus the steady creep strain $\dot{\varepsilon}_{ss} \bullet t$ ($\varepsilon - \dot{\varepsilon}_{ss} \bullet t$) from the creep curves, as it is illustrated in Fig. 4-32. A group of load change creep tests were done for further investigating of the linear hardening stage and there is a typical curve of load change test at 200°C (473K) from 50MPa to 70MPa shown in Fig. 4-33, from which we can learn that the hardening happens at the first loading stage only.

A TEM image of the A356-T6 alloy after 24 hours creep test and just reached the steady stage creep is shown in Fig. 4-34. Not much dislocation can be found in this stage, a reasonable conjecture for the main mechanism of creep at the primary and secondary stage is dislocation generation and annihilation interaction. The rate of dislocation generation is much faster than annihilation at the fast decelerating stage of the primary stage, but the rate of generation decelerates and annihilation accelerates when the density of dislocation increases, and then balanced at the linear hardening stage.

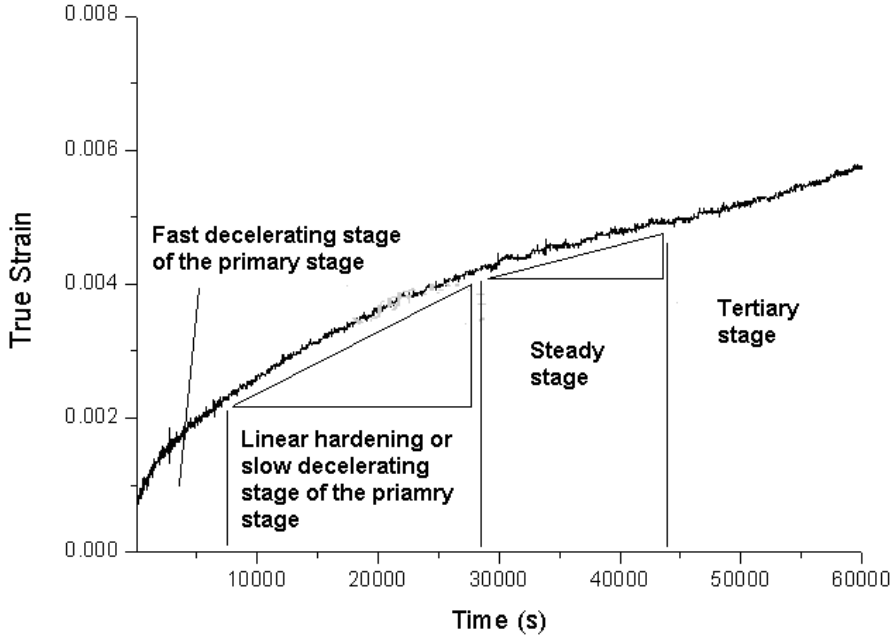

Fig. 4-30 A typical creep curve of the A356-T6 cast alloy.

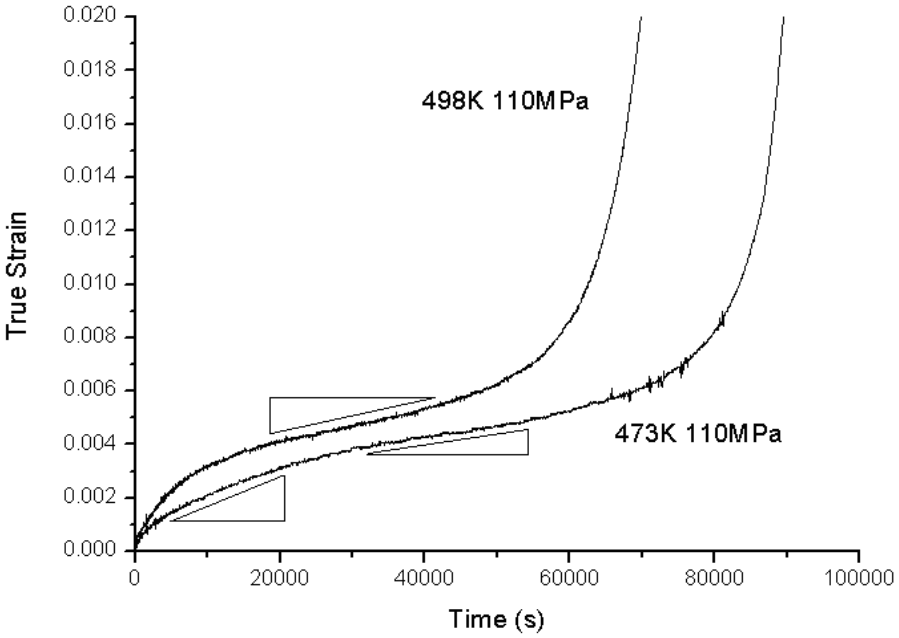

Fig. 4-31 A comparison of the creep curves of A356-T6 cast alloy at 200°C (473K) and 225°C (498K).

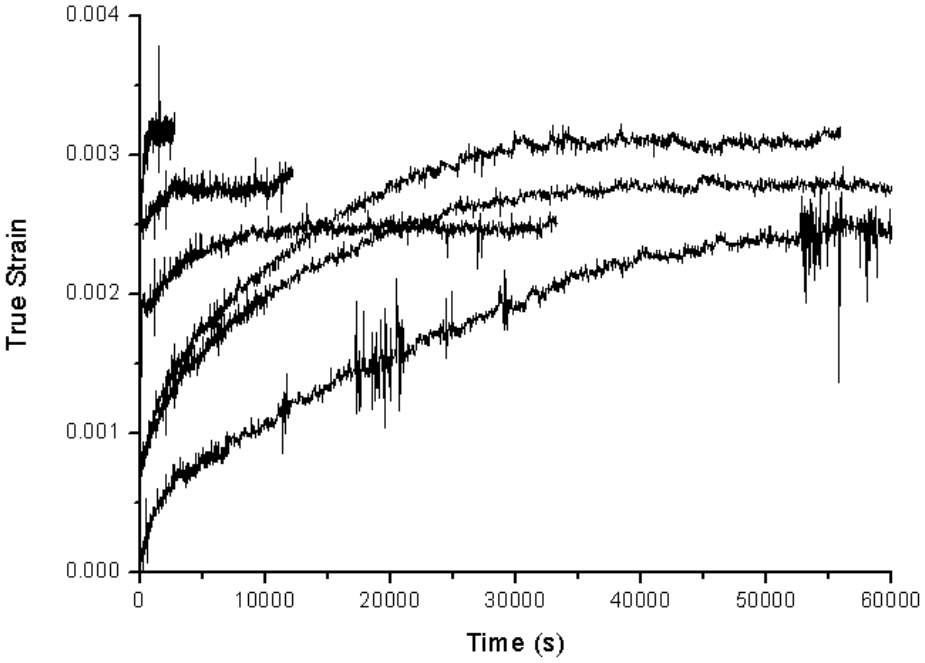

Fig. 4-32 Creep curves with minus the true steady creep strain ($\varepsilon - \dot{\varepsilon}_{ss} \bullet t$) of the A356-T6 cast alloy at 200°C (473K).

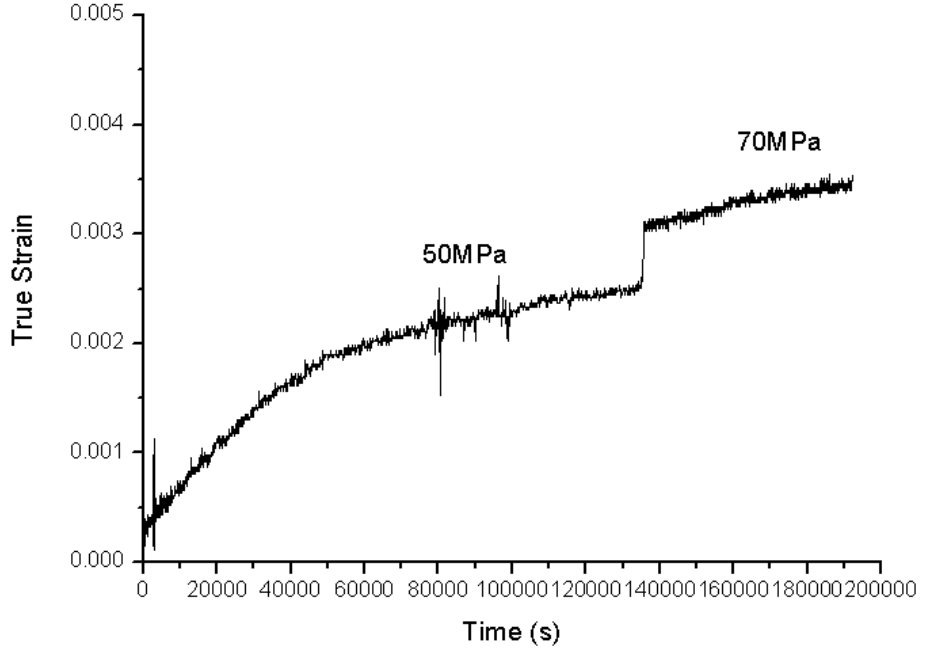

Fig. 4-33 Creep curve of change load test of the A356-T6 alloy at 200°C (473K).

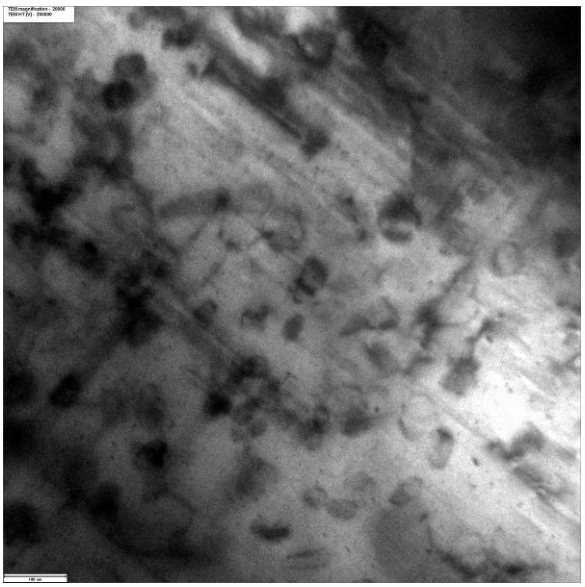

Fig. 4-34 TEM image of A356-T6 alloy at steady stage at 200°C (473K).

4.5. Modeling of creep of the SSM A356 alloy

4.5.1 Modeling of primary stage of creep curve

Equation (31) is obtained by logarithmically expanding equation (8), m can be got by least squares linear fitting of the strain-time curve of the primary state, where n is already learned by plot $\log_{10}$(minimum creep rate) to $\log_{10}$(stress), *A* can be calculated by equation (31) with fixed n and m and then the *A*, *m* and *n* could be adopted to the equations of time or strain hardening theories. However, in this study, it was found that the linear fitting method for calculating the parameter *m* is not very good fit because it needs carefully defining of the primary creep stage and do linear fit one by one, otherwise the precision of fitting will be unreliable, on the other hand, it was observed that not every logarithmic time-strain curve is well linearized, for example Fig. 4-35. Furthermore, the author tried his own way for parameter *m* calculation, by using least square nonlinear fitting on time-strain curve with initial value obtained by the Levenberg-Marquardt global optimization algorithm. The result of creep curves at 200 °C is demonstrated in Fig. 4-36. It is learned that the time hardening theory is not very suitable for modeling the A356-T6 alloy, because of the large primary stage as discussed in previous section.

$$\log_{10}\varepsilon = \log_{10} A + n\log_{10}\sigma + m\log_{10} t \tag{31}$$

There is another way to model the large primary stage including linear hardening stage is the use of the power low relationship equation (3), the stress

exponent of the linear hardening is plotted in Fig. 4-37 by following equation (2) and activation energy of the linear hardening is obtained by the equation (30) and shown in Fig. 4-38, it is averagely 97 kJ/mol, or we could also defined the activation energy as activation energy of creep minus 97 kJ/mol = 56 kJ/mol.

At the same time, some statistical relationship of total time of the linear hardening stage has to be found in order to well describe the linear hardening stage and it is plotted in Fig. 4-39, and Boltzmann Sigmoid Equation (32) was used to import to conclude this relationship at 175 and 200°C.

$$t_{LH} = A_2 + (A_1 - A_2) / (1 + \exp((\sigma - \sigma_0) / d\sigma)) \quad (32)$$

where t_{LH} is time of linear hardening stage, σ is stress, σ_0 is medium value of the sigmoid and A_1, A_2 are constants. Unfortunately, database of this research is not enough to determine the relationship of parameters between different temperatures, so unification equation was not available to be constructed.

There are two ideas to model the primary stage and the linear hardening stage, one is separate strain into two parts, strain of primary stage and strain of linear hardening stage,

Unfortunately, it is hard to conclude the less regular result into an equation. Therefore, a new approach should be found to model this special and less statistical phenomenon.

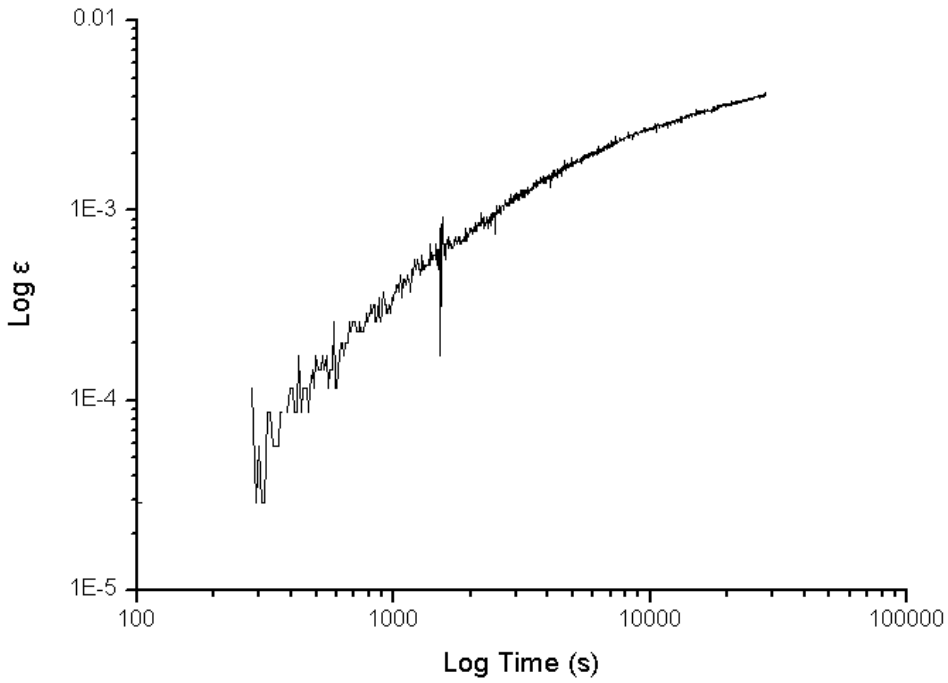

Fig. 4-35 Logarithmic time-strain curve of creep test at 225°C, 90MPa of the A356-T6 cast alloy.

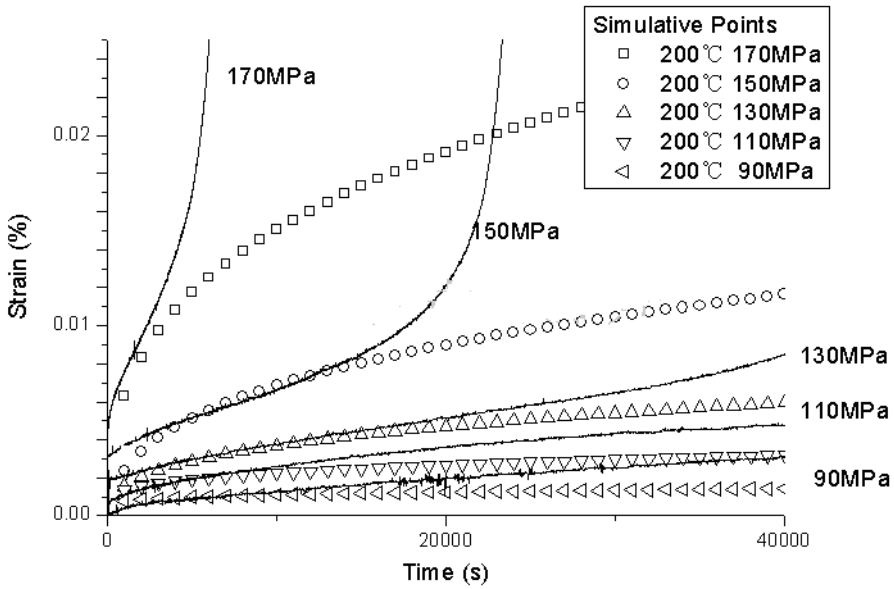

Fig. 4-36 Simulation of primary stage of creep curves of A356 cast alloy at 200°C, the solid lines are experimental curve and the hollow lines are simulative curve by the time hardening equation.

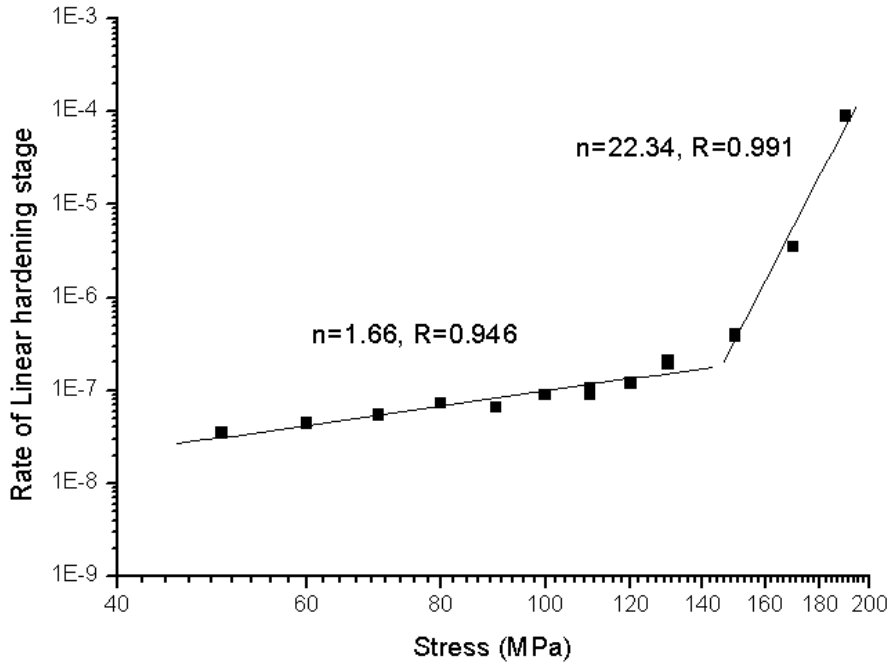

Fig. 4-37 Stress exponent of linear hardening stage at 200C° (473K) of the A356-T6 cast alloy.

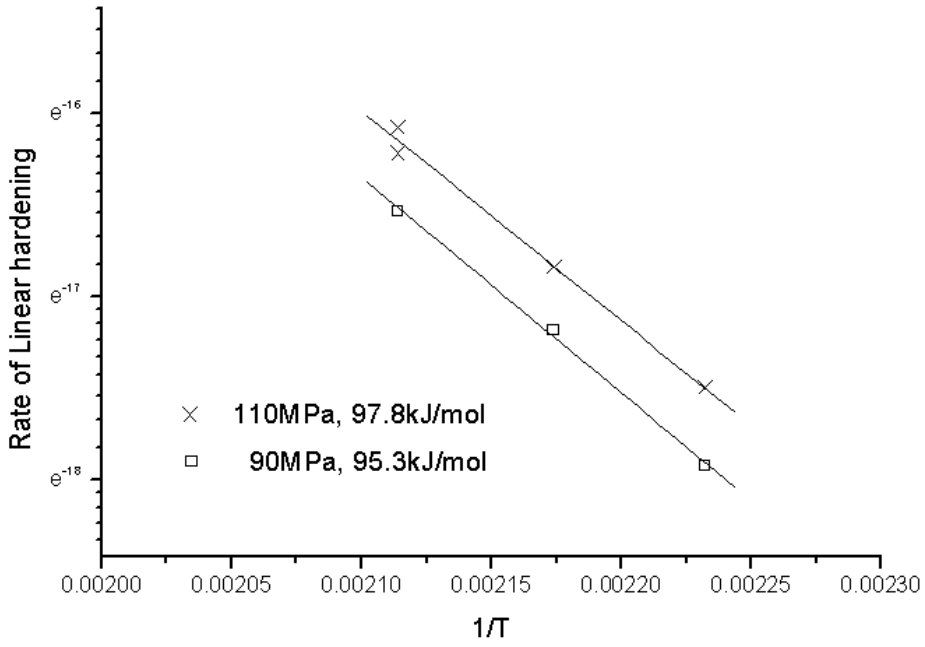

Fig. 4-38 Activation energy of linear hardening stage at 200C° (473K) of the A356-T6 cast alloy.

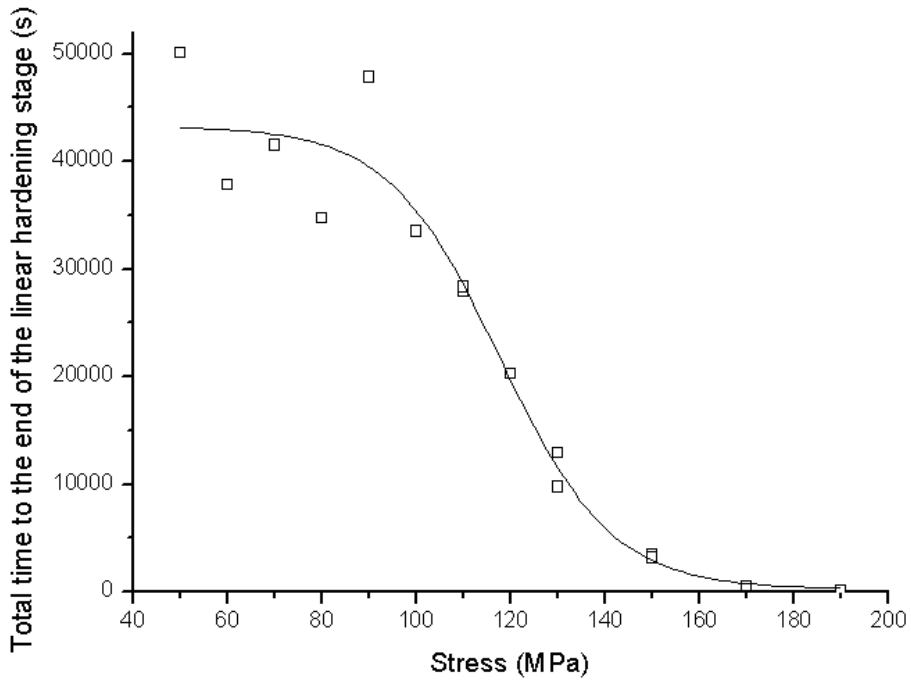

(A)

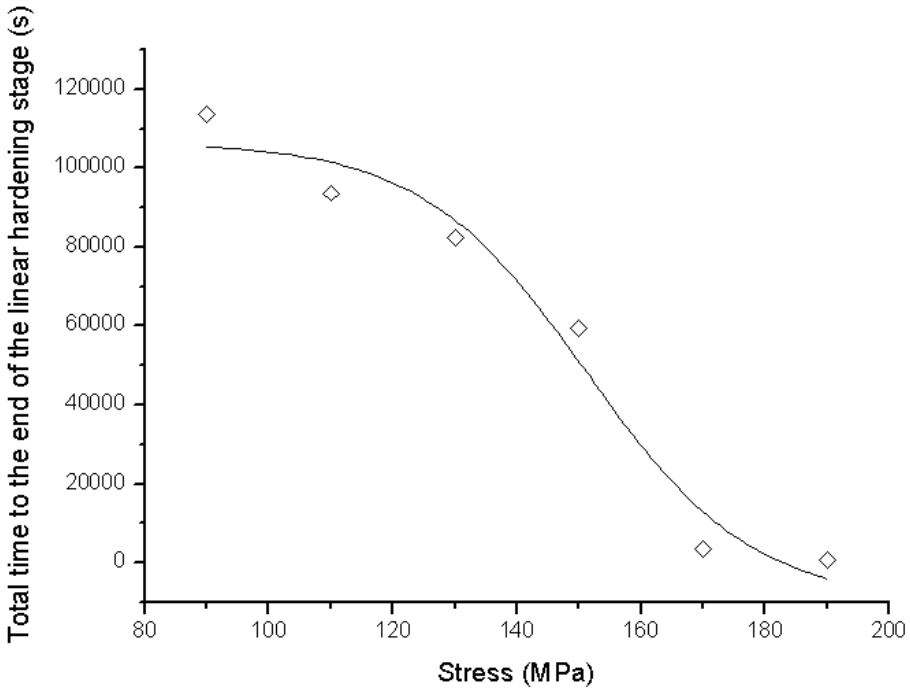

(B)

Fig. 4-39 Total time to the end of linear hardening stage at 200C° (473K) (A) and 175C° (448K) (B) of the A356-T6 cast alloy

4.5.2 Modeling of both primary and linear hardening stage by some novel equations

In order to solve the problem in paragraph 4.4.1, an arctangent equation (34) was imported to modeling the large primary stage of the creep curves, and later was modified into novel equations (35), (36) and (37) were proposed in this study, where n_{LH} is stress exponent of the linear hardening stage, n_c is stress constant of the value of B, A is a constant corresponding to total creep strain before steady stage, B is a constant of the shape of the linear hardening stage, B_2, A_C and B_C are constants plays similar role as A and B, A_T and B_T are constants similar as A and B but fixed with temperature, and C is a materials constant which unit is kJ/mol.

$$\varepsilon = \sigma E + \dot{\varepsilon}_{\min} t + A\arctan(Bt) \tag{34}$$

$$\varepsilon = \sigma E + \dot{\varepsilon}_{\min} t + A\arctan(B_2 \sigma {n_{LH}}^2 t) \tag{35}$$

$$\varepsilon = \sigma E + \dot{\varepsilon}_{\min} t + A_T \arctan(B_T \sigma^{n_c} t) \tag{36}$$

$$\varepsilon = \sigma E + \dot{\varepsilon}_{\min} t + A_C \arctan(B_C \sigma^{n_C} \exp(C/RT) t) \tag{37}$$

$$\varepsilon = \sigma E + \dot{\varepsilon}_{\min} t + A_C \arctan(B_C \sigma^{n_c} t) \tag{38}$$

There are two way to find out the best value of the constant A and B in equation (35). One is eyeballing method, define A by total strain before steady stage and determine B by observe the shape of the linear hardening stage, but both efficiency and precision of this method is low. Another solution is the author's creation which introduced in the last paragraph, nonlinear fitting by Levenberg-Marquardt global optimization algorithm.

According to the experimental data and the nonlinear fitting by Levenberg-Marquardt global optimization algorithm method, A and B_2 of the semi-solid alloy A356-T6 G+H is about 0.01326 and 6.39E-7 and as it is shown in Fig. 4-40 that unlike the time hardening theory, the numerical regenerated creep curve made by equation (35) is highly correspond to the experimental curve in a very wide range of stress, which is from $0.25\sim0.85\sigma_{UTS}$.

However, in one hand, because of the limitation of the experience some times it is not easy to find out the value of n_{LH}, in the other hand it is worth while to fix the equation to adapt with various temperature levels, so the author would like to propose equation (36) for fitting the data in the primary stage, though there are some disadvantages of equation (36) such as it does not work well when stress is above $0.8\sigma_{UTS,}$ on the other hand, the advantages of this equation is it does not have relationship with n_{LH} and can adapt with creep curves at different temperature levels. In this case the value of A_T and B_T might be constants or other kind of relationship of temperature, and n_c could be approximately considered as a constant.

As it is shown in Fig. 4-41 that the A_T is not sensitive with temperature and stress, so it could approximately considered as a constant A_C when the temperature range is not too wide. According to Fig. 4-42 and Fig. 4-43 that value of *Ac*, n_c, *C* and *Bc* of equation (37) in this case are approximately 0.001326, 5.081, 135.4kJ/mol and 2.26E-27, respectively.

Unfortunately, the equation (37) may not be the perfect unification equation, because by the limitation of database of this study, there are not enough data to test this equation. However, all of these novel equations gave an idea of modeling by image method and it could be perfect and improved in the future. Moreover, when the temperature is constant, B_T can be considered as a constant B_C, and then a simplified equation was obtained as equation (38).

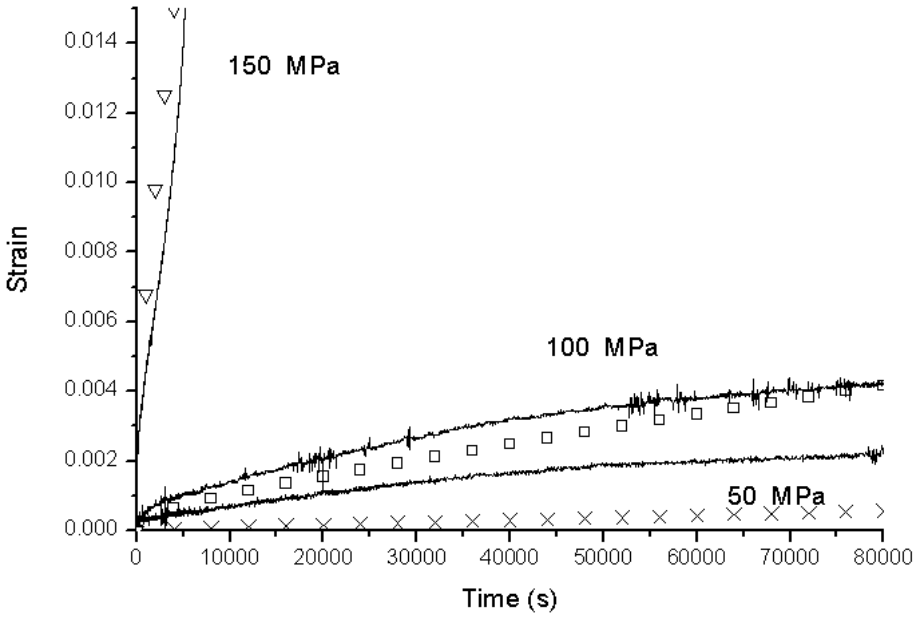

(A)

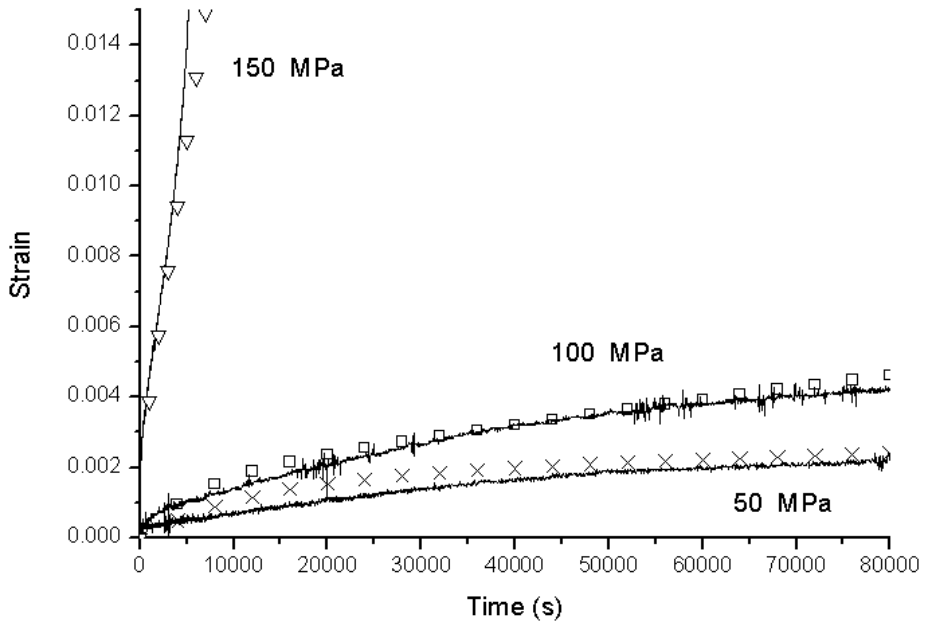

(B)

Fig. 4-40 A comparison of experimental creep curve (solid lines) and numerical regenerated creep curve (plots) by time hardening theory (A) and equation (35) proposed in this study.

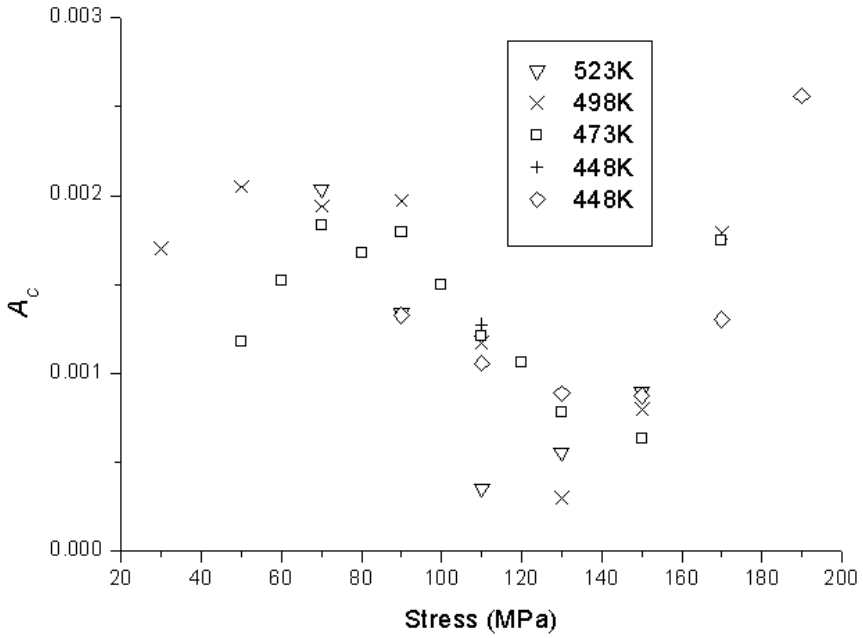

Fig. 4-41 Relationship between temperature, stress and constant *Ac*.

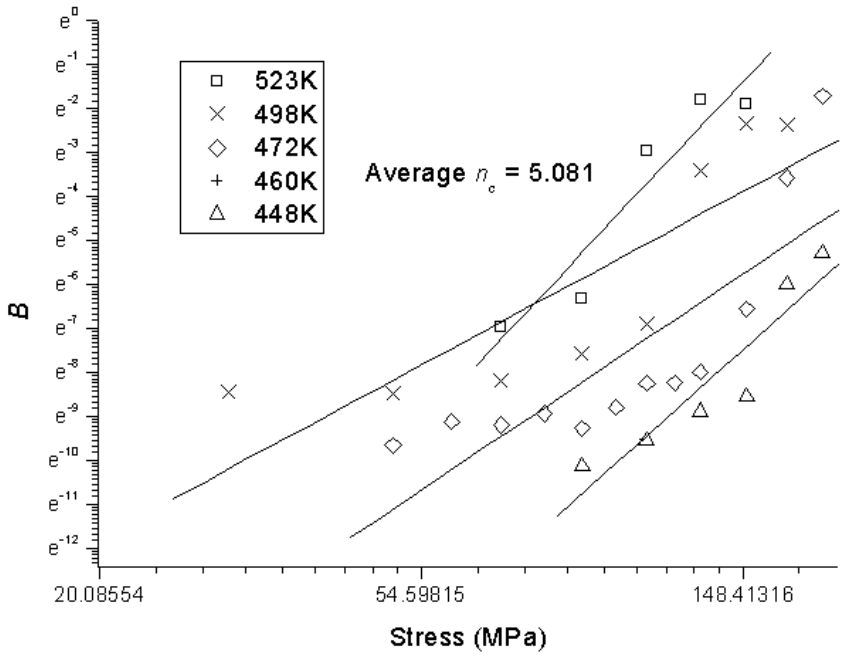

Fig. 4-42 Value of stress exponent n_c of the equation (37).

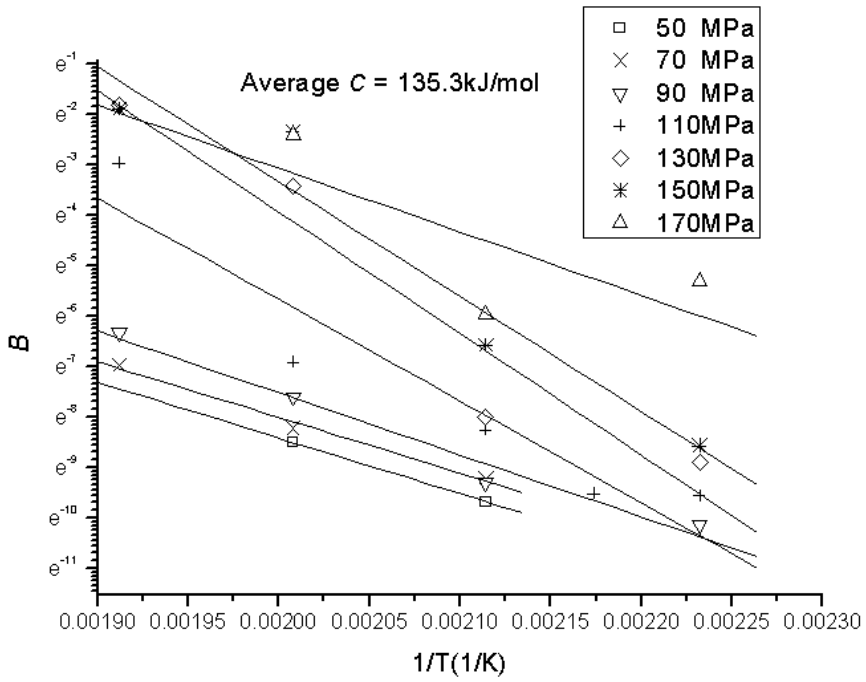

Fig. 4-43 Value of constant C of the equation (37).

4.5.3 Modeling of tertiary stage and total of creep curve

Tertiary stage of creep curves of the G+H A356-T6 cast alloy were modeled and some of the results are shown in Fig. 4-44, in which the solid lines are experimental data at 200°C and the hollow points are simulative data computed by the damage equations (12) and (13). The damage tolerance factor at stress levels of 110, 130, 150 and 170MPa are 4.5, 10.5, 13.2, 29.7 respectively, which proved that the main mechanism begins the tertiary stage of creep is precipitation coarsening [66].

Total creep curve modeling is achieved by equation (35), it is combined by equation (8) and (13) with superposed area subtracted. An example is shown in Fig. 4-45, in which the curves are SSM A356-T6 alloy at 200°C, average value A is about 1.86E-15, n is 5.08~5.23, m is around 0.35, λ is the same as listed in the last paragraph. It is learned that the result is reasonable but not perfect, which means the hardening-damage interaction conjecture can not perfectly model the creep behavior of G+H A356-T6 alloy, though it is quite suitable for some other kind of metals and alloys.

In the author's opinion, it probably because as it was introduced previously, the Kachanov damage theory and equation (11) defined the virgin metal before creep test as a piece of perfect metal, and creep damage accumulates during

creep until fracture, however, the point is, none of virgin metal in the lab is perfect, especially the cast alloys, instead, there are quite much defects in the alloys. These defects substantially decrease the plasticity of the alloy and more or less lead an excursion between the creep regenerated curve and experimental curve. There are three solutions may help to solve the problem, first is to perform the multi-axial creep test by using notch specimens, second is to analyze stress concentration by micro or meso mechanics, and the last solution is to modify the Kachanov equation to adapt the imperfect alloys, it is obviously that the third method is the easiest way to achieve. The author modified the Kachanov equation (13) by approximately presuming that the defects in the virgin metal is also a kind of damage, though it might be unreasonable in the micro mechanics perspective, however it is a easy way to obtain an high precision results with low cost, and the modified equation is equation (39), where t_0 is a parameter that assume the alloy already been crept and got some damage (defects) for t_0 time before the real creep test.

$$\varepsilon_c = A\sigma^n t^m + \varepsilon_t[1-(1-\frac{t}{t_r})^{1/\lambda}] - \dot{\varepsilon}_m t \tag{38}$$

$$\varepsilon_c = (\varepsilon_f \quad or \quad \varepsilon_t)[1-(1-\frac{t+t_0}{t_r+t_0})^{1/\lambda}] \tag{39}$$

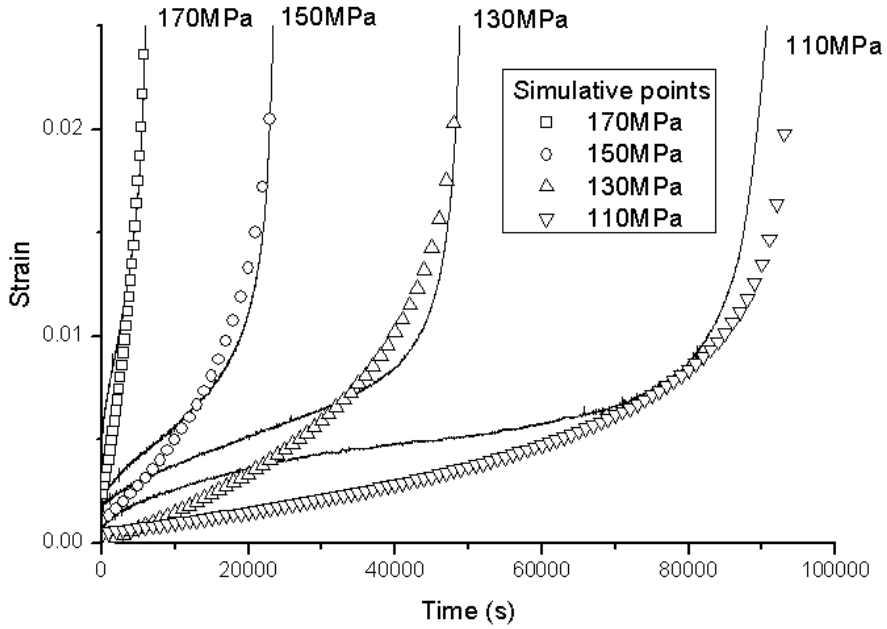

Fig. 4-44 Simulation of tertiary stage of creep curves of SSM A356-T6 alloy group 10 at 200°C, the solid lines are experimental curve and the hollow lines are simulative curves by the Kachanov equation.

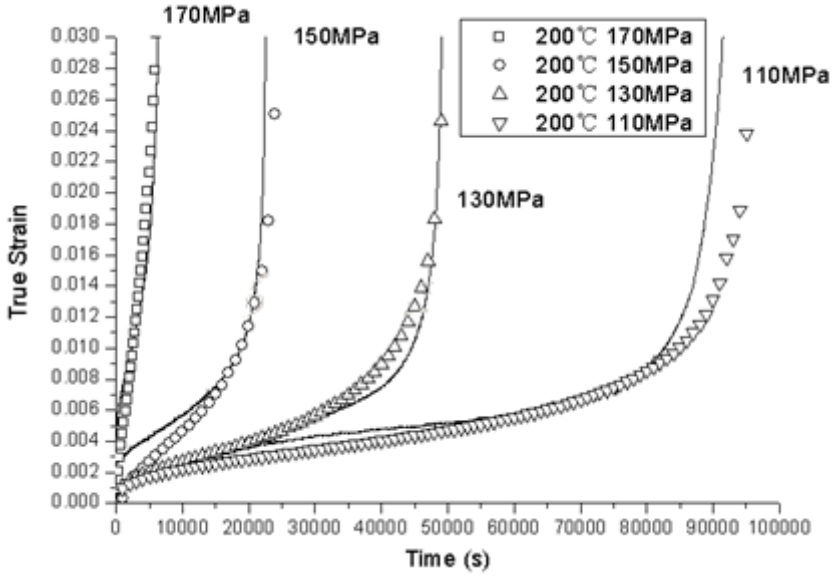

Fig. 4-45 Simulation of total creep curve of SSM A356-T6 alloy by the hardening-damage interaction theory.

4.6. Creep rupture life prediction of the SSM A356 alloy

A Monkman-Grant relationship is shown in Fig. 4-46, it is clear that the data is more convergent in the area of small stress than in the large stress area.

As it was introduced in the chapter 2 that the Larson-Miller extrapolation method is the most widely used method in the industrial applications and the Dorn-Orr-Sherby extrapolation is more close to the nature of materials, so that both of them have been used for normalizing the creep rupture data of the SSM A356 alloy G+H.

The Larson-Miller method assumes that the creep rupture data with different stress levels would converge into a point in the log(*tr*)-(1/T) coordinate, as it is illustrated in Fig. 4-47, but it does not happen in this research. Instead, all the data of the SSM A356 alloy G+H is divergent, or at least should be regarded as approximately parallel, as shown in Fig. 4-48, hence it might be concluded that the Larson-Miller method is not suitable for predicting the SSM A356 alloy.

Unlike Larson-Miller parameter, the Dorn-Orr-Sherby method conjectures that creep rupture data at different stress levels are parallel with each other, as it is sketched in Fig. 4-50. The result shown in Fig. 4-51 is more satisfactory

than the one obtained by the Larson-Miller method.

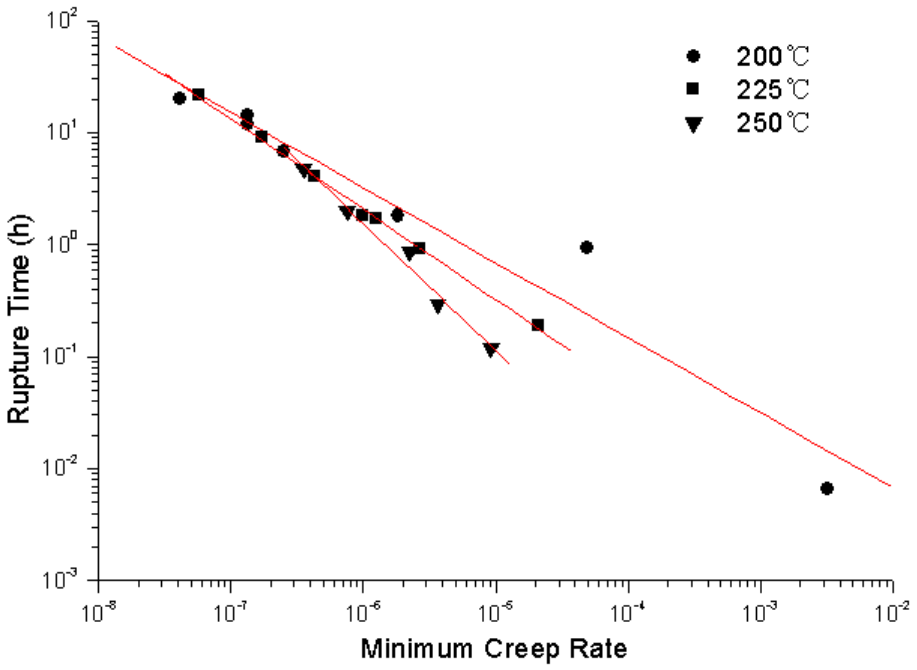

Fig. 4-46 Monkman-Grant relationship of the SSM A356 alloy G+H.

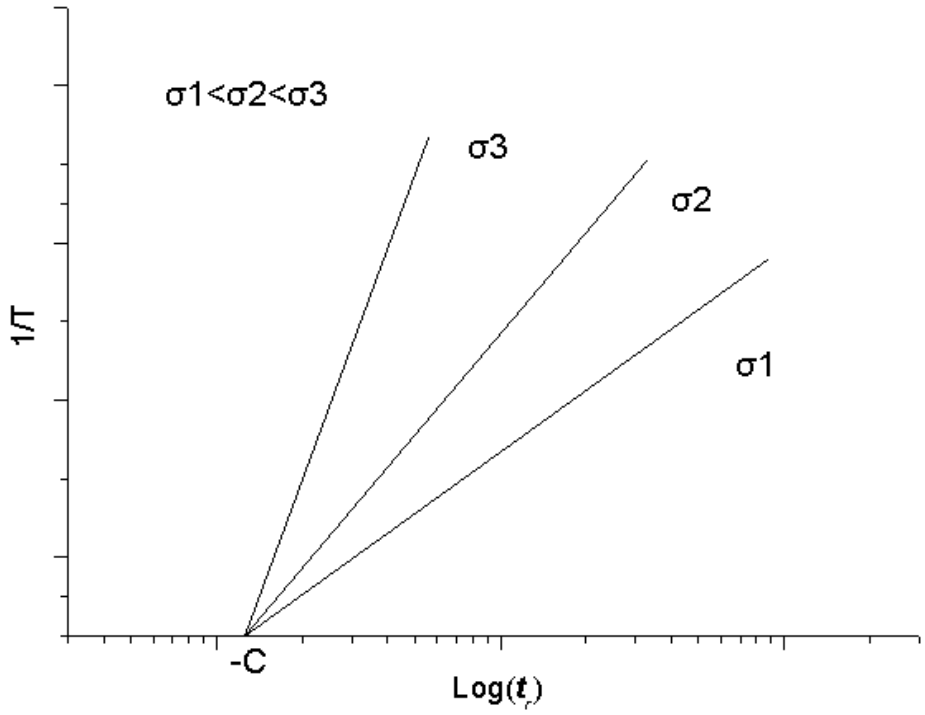

Fig. 4-47 Sketch of extrapolation convergence of the Larson-Miller method.

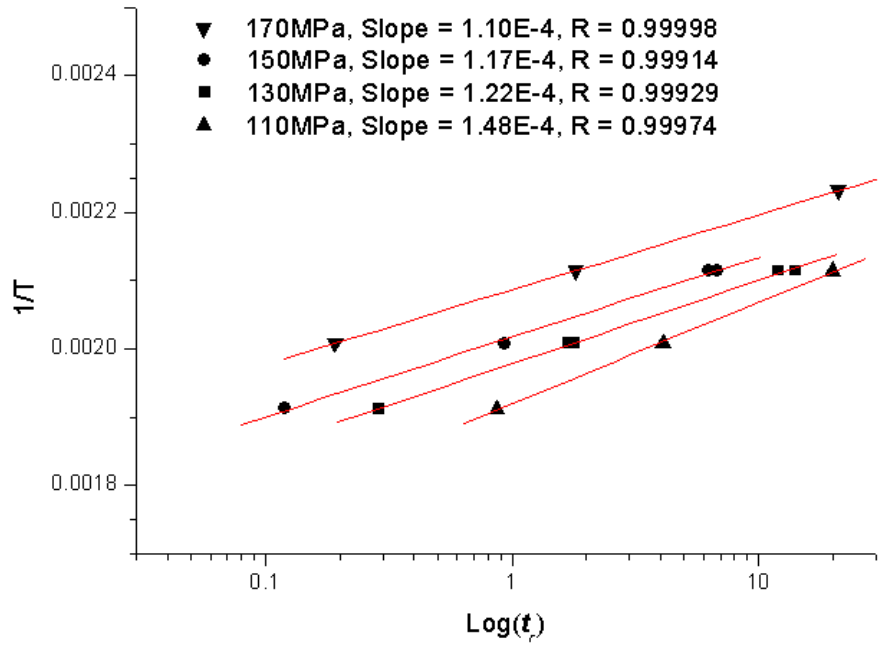

Fig. 4-48 Creep rupture data normalization of the SSM A356 alloy G+H by using the Larson-Miller extrapolation method.

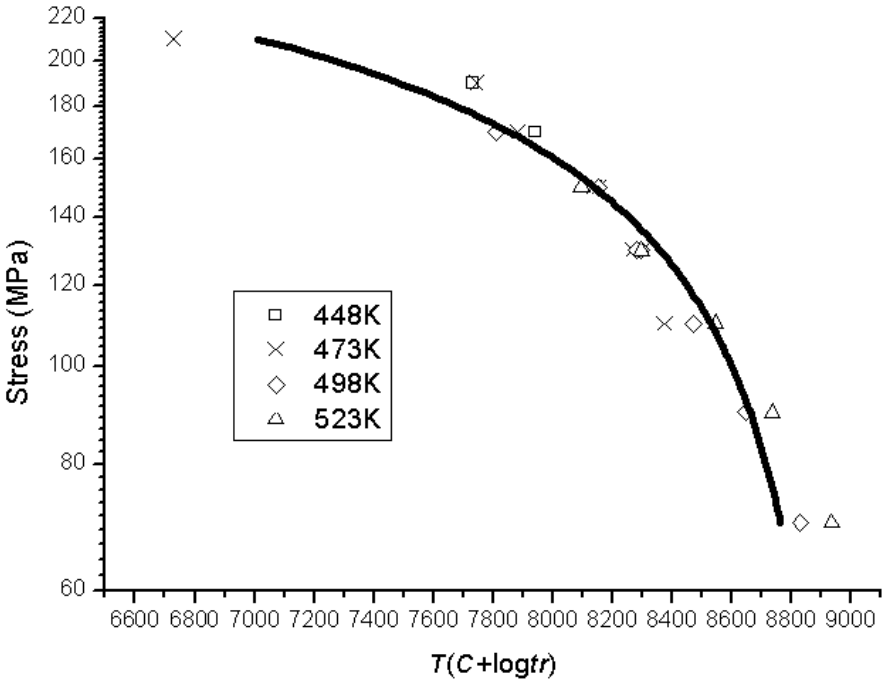

Fig. 4-49 Creep rupture life of the SSM A356 alloy G+H extrapolation by using the Larson-Miller method.

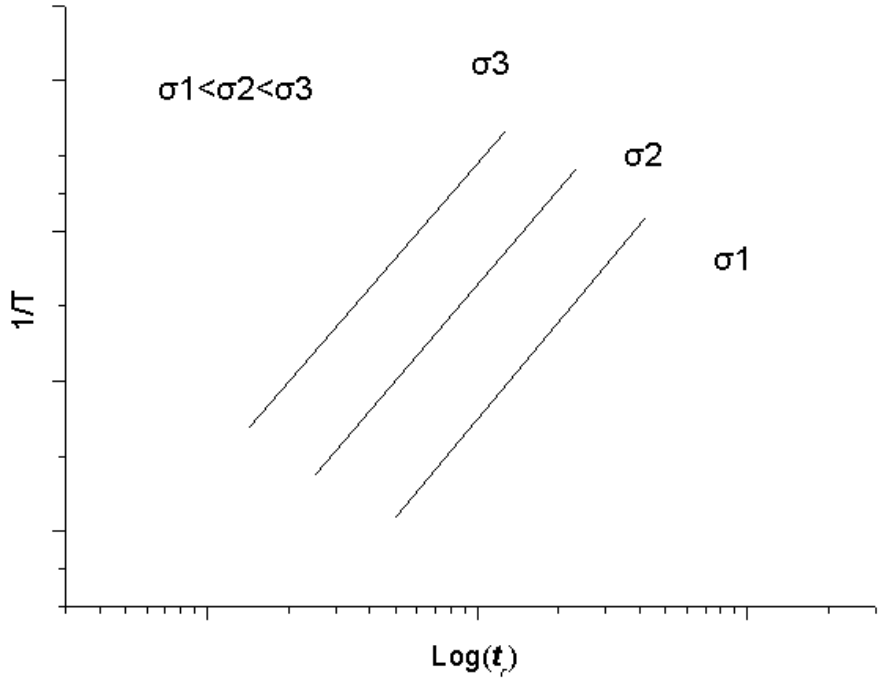

Fig. 4-50 Sketch of parallel stress levels of the Dorn-Orr-Sherby extrapolation method.

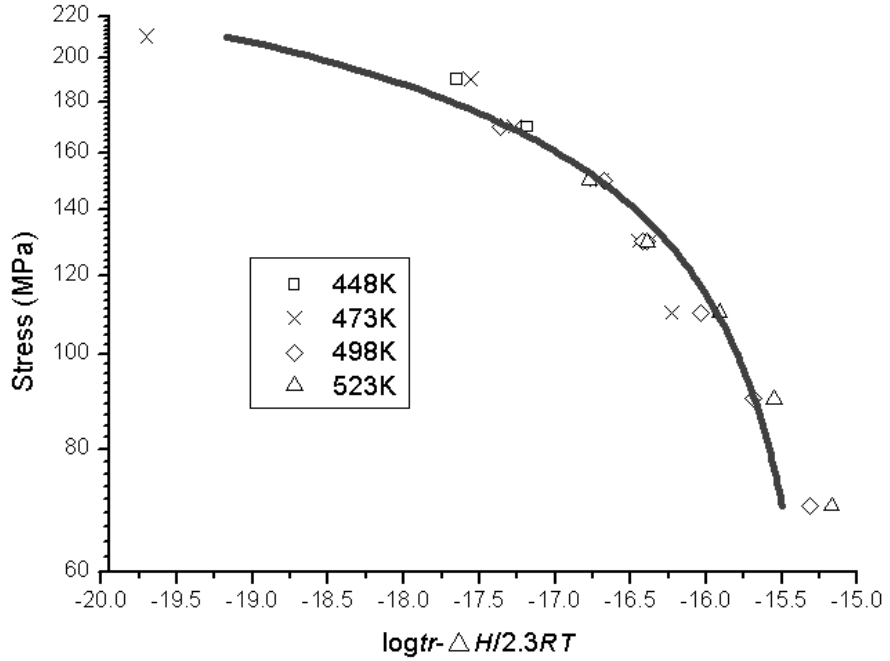

Fig. 4-51 Creep rupture life of the SSM A356 alloy G+H extrapolation by using the Dorn-Orr-Sherby method.

4.7. Conclusions

A group of A356 alloy was cast with conventional liquid casting and the Gas-Induced Semi-Solid (GISS) casting, and globular microstructure was obtained by the GISS casting. Mechanical properties of the alloys were further improved by T6 heat treatment with under, peak and over aged artificial aging.

Room temperature tensile properties (25°C, 298K) of A356-T6 alloy produced by different processes including both conventional liquid casting and the GISS casting. It was learned that the GISS process plus holding is good for producing globular α grain, but the alloys produced by short time GISS process (5s and 10s) without holding has smaller α grain and higher density of silicon particle.

Effects of average size of α grain, average size of silicon particle, shape factor, total volume of α phase and density of silicon particle on tensile properties were investigated and it was pointed out that these factors substantially affect but none of them could dominate the tensile properties. It was learned that the group 2 alloy produced by the GISS process has the highest tensile strength at room temperature (331.6±2.7MPa, strain rate 0.001/s) and it might indicated that smaller α grain size and higher density of silicon particle provide better tensile strength.

Tensile properties at temperature range of 25~250°C (298~523K) of the A356 aluminum low pressure squeeze cast alloys were investigated and satisfactory results were obtained by comparing to the report from the handbooks and other researchers. Work softening occurred during tensile test at 250°C indicated that the A356 aluminum alloy is not suitable to service at such high temperature.

A level arm creep test machine was successfully designed and fabricated. The error of temperature, force and displacement recording were controlled to a satisfactory range (±1°C, ±0.4kg and ±0.001μm, respectively) by strictly adjustment.

Creep behaviors at 175~250°C (448~523K) of the low pressure squeeze cast A356-T6 aluminum alloys produced by conventional liquid casting process (CLC), GISS process and GISS plus holding period were investigated. Anti-creep properties of the CLC alloy and GISS alloy are similar but G+H alloy is lower. According to the microstructure it is reasonable to infer that density of silicon particle is a key factor which affects creep properties, and higher density of silicon particle can obstruct the dislocation flow more efficiency. Activation energy of creep of the CLC, GISS and G+H alloys are 159.8, 163.1 and 144.5 kJ/mol respectively, and they are close to the activation energy of self-diffusion of pure aluminum (142 kJ/mo). As it is generally believed that the higher activation energy means better the anti-creep property.

Anti-creep properties of the GISS + Holding alloy with different heat treatment process were also be tested and the under aged A356 alloy it better than the as-solutioned, peak and over aged ones. Some previous researchers pointed out that this is because the precipitates of the over aged alloy are too coarse and lead brittleness to the alloy.

Large primary stage of creep curves of the A356-T6 alloys was

observed and it is probably governed by dislocation generation, dislocation hardening or secondary phase precipitating process.

A new approach for obtaining the best values for creep modeling by method of Marquardt was invented. Values defining of the constant of the constitutive equation of creep behavior became much easier and faster by using this method.

Several novel equations was created, which could model the primary stage of creep curves with good precision.

Kachanov damage theory for modeling the tertiary creep stage was proposed to import a pre-damage-time parameter but there is not enough data to prove this modified equation in this study.

Monkman-Grant, Larson-Miller and Dorn-Orr-Sherby creep life prediction theories were used to conclude creep rupture life of the GISS A356-T6 aluminum alloys.

REFERENCES

[1] V. S. Zolotorevsky, N. A. Belov and M. V. Glazoff, “Casting Aluminum Alloys”, pp, ix, Alcoa Technical Center, Alcoa Center, PA, U.S.A., Oct., 2007.

[2] H. Ye, “An Overview of the Development of Al-Si-Alloy Based Material for Engine Applications”, Journal of Materials Engineering and Performance, Vol. 12(4), 2003.

[3] J. L. Murray, A. J. McAlister, “Al-Si Phase Diagram”, ASM Metal Handbook 3, Alloy Phase Diagrams, 1984.

[4] ASTM International, “ASTM B 108 - 03a, Standard Specification for Aluminum-Alloy Permanent Mold Casting”, Copyright, ASTM International, 100 Barr Harbor Drive, PO Box C007, West, Conshohocken, PA 19428-2959, United States.

[5] M. E. Kassner, M-T Perez-Prado, “Fundamentals of Creep in Metals and Alloys”, ISBN0-08-043637-4, Elsevier, 2004.

[6] F. Philips, Philos. Mag. 9(1905)513.

[7] E. N. Da, C. Andrade, Proc. R. Soc. A84(1910)1-13.

[8] J. A. Lee, “Cast Aluminum Alloy for High. Temperature Applications”, Automotive Alloys, 2003.

[9] K. Young, P. Eisen, “SSM (semi-solid metal) technological alternatives for different applications, in: G.L. Chiarmetta (Ed.), Proceedings of the Sixth International Conference on Semi-solid Processing of Alloys and Composites,” 2000, pp. 41-46.)

[10] J. Wannasin, S. Janudom, T. Rattanochaikul, R. Canyook, R. Burapa, T. Chucheep, S. Thanabumrungkul, “Research and Development of Gas Induced Semi-solid Process for Industrial Applications”, Transactions of Nonferrous Metals Society of China, P. R. China, 2010.

[11] J. Wannasin, S. Junudom, T. Rattanochaikul, M. C. Flemings, “Development of the Gas Induced Semi-Solid Metal Process for Aluminum Die Casting Applications”, Solid State Phenomena, Vols. 141-143 (2008) pp 97-102, Switzerland, 2008.

[12] J. C. Gibeling, “Creep and Creep-Rupture Properties”, ASM Metal Handbook, vol. 8, Mechanical Testing and Evaluation, 2000.

[13] R. E. Reed-Hill, R. Abbaschian, Physical Metallurgy Principles, third edition, ISBN 0-534-98236-0, Pws-kent Publishing Company, Boston, USA.

[14] C. R. Brooks, “Principles of Heat Treating of Nonferrous Alloys”, Vol. 4 Heat Treating, ASM Metal Handbook, 1991.

[15] C. R. Brooks, “Heat Treating of Aluminum Alloys”, Vol. 4 Heat Treating, ASM Metal Handbook, 1991.

[16] M. H. Jacobs, “Precipitation Hardening”, Talat Lecture 1204, EAA – Europe Aluminum Association, 1999.

[17] W. M. von Haaften, W. H. Kool, L. Katgerman, “Tensile Behaviour of Semi-Solid Industrial Aluminum Alloys AA3104 and AA5182, Materials Science & Engineering A, 2002.

[18] C. Park, S. Kim, Y. Kwon, Y. Lee, J. Lee, “Effect of Microstructure on Tensile Behavior of Thixoformed 357-T5 Semi-solid Al Alloy, Metallurgical and Materials Transactions A, Vol. 35A, 2004

[19] Y. B. Yu, P. Y. Song, S. S. Kim and J. H. Lee, Possibility of improving tensile strength of semi-solid processed A356 alloy by a post heat treatment at an extremely high temperature, Scripta Materialia, Vol. 41, No. 7, pp. 767-771, 1999.

[20] H. M. Guo, Pressurized solidification of semi-solid aluminum die casting alloy A356, Journal of Alloys and Compounds, 485 (2009) 812-816, 2009

[21] H. Moller, Influence of temper condition on microstructure and mechanical properties of semisolid metal processed Al–Si–Mg alloy A356, International Journal of Cast Metals Research, VOL 22, NO 6 421, 2009.

[22] C. D. Lee, “Effects of Microporosity on Tensile Properties of A356 Aluminum Alloy”, Materials Science & Engineering A pp. 249-254, 2007.

[23] K. Lee, Y. N. Kwon, S. Lee, “ Correlation of Microstructure with Mechanical Properties and Fracture Toughess of A356 Aluminum Alloys Fabricated by Low-Pressure-Casting, Rheo-Casting, and Casting-Forging Processes”, Engineering Fracture Mechanics, 75, 2008.

[24] R. Burapa, S. Janudom, T. Chucheep, R. Canyook, J. Wannasin, “Effects of Primary Phase Morphology on Mechanical Properties of Al-Si-Mg-Fe Alloy in Semi-Solid Slurry Casting Process”, Transactions of Nonferrous Metals Society of China, 2010.

[25] W. N. Findley, J. S. Lai, K. Onaran, Creep and Relaxation of Nonlinear Viscoelastic Materials, Dover Publications, INC., New York, ISBN 0-486-66016-8, 1989.

[26] R. K. Penny, D. L. Marriott, Design for Creep, second edition, Chapman & Hall, ISBN 0 412 59040 9.

[27] F. Abe, T.-U. Kern and R. Viswanathan, Creep-resistant steels, Woodhead Publishing Limited, Cambridge England.

[28] S. Spigarelli, Creep of Aluminum and Aluminum Alloys, EAA-European Aluminum Association, 1999.

[29] J. C. Dandrea, “Creep and Creep Recovery of Cast Aluminum Alloys”, Mech Time-Depend Mater, 2009.

[30] T. G. Langdon, “Transition in Creep Behavior”, Materials Transactions, JIM, Vol. 37, pp. 359-362, 1996.

[31] W. X. Song, Theory of Metals, Second Edition, ISBN 978-7-5024-0475-8, Metallurgical Industry Publishing Company, Peking, China.

[32] N. C. Guo, Z. J. Guo, Q. Y. Gong, “The Superplasticity of Commercials Aluminum Alloy”, Journal of Materials Processing Technology, Vol 21, Issue3, pp. 285-294, 1990.

[33] R. K. Islamgaliev, N. F. Yunusova, R. Z. Valiev, N. K. Tsenev, V. N. Perevezentsev, T. G. Langdon, “Characteristics of Superplasticity in an Ultrafine-grained Aluminum Alloy Processed by ECA Pressing”, Scripta Materialia, Vol. 49, Issue 5, pp. 467-472, 2003.

[34] T. Tvergarrd, “Mechanical Models of the Effect of Grain Boundary Sliding on Creep and Creep Rupture”, Revue Phys. Appl. 23, pp. 595-604, 1988.

[35] J. Dunnwald, E. El-Maged, “Description of the Creep Behaviour of the Precipitation-Hardened Material Al-Cu-Mg Alloy 2024 Unsing Finite Element

Computations Based on Microstructure Mechanical Models", Computational Materials Science, pp. 200-207, 1996.

[36] R. N. Lumley, A. J. Morton, I. J. Polmear, *Conference Proceedings ICAA7Mater. Sci. Forum* 331-337, pp/ 1495, 2000.

[37] R. N. Lumley, A. J. Morton, I. J. Polmear, "Enhanced Creep Performance in an Al-Cu-Mg-Ag Alloy Through Underaging", Acta Materialia, Vol. 50, Issue 14, pp. 3597-3608, 2002.

[38] A. M. Abd, El-Khalek, "Steady State Creep and Creep Recovery Behaviours of Pre-aging Al-Si Alloys", Materials Science and Engineering A, pp. 176-181, 2009.

[39] S. Spigarelli, M. Cabibbo, E. Evangelista, S. Cucchieri, "Evaluation of the Creep Properties of an Al-17Si-Mg-0.7Cu Alloy", Materials Letters, 2002.

[40] S. Spigarelli, E. Evangelista, S. Cucchiberi, "Analysis of the Creep Response of an Al-17Si-4Cu-0.55Mg Alloy, Materials Science & Engineering A, 2004.

[41] T. Jaglinski, R. Lakes, "Creep Behavior of Al-Si Die-Cast Alloys", Transactions of the ASME, Vol. 126, 2004.

[42] K. Ishikawa, Y. Kobayashi, "Creep and Rupture Behavior of a Commercial Aluminum-Magnesium Alloy A5083 at constant applied stress", Materials Science & Engineering A, 2004.

[43] K. Naumenko, H. Altenbach, Modeling of Creep for Structural Analysis, Springer, ISBN-10:3-540-70834-0, 2007.

[44] W. Blum, P. Eisenlohr, F. Breutinger, "Understanding Creep-a Review", Metallurgical and Materials Transactions A, Vol. 33A, 2002.

[45] R. E. Reed-Hill, R. Abbaschian, Physical Metallurgy Principles, third edition, ISBN0-534-92173-6, Pws-Kent Publishing Company, Boston.

[46] F. R. N. Nabarro, H. L. de Villiers, the Physics of Creep, Taylor & Francis Ltd, 1995, ISBN0850668522.

[47] W. Blum, P. Eisenlohr, Dislocation mechanics of creep, Materials Science and Engineering A, 510-511(2009)7-13.

[48] ASTM International, "ASTM E18-03, Standard Test Methods for Rockwell Hardness and Rockwell Superficial Hardness", Copyright, ASTM International,

100 Barr Harbor Drive, PO Box C007, West, Conshohocken, PA 19428-2959, United States.

[49] ASTM International, “ASTM E112–96, Standard Test Methods for Determining Average Grain Size”, Copyright, ASTM International, 100 Barr Harbor Drive, PO Box C007, West, Conshohocken, PA 19428-2959, United States.

[50] ASTM International, “ASTM E8–08, Standard Test Methods for Tension Testing of Metallic Materials”, Copyright, ASTM International, 100 Barr Harbor Drive, PO Box C007, West, Conshohocken, PA 19428-2959, United States.

[51] J. R. Davis, Properties of Aluminum and Aluminum Alloys, Aluminum and Aluminum Alloys, ASM Specialty Handbook, Vol. 2, The Materials Information Society, pp. 706-731, 1993.

[52] J. G. Kaufman, E. L. Rooy, Aluminum Alloy Castings, ASM international, ISBN:0-87170-803-5, 2004.

[53] R. W. Hertzberg, Deformation and Fracture Mechanics of Engineering Materials, Wiley, ISBN0471012149, 1995.

[54] J. P. Poirier, Creep of Crystals, Cambridge University Press, ISBN0-521-27851-1, 2005.

[55] M. E. Kassner, Taylor hardening in five-power-law creep of metals and Class M alloys, Acta Materialia, 52(2004)1-9.

[56] S. V. Raj, A. D. Freed, A phenomenological description of primary creep in class M materials, Materials Science and Engineering A, 283(2000)196-202.

[57] S. Spigarelli, “Creep of Aluminum and Aluminum Alloys”, Talat Lecture 1253, EAA – European Aluminum Association, 1999.

[58] P. K. Penny and D. L. Marriott, Design for Creep, Chapman & Hall, ISBN0-412-59040-9, 1995.

[59] R. W. Evans, B. Wilshire, Introduction to Creep, Oakdale Printing Company Ltd, Poole, 1999.

[60] B. Wilshire, H. Burt, “Damage Evolution during Creep of Steels”, Pressure Vessels and Piping, 2008.

[61] M. E. Kassner, M. T. Perez-Prado, Fundamentals of Creep in Metals and Alloys, Elsevier, ISBN0-08-043637-4, 2004.

[62] F. Abe, T.-U. Kern and R. Viswanathan, Creep-resistant steels, Woodhead Publishing Limited, Cambridge, England.

[63] ASTM International, "ASTM E139–06, Standard Test Methods for Conducting Creep Creep-Rupture, and Stress-Rupture Tests of Metallic Materials", Copyright, ASTM International, 100 Barr Harbor Drive, PO Box C007, West, Conshohocken, PA 19428-2959, United States.

[64] K. C. Ho, J. Lin, T. A. Dean, "Constitutive Modelling of Primary Creep for Age Forming and Aluminum Alloy", Journal of Materials Processing Technology, 2004.

[65] O. D. Sherby, E. M. Taleff, Influence of grain size, solute atoms and second-phase particles on creep behavior of poly crystalline solids, Materials Science & Engineering A, 322(2002)89-99.

[66] J. Betten, Creep Mechanics, Springer, ISBN-978-3-540-85050-2, 3rd Edition.

CIRRICULUM VITAE

Name Mr. Yi Zhou

Student ID 5110120132

Educational Attainment

Degree	Name of Institution	Year of Graduation
Bachelor of Materials Engineering	JiangXi University of Science and Technology	2007

List of Publication and Proceeding

Y. Zhou, T. Plookphol, S. Wisutmethangoon, J. Wannasin, “High-Temperature Tensile Properties of Semi-Solid Aluminium Alloy A356-T6 Produced by the GISS Process”, Proceedings of the MESO Mechanics International Conference 2010, PP. 367-370, Taipei, Taiwan, June 2010.